The *In Vitro* Pharmacology of Cannabidivarin (CBDV)

A Thesis Submitted to the

College of Graduate and Postdoctoral Studies

In Partial Fulfillment of the Requirements

For the Degree of Master of Science

In the Toxicology Graduate Program

University of Saskatchewan

Saskatoon

By

Jennifer Le

PERMISSION TO USE

In presenting this thesis in partial fulfillment of the requirements for a degree of Master of Science from the University of Saskatchewan, I agree that the University Libraries can make it freely available for inspection. I further agree that permission for copying of this thesis in any manner, in whole or in part, for scholarly purposes may be granted by the professors who supervised my thesis work or, in their absence, by the Dean of the College in which my thesis work was done. It is understood that any copying or publication or use of this thesis or parts for any financial gain shall not be allowed without my written permission. It is also understood that due recognition shall be given to me and to the University of Saskatchewan in any scholarly use which may be made of any material in my thesis.

Request for permission to copy of to make other uses of materials in this thesis in whole or part should be addressed to:

Toxicology Centre
44 Campus Drive
University of Saskatchewan
Saskatoon, Saskatchewan, S7N 5B3
Canada

OR

Dean of the College of Graduate and Postdoctoral Studies
110 Science Place
University of Saskatchewan
Saskatoon, Saskatchewan, S7N 5C9
Canada

ABSTRACT

Cannabis and the family of cannabinoids were first popularized due to the psychoactive profile elicited by a major cannabinoid, Δ^9-tetrahydrocannabinol (THC). In recent decades, the rejuvenation and rapid increase in popularity of cannabinoid research arose due to another major cannabinoid, cannabidiol (CBD), and its therapeutic potential in inflammation, neurological disorders, and many other diseases. However, to standardize the medical and recreational use of *Cannabis*, the lesser-known cannabinoids including cannabidivarin (CBDV) also require pharmacokinetic (PK) and pharmacodynamic (PD) evaluations. While CBD and CBDV are similar in structure and other aspects, such as therapeutic potential as an anti-epileptic and anti-inflammatory agent, a complete understanding of the pharmacological profile for CBDV is lacking. The aim of this thesis was to perform PK and PD evaluations of CBDV utilizing various *in vitro* methods for two purposes: 1) to support current and future literature, and 2) to present alternatives to animal and human testing.

First, the plasma protein binding characteristics of CBDV in human pooled plasma was studied using a three-solvent extraction protocol, allowing for the prediction of the unbound fraction as well as the binding fractions of CBDV to various plasma proteins. Next, the metabolic stability of CBDV was assessed via the substrate depletion method and the linear extrapolation stability assay with human liver microsomes to determine *in vitro* intrinsic clearance. Intestinal permeability was determined via a Transwell® system comprised of human colorectal adenocarcinoma cell (Caco-2), a model of the intestinal epithelium; however, due to lack of CBDV detection in the receiver compartments of the Transwell®, limitations of the current gold-star method were examined instead. In terms of PD assessment, human induced pluripotent stem cells (iPSCs) were cultured and used to grow brain organoids, which are multi-cellular and self-organizing three-dimensional aggregates capable of mimicking the human brain. The brain organoids exposed to an inflammatory stimulus were used for the preliminary screening of anti-inflammatory potential of CBDV. These studies revealed that plasma protein binding of CBDV was determined to be not clinically significant due to the highly unbound fraction (> 20%); however, CBDV is a high clearance drug due to its high unbound intrinsic clearance value (> 100.0 µL/min/mg). Brain organoids, in response to lipopolysaccharide (LPS) stimulation, revealed potential anti-inflammatory effects with CBDV treatment.

Our data suggests these studies are valuable assets capable of determining *in vitro* human PK parameters of CBDV, which are currently understudied and unreported, as is its role in the inflammatory response. This thesis provides the groundwork for future studies and demonstrates that *in vitro* models could be a useful tool to compare with traditional *in vivo* methods.

ACKNOWLEDGEMENTS

Of my time as a graduate student at the University of Saskatchewan, I have been grateful to learn and grow from the experience thanks to my supervisors, committee members, lab colleagues, family, and friends.

First, I would like to thank my supervisors, Dr. Jane Alcorn and Dr. Darrell D. Mousseau, not only for this amazing opportunity in *Cannabis* research, but for their guidance, support, generosity and understand during this time. I am thankful of Dr. Alcorn's expertise and guidance in both experimentation and writing; with meticulously detailed feedback, her words greatly helped to shape my research and writing skills. I am also grateful of Dr. Mousseau's expertise and guidance; his support in the laboratory and his feedback in the writing process were of great benefit. I would like to give thanks to committee members, Dr. John Howland and Dr. Barry Blakley, as well as a previous committee member, Dr. Mark Wickstrom, for all of their expertise and dedication. A special thank you to Dr. Tyler J. Wenzel whose immense support, reassurance, and guidance inspired me to become a better researcher and person. As for my colleagues, I am grateful to Jim He, Dr. Frank De Silva, and Morgan Beattie for their assistance in experimentation and providing an incredible lab environment. I would also like to thank Ryan Heistad, Deborah Michel, and Stephanie Vuong for their support as technicians in their respective fields.

Special thanks to my mother and father, Nga Thi Tran and Johnny Le, as well as the rest of my family for the endless love, encouragement, and support during my master's program; I hope that they are as equally proud of me as I am of them. Finally, thank you to all my friends who kept me sane during the trying times of the pandemic, especially to Saili Bundele; a friend, mentor, and sister.

Thanks to the Zigurds and Hildegarde Lejins Fund and the Dr. H. B. (Bruno) Schiefer Graduate Student Travel Award at the University of Saskatchewan for the generous philanthropic financial support of this research project.

TABLE OF CONTENTS

LIST OF TABLES

LIST OF FIGURES

LIST OF ABBREVIATIONS

2-AG	2-Arachidonoylglycerol
2D	Two-dimensional
3D	Three-dimensional
AA	Arachidonic acid
AAG	α_1 acid glycoprotein
ACN	Acetonitrile
ADME	Absorption, distribution, metabolism, and elimination
AEA	Anandamide
AED	Antiepileptic drugs
ANOVA	One-way analysis of variance
ATCC	American Type Culture Collection
AUC	Area under the curve
BBB	Blood-brain barrier
bFGF	Basic fibroblast growth factor
BMEC	Brain microvascular endothelial cells
BSA	Bovine serum albumin
Caco-2	Human colorectal adenocarcinoma cells
CB1R	Cannabinoid receptor 1
CB2R	Cannabinoid receptor 2
CBD	Cannabidiol
CBD-D_3	Cannabidiol-D_3
CBDV	Cannabidivarin
Cl_H	Hepatic clearance
Cl_{int}	Intrinsic clearance
$Cl_{int,u}$	Unbound intrinsic clearance
CNS	Central nervous system
CO_2	Carbon dioxide
CSF	Cerebral spinal fluid
CYP	Cytochrome P450 enzyme

dH_2O	Deionized water
DI	Deionized
DGLα	Diacylglycerol lipase-alpha
DMEM	Dulbecco's modified Eagle medium
DMSO	Dimethyl sulfoxide
EB	Embryoid body
eCB	Endocannabinoid
ECS	Endocannabinoid system
ESC	Embryonic stem cells
ESI	Electrospray ionization
Eq	Equation
FBS	Fetal bovine serum
FDA	U.S. Food and Drug Administration
f_u	Unbound fraction
GAPDH	Glyceraldehyde 3-pohsphate dehydrogenase
GPCR	G protein-coupled receptor
HBSS	Hank's balanced salt solution
HCl	Hydrochloric acid
hESC	Human embryonic stem cells
HEPES	N-2-hydrozyethylpiperazine-N'-2-ethanesulfonic acid
HK_2PO_4	Potassium phosphate dibasic
HLMs	Human liver microsomes
HPLC	High-performance liquid chromatography
hPSC	Human pluripotent stem cells
HQC	High quality control
IBA1	Ionized calcium binding adaptor molecule 1
IgG	Immunoglobulin G
IL	Interleukin
iNOS	Inducible nitric oxide synthase
i.p.	Intraperitoneal
iPSCs	Induced pluripotent stem cells

IS	Internal standard
i.v.	Intravenous
K_2HPO_4	Dipotassium phosphate
kDa	Kilodalton
k_{dep}	Substrate depletion rate constant
Klf4	Kruppel-like factor 4
K_m	Michaelis-Menten constant
LC-MS	Liquid chromatography-mass spectrometry
LC-MS/MS	Liquid chromatography-tandem mass spectrometry
LDH	Lactate dehydrogenase
LESA	Linear extrapolation in the stability assay
LFP	Local field potential
LLOQ	Lowest limit of quantification
LOD	Limit of detection
LPS	Lipopolysaccharide
LQC	Low quality control
LY	Lucifer yellow
MEM-NEAA	Minimum essential medium non-essential amino acid
$MgCl_2$	Magnesium chloride
MQC	Medium quality control
NaCl	Sodium chloride
NADPH	Nicotinamide adenine dinucleotide phosphate
NO	Nitric oxide
NSB	Non-specific binding
NSCs	Neural stem cells
Oct	Octamer-binding transcription factor
PBS	Phosphate buffered saline
PD	Pharmacodynamic(s)
PK	Pharmacokinetic(s)
PNS	Peripheral nervous system
p.o.	per os

PPAR	Peroxisome proliferator-activated receptor
PPB	Plasma protein binding
PSCs	Pluripotent stem cells
QC	Quality control
$\boldsymbol{R^2}$	Coefficient of determination
RA	Retinoic acid
RIPA	Radioimmunoprecipitation assay buffer
ROCK	Rho-associated protein kinase
R.S.D.	Relative standard deviation
S.D.	Standard deviation
SDS	Sodium dodecyl sulfate
Sox2	Sex-determining region Y
SPE	Solid phase extraction
$\boldsymbol{t_{1/2}}$	Half-time
TBS	Trisaminomethane-buffered saline
TBS-T	Trisaminomethane-buffered saline with TWEEN® 20
TEER	Transepithelial electrical resistance
TEMED	Tetramethylethylenediamine
THC	Δ^9-Tetrahydrocannabinol
THCV	Δ^9-Tetrahydrocannabidivarin
TMEM119	Transmembrane protein 119
TNF-α	Tumor necrosis factor α
TRIS	Trisaminomethane
TRP	Transient receptor potential cation channel
TRPV1	Transient receptor potential vanilloid 1
TWEEN® 20	Polysorbate 20
$\boldsymbol{V_d}$	Volume of distribution
VEGF	Vascular endothelial growth factor

1. INTRODUCTION

Cannabis and the family of cannabinoids have been popularized in recent decades due to their therapeutic potential in inflammation, neurological disorders, and many other diseases. One of the main cannabinoids, cannabidiol (CBD), is of particular interest, but many other phytocannabinoids exist with the possibility of similar or greater potential therapeutic benefits. A lack of pharmacokinetic (PK) and pharmacodynamic (PD) data, though, exists for these lesser-known cannabinoids, but will be necessary to understand any medicinal and non-medicinal use. In vitro methodologies pose an opportunity to understand human PK and PD characteristics without the requirement of any human clinical trial strategies or *in vivo* preclinical animal models. A new technology of three-dimensional (3D) cell cultures using stem cells, called 'organoids', is also gaining popularity as a potential alternative to *in vivo* animal testing and drug assessment prior to clinical trials. This is possible due to the organoids' ability to produce multiple, self-organizing cell types, mimicking the *in vivo* cytoarchitecture and one or more functions of the organ of interest. The purpose of this thesis was to assess *in vitro* pharmacology of a lesser-known cannabinoid, cannabidivarin (CBDV), which is gaining recognition for its potential antiepileptic properties, using *in vitro* PK methods and to incorporate organoids as part of the PD assessment.

2. LITERATURE REVIEW

2.1. *Cannabis* Overview

Cannabinoids are a class of naturally occurring, lipophilic compounds that can derive from the *Cannabis* plant (Huestis et al., 2019). Multiple strains of *Cannabis* exist based on phenotypic traits, with the most well-known cultivars being *Cannabis sativa* and *Cannabis indica*, two subspecies of *Cannabis sativa L.* (Klumpers & Thacker, 2019). All strains contain well over 100 potentially bioactive compounds with psychoactive Δ^9-tetrahydrocannabinol (THC) and its structural isomer, cannabidiol (CBD), as the most well-studied compounds. These two cannabinoids share the same molecular formula and weight ($C_{21}H_{30}O_2$; molecular weight 314.5 g/mol), as well as physiochemical properties such as their poor solubility in water (Calapai et al., 2020; Huestis et al., 2019; Klumpers & Thacker, 2019). Compounds such as CBD, THC, and other plant-derived cannabinoids, also known as phytocannabinoids, can interact with the endocannabinoid system (ECS) to mediate their effects (Klumpers & Thacker, 2019). It was profiled as early as the 1970s in humans that THC is one of the main psychoactive constituents in *Cannabis* and that its metabolite, 11-OH-THC, is also partly responsible for the psychotropic effects (Lemberger, Martz, & Rodda, 1973). While THC gained popularity due to its ability to elicit the 'high' associated with *Cannabis*, CBD has become more significant in recent decades because of its potential therapeutic benefits without the negative effects associated with THC (Klumpers & Thacker, 2019).

2.1.1. Cannabidiol

Cannabidiol (CBD) was discovered in the 1940s but was widely underestimated in research due to its 'non-*Cannabis* like' psychoactive effects, categorizing it as an inactive and minor compound, unlike THC (Adams, Hunt, & H. Clark, 1940; Mechoulam, Shani, Edery, & Grunfeld, 1970). In the early stages of *Cannabis* research, despite some promising results as an antiemetic and appetite stimulant, multiple adverse effects such as general weakness, nausea, disorientation, hallucinations, and vomiting proved difficult to market *Cannabis* treatment in humans (Whiting et al., 2015). Later, during the early 1970s, experiments utilizing CBD originally focused on its pharmacological interaction with THC, which showed CBD's ability to decrease the amount of THC's adverse effects and to potentiate THC's therapeutic benefits that researchers originally associated with *Cannabis* (Boggs, Peckham, Boggs, & Ranganathan, 2016). Studies that focused

solely on CBD treatment show greater tolerability in patients with little to no adverse effects and without any *Cannabis*-like (e.g., THC-like) intoxication or euphoria (Boggs et al., 2016; Grotenhermen, Russo, & Zuardi, 2017). In the recent decades, CBD has been studied for its range of potential usage as an antiemetic, anticonvulsant, analgesic, anti-inflammatory, anxiolytic for social anxiety and depression, as well as neuroprotective treatment against schizophrenia, Parkinson's, and Alzheimer's disease (Aso & Ferrer, 2014; Beale et al., 2018; Chagas et al., 2014; Drożak, Skrobas, & Drożak, 2022; Huestis et al., 2019; McGuire et al., 2018; Solowij et al., 2018; Whiting et al., 2015; Zuardi, 2008).

2.1.2. Cannabidivarin

While CBD and THC are the most studied members of the cannabinoid family, over 100 other phytocannabinoids have been discovered. It is only in recent years that researchers began to study the lesser-known phytocannabinoids for potential therapeutic applications. Many analogues of CBD share similar physicochemical characteristics and clinical effects; however, there is an important knowledge gap regarding the pharmacokinetic (PK) and pharmacodynamic (PD) profiles of these other cannabinoids. A related phytocannabinoid currently of interest is cannabidivarin (CBDV), the *n*-propyl analogue of CBD that was officially documented in 1969 (Vollner, Bieniek, & Korte, 1969). This compound is found at high concentrations in *C. indica* and acts as the plant precursor to tetrahydrocannabivarin (THCV), which is the *n*-propyl analogue to THC (Rock, Sticht, Duncan, Stott, & Parker, 2013). While CBDV can isomerize into THCV under acidic conditions, it is unknown whether stomach pH leads to isomerization *in vivo* (Deiana et al., 2012). Despite its popularity, there is still a lack of literature to establish the complete pharmacological profile of this phytocannabinoid. Like other phytocannabinoids, CBDV is known to interact with the endocannabinoid system (Zamberletti et al., 2019).

2.2. The Endocannabinoid System and its Receptors

Discovered in the early 1990s, the endocannabinoid system (ECS) consists of various receptors, enzymes, and endogenous cannabinoids (eCBs) that play a significant role in maintaining homeostasis of the body for multiple different functions (Klumpers & Thacker, 2019). This includes memory and learning, perception, mood, feeding behaviour, pain, and cardiovascular functions (Vučkovic, Srebro, Vujovic, Vučetic, & Prostran, 2018). The main receptors responsible in the ECS include cannabinoid type 1 receptor (CB1R) and cannabinoid type 2 receptor (CB2R),

both of which belong to the G protein-coupled receptor (GPCR) family and can be found in the central nervous system (CNS) (Huestis et al., 2019) (**Figure 2.1**). The CB1R is one of the most abundant receptors in the brain, present on the axon terminals and pre-terminal axon segments of neurons in the cortex, basal ganglia, hippocampus, and cerebellum (Huestis et al., 2019; Lu & Mackie, 2016). The CB2R has lower expression in the CNS than the periphery; however, it is expressed in microglia, vascular elements, and neurons during pathological conditions (e.g., during inflammation, tissue injury) and is therefore associated with the immune system. Different receptors that are also engaged in the system include other GPCRs, transient receptor potential cation channels (TRPs), and nuclear peroxisome proliferator-activated receptors (PPARs) (Ao et al., 2020; Huestis et al., 2019).

As a neuromodulatory system, ligands such as eCBs are retrograde messengers, in that they are synthesized in the post-synaptic terminal and are released into the synapse where they act upon pre-synaptic receptors (Lu & Mackie, 2016), unlike traditional synaptic transmission which acts postsynaptically (Klumpers & Thacker, 2019). The precursors to eCBs are stored in lipid membranes of postsynaptic neurons, until needed for synthesis and signalling (Lu & Mackie, 2016). By acting upon presynaptic CB1R and CB2R, eCBs inhibit synaptic transmission. The first identified eCBs and the most well-known ligands to the ECS are anandamide (AEA) and 2-arachidonoyl glycerol (2-AG) which act upon CB1R, CB2R, TRP, PPAR-α, and PPAR-γ (Huestis et al., 2019; Lu & Mackie, 2016). Although both AEA and 2-AG are synthesized from arachidonic acid, the intrinsic efficacy of each eCB varies, especially among the cannabinoid receptors. The principal ligand for CB1R is AEA while the principal ligand for CB2R is 2-AG; however, 2-AG is a strong agonist for both CB1R and CB2R and AEA is a low efficacy agonist of CB1R with even lower efficacy for CB2R (Lu & Mackie, 2016).

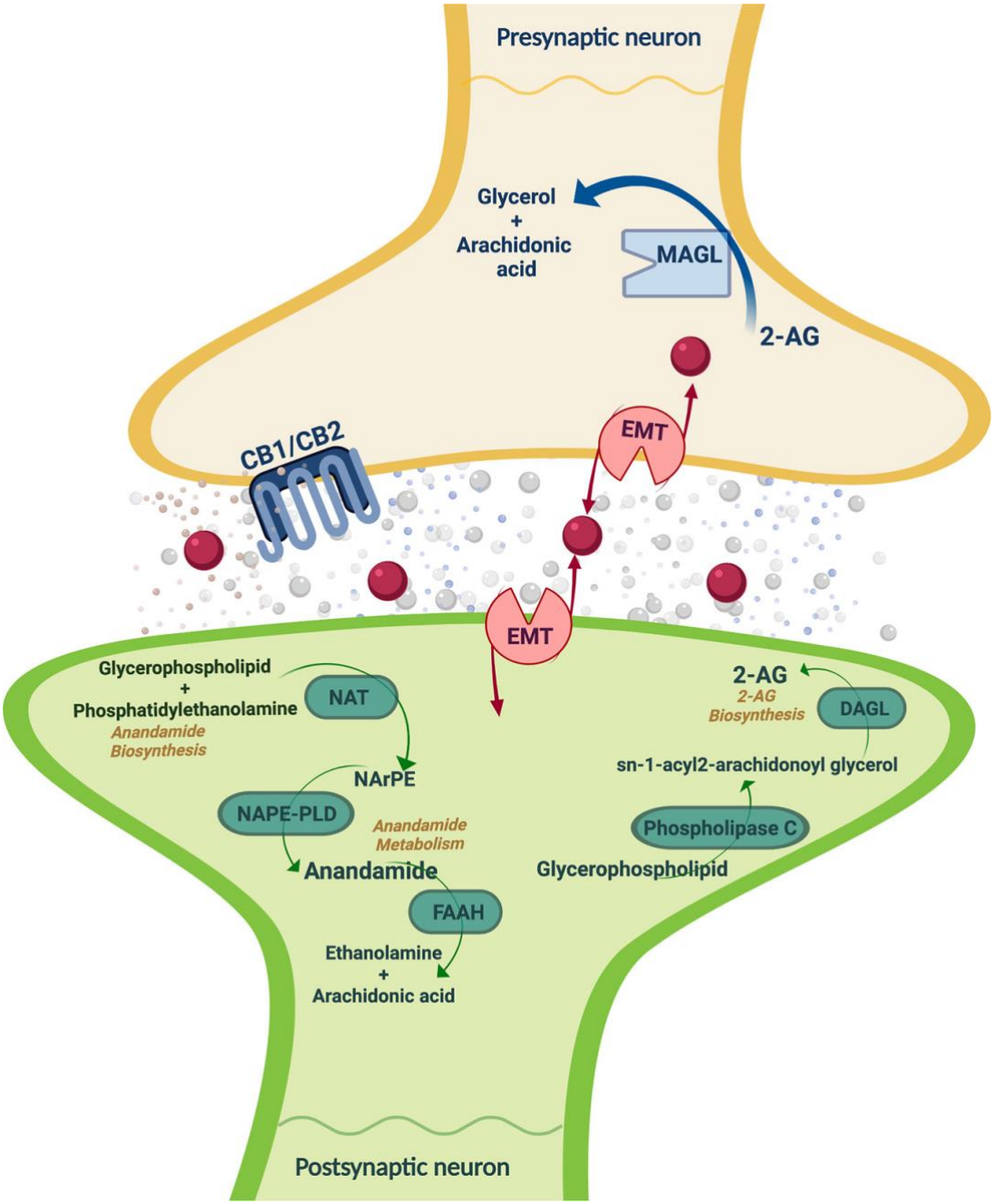

Figure 2.1. Schematic of the endocannabinoid system (ECS) signalling and endocannabinoid (eCB) synthesis and metabolism with the retrograde messengers (e.g., eCBs, phytocannabinoids) represented as red dots. 2-AG = 2-arachidonoylglycerol; CB1/CB2 = cannabinoid ½ receptor; DAGL = diacylglycerol lipase; EMT = endocannabinoid membrane transporter; FAAH = fatty acid amide hydrolase; MAGL = monoacylglycerol lipase; NAPE-PLD = N-acyl-phosphatidylethanolamine specific phospholipase; NarPE = N-arachidonoyl phosphatidylethanolamine; NAT = N-acyl transferase. Front Psychiatry © Navarrete et al. (2020), Creative Commons Attribution 4.0 International License. Image created with BioRender.com.

2.3. Pharmacological Mechanisms of Cannabinoids

Limited pharmacological data is available regarding cannabinoid pharmacokinetics (PK) and pharmacodynamics (PD) to help guide healthcare practitioners, clinicians, and patients (Huestis et al., 2019; Lucas, Galettis, & Schneider, 2018). Due to the multiple types of medicinal and non-medical *Cannabis* products, dosages, and variations of administration routes (ex., inhalation via smoking, inhalation via vapours, intravenous (i.v.) administration, etc.), PK descriptions of cannabinoids can vary greatly in the literature. For example, inhalation studies reported that CBD and THC bioavailability ranges from 10 to 35%, with significant intra- and intersubject variability (Gaston & Friedman, 2017; Lucas et al., 2018). The general consensus is that due to their lipophilic nature, cannabinoids rapidly distribute to highly vascularized organs (e.g., lung), including the brain due to its ability to easily diffuse across the blood-brain barrier (BBB), and accumulates into adipose tissue with subsequent release and redistribution, leading to several weeks of cannabinoid activity within the body (Calapai et al., 2020; Klumpers & Thacker, 2019; Lucas et al., 2018). In terms of PD, THC is a partial agonist of both CB1R and CB2R and the psychoactive effects primarily seen with *Cannabis* is attributed to THC's partial agonist activity at CB1R in humans (Huestis et al., 2001; Klumpers & Thacker, 2019). On the other hand, CBD has very low affinity for CB1R or CB2R yet is able to heighten the pharmacological profile of THC through CB1R as a negative allosteric modulator (Hayakawa et al., 2008; Laprairie, Bagher, Kelly, & Denovan-Wright, 2015). Aside from receptor recognition and activity, the full mechanism of CBD and THC are unknown (Huestis et al., 2019).

2.3.1. Pharmacokinetics

The comparison between CBDV and CBD is often made in terms of PK characteristics. Both cannabinoids are highly lipophilic and have poor oral bioavailability at approximately 6% (Gaston & Friedman, 2017), although the accuracy of the estimate is questionable since it is the result of a study conducted in 1981 that focused more so on THC, CBD, and cannabinol (Agurell et al., 1981). Oral (25 – 800 mg/day) and i.v. bolus (5 mg) dosing of CBDV in human participants is well-tolerated and CBDV rapidly metabolizes in the liver to 7-OH-CBDV and 7-COOH-CBDV (Morano et al., 2020). Whether hepatic metabolism is the primary elimination pathway remains unknown, as does the identity of the major xenobiotic metabolizing enzyme(s) responsible for the production of CBDV metabolites. It has also been reported that CBDV has a large volume of

distribution (V_d) of 32 L/kg and reaches maximum plasma concentrations within 3 h of oral administration (Morano et al., 2020).

Preclinical evaluations using rat and mouse models suggest important species differences in the absorption and disposition of CBDV (Deiana et al., 2012). Following a single intraperitoneal (i.p.) or per os (p.o.) dose of CBDV (60 mg/kg) post-fasting, CBDV was generally rapidly absorbed in rat and mouse, independent of administration route. However, the mouse model resulted in higher CBDV concentrations when administered i.p. as compared to p.o., while the opposite was true in rats that displayed higher concentrations from p.o. dosing. Overall, rats displayed higher brain concentrations, and plasma AUC values are lower than AUC values for the brain regardless of the route of administration. Rats also displayed a large variability in the time to reach maximum plasma and brain concentrations (t_{max}), with times ranging from 0.5—4 h. In mice, the brain concentration (C_{max}) were three-to-five times higher following i.p. (versus p.o.) dosing and nearly eight times higher for the plasma C_{max}, while t_{max} of mice are often seen at 0.5—1 h for both routes of administration.

Curiously, the same article states "no differences occurred in elimination half-lives between tissues" yet it still reports that both brain and plasma elimination half-life ($t_{1/2}$) administered i.p. (232 min and 239 min) were shorter than the half-lives of CBDV administered p.o. (383 min and 399 min) in rats (Deiana et al., 2012). Additionally, in the mouse brain, elimination half-life from i.p. (96 min) was comparatively shorter than brain elimination half-life after oral treatment (204 min). Although the researchers disclose that no i.v. administrations were performed and therefore, only the apparent elimination half-life could be determined, this still should not allow for the differences in elimination half-life unless flip flop kinetics is seen in either route. This would only be true if the absorption rate constant is significantly lower than the elimination rate constant but requires i.v. data for confirmation. Additionally, this means that the absolute exposure could not be determined either without i.v. data.

The species differences in the brain elimination half-life may relate to species differences regarding the BBB. In rats, the greater brain/plasma ratio may be due an ability of the rat BBB to transport CBDV compared to the mouse BBB (Deiana et al., 2012). These factors can have significant impact on the volume of distribution and, therefore, influence elimination half-life. In mice, elimination half-lives are shorter and since it is independent of the route of administration,

this may suggest that in addition to a lower volume of distribution, mice have a higher hepatic xenobiotic metabolism rate compared to rats (Deiana et al., 2012). Since species differences of PK profiles is well known and often poorly extrapolates to humans, evaluations of human PK pose challenges, particularly in the absence of safety information that would allow for human clinical trial investigations. Despite the lack of *in vitro* PK/PD and animal studies, there are case studies and clinical trials for the therapeutic use of CBDV, namely in seizure patients.

2.3.2. Pharmacodynamics

Certain phytocannabinoids, such as THC and CBD, interact with the ECS in a similar manner to the eCBs; however, the binding affinity for the CB receptors for each cannabinoid varies, as well as their effects on the receptor (Klumpers & Thacker, 2019). The scant data regarding the mechanisms of CBDV suggests similarity to CBD, especially regarding the lack of psychoactive effect and its potential therapeutic benefits for seizure patients. Since more is known about CBD's pharmacological properties, it is thought that, because of shared targets, CBDV may also act via the same mechanisms to produce its overall anticonvulsant effect.

Hill et al. (2012) are the first to describe the anticonvulsant properties of CBDV in four different *in vitro* and *in vivo* seizure models: (a) maximal electroshock and (b) audiogenic seizure models in mice and (c) pentylenetetrazole- and (d) pilocarpine-induced seizures in rats. *In vitro* multi-electrode array (MEA) recordings performed on hippocampal slices show a decrease in the amplitude and duration of epileptiform local field potentials (LFPs) after CBDV dosing as well as significantly decreased LPF frequency (Hill et al., 2012). This decreased epileptiform activity characterizes the anticonvulsant profile of CBDV. In the same study, co-administration of i.p. or p.o. dosing of CBDV with antiepileptic drugs (AEDs) valproate, ethosuximide, or phenobarbital showed a decrease in severity and percent of animals that developed tonic-clonic convulsions, and an increase in onset latency from all seizure models except for the pilocarpine-induced seizure in rats. Additionally, the statistical analysis showed that the effects of CBDV were independent of the actions of AEDs (Hill et al., 2012). Because this suggests that since there are no negative drug-drug interactions, CBDV is considered well-tolerated when co-administered with the AEDs employed in the study.

The apparent efficacy of CBDV in mouse seizure models and similarities to CBD has led to CBDV's use in clinical trials and patient-specific cases for seizures. In 2015, a phase II,

randomized, placebo-controlled trial was conducted to assess the PK profile, safety (part A), and effectiveness (part B) of CBDV treatment with AED in epileptic patients (GW Research Ltd., 2015). Patients (age 18—65 years) in the CBDV group were further separated into three groups: patients on inhibitor AED, inducer AED, and AED with no effect on cytochrome P450 (CYP) enzymes. However, the trial failed to meet its primary endpoint of seizure treatment and the results have yet to be published (GW Pharmaceuticals, 2018). In 2016, a case study was released regarding a 19-year-old male patient affected by symptomatic partial seizures who started to self-medicate using oral administration of 300-400 mg *Cannabis* extract, twice daily (Morano et al., 2016). The report includes clinical and video electroencephalogram evaluations and CBDV serum levels, which were periodically measured, and the results suggest that the dramatic clinical improvement may have occurred at high CBDV plasma concentration. However, it should be noted that the *Cannabis* was produced in the patient's household without regulatory oversight, and that the individual also continued their AED while using *Cannabis* (Morano et al., 2016).

The activity of CBDV may be cannabinoid receptor-independent as studies have indicated low binding affinity to the receptors (Gaston & Friedman, 2017). Yet one study demonstrates that the link between CBDV-rich extract and anti-convulsant properties in mice is potentially linked to the agonistic effects of CBDV on CB1R (Hill et al., 2013). Using a displacement binding assay with whole mouse brain and hCB1R-CHO cell membranes, CBDV-rich *Cannabis* extract was able to displace the CB1R radioligand, [^{3}H]CP55940, in both models, although compared to purified CBDV, [^{3}H]CP55940 showed greater affinity for CB1R (Hill et al., 2013). An evaluation of ability of CBDV to exhibit inverse agonism at CB1R in a rat model of nausea indicated that CBDV could suppress lithium chloride-induced gaping, the behaviour of nausea in rats (which are incapable of vomiting) (Hill et al., 2013; Parker & Limebeer, 2006). Therefore, CBDV displays anti-nausea potential, but this is likely not due to CB1R inverse agonism since the profile of activity did not parallel positive controls, e.g. rimonabant and AM251 (Hill et al., 2013).

2.4. Cannabinoids and Inflammation

For the purpose of this thesis, while cannabinoids such as CBD have therapeutic benefits for neurological diseases and non-neurological diseases, such as colitis and arthritis, the anti-inflammatory and pro-inflammatory responses of cannabinoid treatment in only neurological diseases will be discussed. (Nagarkatti, Pandey, Rieder, Hegde, & Nagarkatti, 2009).

Despite only making up 5-15% of the cell population in the brain, microglia are the most significant resident immune cells that are involved in both neuroprotection and neuronal damage (Lu & Mackie, 2016; Thion, Ginhoux, & Garel, 2018). When microglia are activated in response to injury, bacterial viruses, or inflammation, microglia begin to proliferate, migrate, and synthesize and secrete pro-inflammatory cytokines, which include IL-1β, IL-6, tumour necrosis factor-α (TNF-α) (Ohsawa, Imai, Sasaki, & Kohsaka, 2004; Puffenbarger, Boothe, & Cabral, 2000). This also results in the production of nitric oxide (NO) and other reactive oxygen species (ROS), which, at constantly high levels, ultimately contribute to tissue damage (Chen et al., 2018; Puffenbarger et al., 2000; Sonar & Lal, 2019; Thion et al., 2018). Activation of microglia can also be seen via upregulation of markers such as inducible nitric oxide synthase (iNOS), ionized calcium binding adaptor molecule 1 (IBA1), and transmembrane protein 119 (TMEM119) (Ito, Tanaka, Suzuki, Dembo, & Fukuuchi, 2001; Ruan & Elyaman, 2022; Sonar & Lal, 2019). This type of sustained neuroinflammatory response contributes to CNS degeneration and promotes progression of various neurological degenerative disorders such as Alzheimer's disease, Parkinson's disease, and epilepsy (Chen et al., 2018; Minett et al., 2016).

The upregulation of CB2R expression in microglia, as well as vascular elements and neurons during pathological conditions, suggests that many of the anti-inflammatory properties of cannabinoids may occur via the ECS (Lu & Mackie, 2016). However, this does not mean that the inflammatory responses can only be mediated via the two cannabinoid receptors. In one study, cultured neonatal rat cortical microglial cells were treated with cannabinoids and later exposed to bacterial lipopolysaccharide (LPS, 10 ng/mL) to determine any effect(s) on LPS-inducible expression of cytokine mRNAs (Puffenbarger et al., 2000). A substantial decrease in LPS-stimulated mRNA expression of IL-1α, IL-1β, IL-6 and TNF-α was seen in microglia treated with THC (10 μM), resulting in a similar yet greater response than treatment with the eCB, anandamide (AEA). However, this inhibition of cytokine mRNA expression was independent of either CB1R or CB2R as the CB1-selective and CB2-selective antagonists, SR141716A and SR144528, were unable to reverse the inhibition by levonantradol (Puffenbarger et al., 2000). This suggests that the anti-inflammatory effects of cannabinoids in reducing microglial cell activation could also be mediated through a separate pathway from the main cannabinoid receptors of the ECS.

The complete mechanism of action for CBDV, while still unknown, and its anti-epileptic potential are both often attributed to TRP activation, specifically via the vanilloid receptor 1 (TRPV1). TRPV is a nociceptive (sensory), cation ion channel of the group 1 subfamily that was first discovered in *C. elegans* worms and rats during the search for channels activated by capsaicin, an inflammatory vanilloid compound which is known best as the active ingredient in 'hot' peppers (Venkatachalam & Montell, 2007). In 2011, CBDV is shown to activate and desensitize TRPV1 via increased intracellular calcium (Ca^{2+}) in a study that used transfected human recombinant TRPV1 in HEK-293 cells and capsaicin (0.1 μM) to assess the antagonistic/desensitizing behaviour of the phytocannabinoids at TRP receptors (De Petrocellis et al., 2011). Iannotti and colleagues (2014) took this notion a step further due to the previous implications of TRPV1 in the onset and progression of certain epilepsies. It is later confirmed through the use of patch-clamping analysis, that CBDV dose-dependently acts upon TRPV1 and TRPV2, and multi-electrode arrays of rat hippocampal tissue confirmed that CBDV also reduces amplitude of epileptiform bursts (Iannotti et al., 2014). The desensitization of TRPV1 via CBDV also shows other potential therapeutic benefits as excessive Ca^{2+} promotes impairment of the nociceptor function of TRPV1 and is implicated in providing relief to inflammatory pain (Kargbo, 2019).

Though CBDV is considered a partial antagonist and has little affinity for CB1R or CB2R, it can act upon other receptors involved in the ECS and various cell types (Gaston & Friedman, 2017). CBDV is an agonist for TRPV1/2 and TRPA1, an antagonist for TRPM8, and an inhibitor for diacylglycerol lipase-alpha (DGLα), the enzyme responsible for 2-AG synthesis (De Petrocellis et al., 2011; Lu & Mackie, 2016; Morano et al., 2020). Protective effects of CBDV were shown in an ischemic BBB model, consisting of human brain microvascular endothelial cells (BMECs), pericytes, and astrocytes, where CBDV reduced levels of IL-6, lactate dehydrogenase (LDH), and vascular endothelial growth factor (VEGF) secretion in astrocytes (Stone, England, & O'Sullivan, 2021). It also increased levels of DNA damage markers. Antagonists for receptors CB1R, CB2R, PPAR-γ, PPAR-α, 5-HT_{1A}, and TRPV1 had no effect on CBDV-mediated decreases in LDH in astrocytes and G-protein receptors, GPR55 and GPR18, were partially implicated in the effects of CBDV (Stone et al., 2021).

2.5. Model Systems to Evaluate the Pharmacology of Cannabidivarin

Absorption, distribution, metabolism, and elimination (ADME) are crucial PK processes required in the drug discovery process to understand safety and efficacy of compounds. Prior to clinical testing, *in vitro* and *in vivo* animal PK/PD assays are utilized to determine the pharmacological properties of new compounds (Li, 2005). "Gold-standard" models are available to understand PK and PD properties, but researchers have proposed revisions and new methods to allow for more robust translations to the human system (Giuliano, Jairaj, Zafiu, & Laufer, 2005; Hubatsch, Ragnarsson, & Artursson, 2007; Sethi, Muralidhara, Bruckner, & White, 2014). Many *in vitro* models derived from human origin have gained popularity as they allow for better extrapolation to human *in vivo* PK/PD without the need to account for interspecies differences when animal model systems are used. (Pearson, 1986). Despite being physiologically limited, *in vitro* methods are beneficial due to their lower cost, higher throughput, faster results, greater experimental control, and reduced animal usage/less ethical concerns (Tang, 2018).

2.5.1. Models to Demonstrate Pharmacokinetics

A number of in vitro model systems are available to understand the PK properties of compounds. Plasma protein binding (PPB) experiments aid in determining the concentration of free drug concentration available to reach the site of action, also known as the unbound fraction (f_u) (Bowman & Benet, 2018). Plasma contains multiple drug-binding components, including albumin, which is makes up the largest proportion (50%) and has two high-affinity binding sites for acidic drugs, and α-1-acid-glycoprotein (AAG), known for a single high-affinity binding site for basic and neutral drugs. To determine PPB, there are three common techniques: ultrafiltration, ultracentrifugation, and equilibrium dialysis, the last of which is considered the gold-standard of testing in the industry (Bowman & Benet, 2018; Cohen, 2004; Sethi, Muralidhara, Bruckner, & White, 2014). However, loss of analyte due to adherence to glass, plastics, and membrane filters have been reported in multiple studies assessing PPB of lipophilic compounds. The nonspecific binding (NSB), among other difficulties such as automation and higher sample requirements, can lead to difficulties in interpretating the true unbound fraction (Cohen, 2004; Sethi et al., 2014). In attempts to avoid NSB, Sethi and team (2014) proposed a new method suitable for lipophilic compounds using a three-solvent extraction technique of isooctane, acetonitrile, and 2-octanol for the unbound, albumin- and/or or α_1-acid-glycoprotein-bound, and lipoprotein-bound fractions,

respectively (Sethi et al., 2014). Results of three pyrethroids at three different concentrations show relatively high absolute recoveries of all three pyrethroids, ranging from 88.2-95.3% and low relative standard deviation (R.S.D.) in human plasma (≤11.9%), as well as suggesting high reproducibility given the low standard deviation in each fraction. Therefore, this method could be advantageous in determining PPB of cannabinoids.

In terms of elimination, hepatic metabolism is considered the primary pathway due to the presence of metabolizing enzymes such as P450s in the liver that are responsible for the elimination of a large majority of drugs (Coe & Koudriakova, 2014). There are numerous *in vitro* methods using human liver-derived systems to determine the intrinsic clearance (Cl_{int}). One of the most well characterized models in drug metabolism is human liver microsomes (HLMs), subcellular fractions of the endoplasmic reticulum that derive from centrifugation of homogenized liver sections, due to their relatively low cost, minimal storage/handling requirements, and straightforward usage (Asha & Vidyavathi, 2010; Li, 2005). Determination of C_{lint} in HLMs may come from use of the metabolite formation method, which focuses on the rate of metabolite production, or the substrate depletion approach, which allows researchers to focus on the metabolism (i.e., depletion) of a single compound concentration over time and is considered more practical in terms of rapid screening (Houston, Kenworth, & Galetin, 2003; Obach, 1999). Additionally, the three most well-known techniques, ultrafiltration, ultracentrifugation, and equilibrium dialysis, firstly determine the f_u in the microsomal fractions, leading to the determination of the intrinsic clearance (Cl_{int}) of a drug (Asha & Vidyavathi, 2010; Li, 2005). However, each technique does not directly calculate for Cl_{int} and faces the same issue regarding NSB of drug to equipment surfaces which can lead to an underestimate of Cl_{int} and the "true" Cl_{int} in the absence of drug binding to HLMs, denoted as the unbound intrinsic clearance ($Cl_{int,u}$). Giuliano and team developed a method to account for NSB directly by extrapolating for $Cl_{int,u}$ using various HLM concentrations for a single drug concentration without the requirement of determining f_u (Giuliano et al., 2005).

Absorption is another key PK process and involves screening for intestinal permeation, which is an important determinant of bioavailability (Li, 2005). The absorption of orally administered compounds may involve four pathways: transcellular absorption, paracellular absorption, transporter-mediated absorption, and transporter-mediated efflux (Bjarnason, 1994).

While many lipophilic compounds, including cannabinoids, can passively diffuse via a concentration gradient, thus undergoing transcellular absorption, this does not exclude them from transport-mediated efflux which could effectively move the compound back into the lumen of the intestine (Alhamoruni, Lee, Wright, Larvin, & O'Sullivan, 2010; Li, 2005). One of the first *in vitro* systems developed to model intestinal absorption and mimic the small intestine epithelium is the human colorectal adenocarcinoma cell line (Caco-2) (Hidalgo, Raub, & Borchardt, 1989). The Caco-2 cells are cultured for up to 21 days on a porous membrane, undergoing spontaneous differentiation until exhibiting characteristics that mimic the *in vivo* intestinal barrier, such as transepithelial electrical resistance greater than 420 $\Omega \times cm^2$ (Hu, Ling, Lin, & Chen, 2004). Also, due to the porous membrane, an apical and basolateral compartment are produced, allowing for the study of transporter-mediated efflux and/or drug excretion. The Caco-2 method is the most well-known and commonly utilized method in its field, as its advantages and limitations are the most well documented and, therefore, is regarded as the "gold-standard" among many pharmaceutical companies in compound screening (Hu et al., 2004).

2.5.2. Models to Demonstrate Pharmacodynamics

Despite the information from clinical trials and animal studies, *in vitro* modelling may allow for a better understanding of CBDV and its PD. Examples of *in vitro* systems include two-dimensional (2D) monocultures, co-cultures, neural stem cells (NSCs), and aggregates of NSCs (i.e. neurospheres), which are used to study neural differentiation and self-renewing capacities, respectively (Lancaster & Knoblich, 2014b). However, such cell systems lack characteristic apical-basal polarity and do not recapitulate complex lineage of neuronal cells and NSCs *in vivo.* Furthermore, prior to the discovery of induction of pluripotent stem cells (PSCs), procuring NSCs from embryonic tissue was difficult and costly. Neural rosettes, 2D neural tube-like structures isolated from neuroepithelium or directed differentiation of PSCs, recapitulate apical-basal polarity & radial organization, resembling the neural tube during brain development. However, this model also displays limitations to overall organization due to its 2D nature. A new technology which could be paired with stem cells, three-dimensional (3D) cell cultures called brain organoids, overcome such limitations with greater potential to recapitulate brain tissue organization and function, displaying the most promise for *in vitro* PD modelling (Lancaster & Knoblich, 2014b).

2.5.3. Brain Organoid Model

Organoids are a 3D cell culture that can be generated from either embryonic stem cells (ESCs) or induced pluripotent stem cells (iPSCs), which are manipulated into developing multiple cell-specific types that spatially organize and function in a similar manner to the organ of interest (Lancaster et al., 2013). The first human ESCs, which were derived from the inner cell masses of a blastocyst, were harvested in 1998 (Thomson et al., 1998). Despite the potential of ESCs, the prohibitive cost and limited supply, as the source is human embryos which are usually donated and produced by *in vitro* fertilization (IVF), has limited their use in research (Takahashi & Yamanaka, 2006; Thomson et al., 1998). In 2006, Yamanaka and Takahashi successfully induced pluripotency in embryonic and adult fibroblasts of mice through transduction of reprogramming factors octamer-binding transcription factor (Oct3/4), sex-determining region Y (Sox2), Kruppel-like factor 4 (Klf4), and the cMyc genes. While there are multiple methods to induce pluripotency, these four factors are the most commonly used and this led to a new classification of stem cells-iPSCs, undifferentiated cells which could be derived from any somatic cell type (Takahashi & Yamanaka, 2006). In 2013, Lancaster and colleagues released the first paper utilizing ESCs and iPSCs to develop brain organoids (Lancaster et al., 2013). In the following year, an official protocol was released and is now the basis of nearly all modified versions for brain organoid development (Lancaster & Knoblich, 2014a). The results of both papers discuss similarities to the *in vivo* human brain and development, specifically using markers of various cell types which also describe spatial organization of the organoids.

The development of brain organoids can be separated into four stages: embryoid body formation, neural induction, neuroepithelial bud expansion, and maturation (Lancaster et al., 2013) (**Figure 2.2**). In the beginning, stem cells are dissociated into single cells that reaggregate into a rounded germinal layer called embryoid bodies (EBs). While there may be a lack of a primitive node to act as a molecular signaling center, as seen *in vivo*, supplemented factors Rho-associated protein kinase (ROCK) inhibitor and basic fibroblast growth factor (bFGF) are used to form the EBs (Lancaster & Knoblich, 2014a). The EBs are then subjected to neural induction media and form neuroectodermal tissue. These then are transferred to Matrigel®, an extracellular matrix that acts as a radial glial scaffolding for the outgrowth of large buds of neuroepithelium. The expansion of the buds also leads to the production of fluid-filled lumens. Embedding the tissue into Matrigel® leads to further expansion and development of various brain regions, also called the maturation stage (Lancaster et al., 2013).

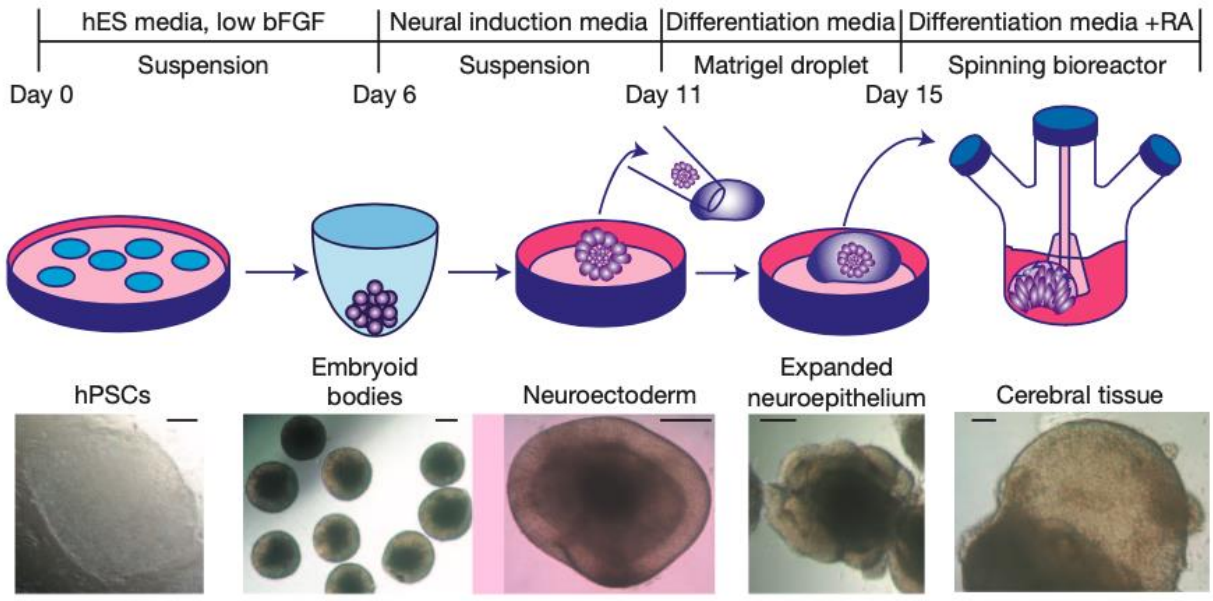

Figure 2.2. The process of brain organoid development in four stages and culture timeline. Once the EB starts to form into neuroectodermal tissue, the organoid must grow within the Matrigel® droplet to allow for buds of neuroepithelium, containing both *neural stem cells (*NPCs*)* and neurons. The use of a spinning bioreactor is used to assist in controlling the development of a necrotic core. bFGF = basic fibroblast growth factor; hES = human embryonic stem cell; hPSCs = human pluripotent stem cells; RA = retinoic acid. Nature © Lancaster et al. (2013). This image has been obtained in accordance with a University of Saskatchewan License agreement.

At the end of day 30, defined brain-like regions are formed (Lancaster & Knoblich, 2014a). Cortical-like regions such as the ventricular zone (PAX6+/SOX2+/Ki-67+), whose markers are indicative of radial glia and NPCs, the intermediate zone (TBR2+), outer subventricular zone (KI-67+/p-Vimentin+), and cortical plate (CTIP2+/MAP2+/TBR1+) are layered in a similar architecture as seen *in vivo* (**Table 2.1**). Specifically, CTIP2 is a marker of deep layer cortical neurons. The layering suggests outward growth of neurons from the centre of the organoid, similar to the production of the six-layered cortex. It is also shown that forebrain and hindbrain identity could be identified in early and 'mature' brain regionalization of the organoid, as well as the midbrain. Additionally, the presence of choroid plexus was determined in 25 of 35 organoids created in the first protocol via immunostaining for transthyretin (TTR), which suggests the potential of CSF production (Lancaster et al., 2013). At this point, expression of synaptic proteins and transporters are present, as well as the presence of networks as seen with spontaneous oscillations.

Table 2.1. A comparison of the expected markers of the brain from the protocol used by STEMCELL Technologies Inc. (STC) which is based on both protocols by Lancaster & Knoblich from 2013 and 2014.

Region	Marker	Lancaster et al., 2013	Lancaster and Knoblich, 2014a	STC Protocol
VZ	PAX6	X (forebrain)	X (radial glia/NPC)	X
	SOX2	X	X (inner radial glia/NPC)	X
OSVZ	Ki-67+			X
	p-Vim		X (mitotic radial glia/NPC)	X
IZ	ASCL1			X
	TBR2		X (intermediate progenitor)	X
CP	TUJ1		X (neuron)	X
	DCX		X (neuron)	X
	MAP2	X (neuron)		X
	TBR1	X (pre-plate)	X (deep layer)	X
	CTIP2	X (early neuron)	X (deep layer)	X
	Reelin (CR cells)	X	X (pre-plate)	
	SATB2		X (surface)	
Choroid plexus	TTR	X	X	

VZ = ventricular zone; OSVZ = outer subventricular zone; IZ = intermediate zone; CP = cortical plate. PAX6 = protein 6; SOX2 = sex determining region Y-box 2; Ki-67+ = marker of proliferation; p-Vim = phospho-vimentin; ASCL1 = achaete-scute homolog 1; TBR2 = T-box brain protein 2; TUJ1 = neuron-specific class III beta-tubulin; DCX = doublecortin; MAP2 = microtubule-associated protein-2; TBR1 = T-box brain protein 1; CTIP2 = B-cell lymphoma/leukemia 11B; SATB2 = special AT-rich sequence-binding protein 2; TTR = transthyretin.

2.5.4. Limitations and Advantages to Brain Organoids

While there are many benefits to using organoids, no single method is absolute nor perfect. Cerebral organoids are useful for modelling early brain development; however, other features of an adult brain fail to form (Lancaster & Knoblich, 2014a). While individual brain regions develop similarly to *in vivo*, 'mature' brain organoids are not reliably organized due to lack of anterior-posterior and dorsal-ventral axes to mimic *in vivo* anatomical orientation. Additionally, the lack of vasculature results in potential nutrient and oxygen deficiency and limits the size of the organoids (Lancaster & Knoblich, 2014b). To address this issue, researchers have employed agitation (i.e., spinning bioreactor) to limit organoid growth or co-cultures with endothelial cells to create vascular-like network (Lancaster & Knoblich, 2014a). Another challenge with organoids is the variability that arises during differentiation and growth, including yield, size, morphology, and cell composition. The differences should consider both intra- and inter-batch variability, as genetic drift can occur over time in the stem cells, and handling techniques (e.g., cryopreservation, thawing, seeding) can result in changes to the differentiation of the stem cells.

Another disadvantage of brain organoids is their inability to mimic all multiple different cell types and function(s) present during and after brain development. While neurons are present, populations of glia cells such as astrocytes, oligodendrocytes, and microglia are not present in the original protocols (Lancaster & Knoblich, 2014a). A surface layer and deep layer of cortical neurons is present in organoids, as suggested by the presence of markers CTIP2 and SATB2; however, organoids will not always display the *in vivo* six-layers structure of the neocortex (Qian et al., 2020). More recently, CB1R was confirmed to be present in brain organoids (Ao et al., 2020; Paraíso-Luna et al., 2020). By exposing developing organoids to THC (1 µM), the authors concluded that the cannabinoid result in downregulation of CB1R, reduce neuronal maturation, and impair neurite outgrowth (Ao et al., 2020). At a higher concentration of THC (2 µM) exposure to the developing brain organoids, CB1R receptor levels remained unchanged, suggesting an absence of receptor desensitization (Paraíso-Luna et al., 2020). However, there is a lack of literature regarding other receptors involved in the ECS which may or may not be present within cerebral organoids.

Nonetheless, the *in vivo*-like characteristics of organoids suggest their potential for many types of investigations including drug assessment, disease modelling, and stem cell therapy (Qian

et al., 2016; S. N. Wang et al., 2020; Yokoi et al., 2021). Organoids can be employed for drug screening without the requirement of whole-organism readouts and can be specified to an individual using patient-specific iPSCs (Artegiani & Clevers, 2018). As mentioned earlier, animal modelling often leads to the challenge of interspecies interpretation for human relevancy since different species have their own unique PK and PD responses. Using human stem cells for organoids, the 3D model contains the human genome and, therefore, allows for a more human-relevant response. Additionally, compared to 2D monocultures and co-cultures, the different cell types in organoids are all derived and differentiated from the same source and are developed not only in the same environment, but also self-organize in a similar manner to *in vivo* tissue. This allows for the study of human organ development without risk to a fetus or mother. Since the development of cerebral organoids mimics the brain during embryogenesis, these can be used to study the effects of xenobiotics on the developing human fetus brain. With the ability of somatic cell reprogramming, patient iPSC-derived organoids can be utilized for disease modelling and drug screening. For example, tumoroids, patient-derived organoids made from tumor biopsy, can be collected and stored for genomic analyses, to perform genotype-phenotype correlation assessments, and drug response screening (Artegiani & Clevers, 2018).

2.5.5. Brain Organoid *Versus* Other Two- and Three-Dimensional Cell Cultures

Relative to 2D cell cultures, brain organoids offer a better model for *in vivo* comparisons as they must have the following characteristics: 1) multiple organ-specific cell types, 2) ability to recapitulate some aspect of organ function, and 3) show spatial restriction and grouping similar to the organ (Lancaster & Knoblich, 2014b). Cells of the brain organoid are in constant contact with the extracellular matrix and other cells due to their 3D nature, mimicking the microenvironment, which allows for greater cell-cell communication and a possible diffusion gradient of nutrients, waste, oxygen, and drug(s) (Białkowska, Komorowski, Bryszewska, & Miłowska, 2020). Consequently, brain organoids offer better *in vitro-in vivo* extrapolation than other 2D cell cultures. Other 3D models are available to researchers and include spheroids, assembloids, and EB-like aggregates that were introduced prior to and after the release of the pivotal Lancaster & Knoblich paper (Andersen et al., 2020; Birey et al., 2017; Lancaster & Knoblich, 2014a; Miura et al., 2020; Ozone et al., 2016).

The original protocol expresses the generation of whole-brain organoids. However, brain organoids can be specified to mimic certain regions of the brain, such as cerebellar, midbrain, forebrain, cortical, and thalamic organoids (Jo et al., 2016; Lancaster & Knoblich, 2014a; Muguruma, Nishiyama, Kawakami, Hashimoto, & Sasai, 2015; Qian et al., 2020; Schukking, Miranda, Trujillo, Negraes, & Muotri, 2018; Trujillo et al., 2019; Xiang et al., 2019). Brain organoids methods have even been developed with potential CSF production capabilities to mimic the *in vivo* barrier (Pellegrini et al., 2020). Due to the lack of certain cell types, brain organoids can also be co-cultured to supplement for neuronal and non-neuronal cell types that do not arise from the self-differentiation process. This includes co-cultures with microglia, BMECs, and tumour cells to better recapitulate the homeostatic brain or brain tumour invasion (Abud et al., 2017; Brownjohn et al., 2018; Krieger et al., 2020; Linkous et al., 2019; Pham et al., 2018; Shi et al., 2020). Researchers have begun to transplant brain organoids into *in vivo* tissue, such as mouse brain, in attempts to vascularize the organoid itself whereby the original microenvironment lacks any circulation (Mansour et al., 2018).

A brain organoid can be characterized as an aggregate formed by a single batch of stem cells that self-differentiate into multiple cell types in a single well, rather than the introduction of other cell types or fusion of the EBs/developing brain organoids/other 3D aggregates which should be clarified as such (Lancaster & Knoblich, 2014a, 2014b). Consequently, assembloids may not be considered brain organoids and should be considered as a fusion of brain organoids/3D aggregates (Andersen et al., 2020; Bagley, Reumann, Bian, Lévi-Strauss, & Knoblich, 2017; Miura et al., 2020; Xiang et al., 2019, 2017). Additionally, when performing literature searches using the term “brain organoids”, search engines often include assembloids and other types of 3D cell cultures, such as serum-free floating culture of embryoid body-like aggregates with quick reaggregation (SFEBq) (Andersen et al., 2020; Ozone et al., 2016). These specifications do not imply that co-cultures, fused organoids, and resembling models should not be utilized but advise the user to be cautious of the differences. **Table 2.2** describes popular journal articles from searches using the term ‘brain organoid’ and can be viewed as a guide for researchers new to the field of brain organoids and/or different types of 3D cell culture modelling.

Table 2.2. Popular journal articles from literature searches using the term "brain organoid".

Reference	Brain organoid	Co-culture	Description
(Lancaster et al., 2013)	Yes	No	First published protocol of (whole-)brain organoid development
(Lancaster & Knoblich, 2014a)	Yes	No	Second published protocol of (whole-)brain organoid; most widely cited
(Muguruma et al., 2015)	Yes	No	Cerebellar organoids
(Ozone et al., 2016)	No	No	Serum-free floating culture of embryoid body-like aggregates with quick reaggregation (SFEBq)
(Qian et al., 2016)	Yes	No	Forebrain, midbrain, and hypothalamic organoids
(Abud et al., 2017)	Yes	Yes	Co-cultured with iPSC-derived microglial-like cells
(Bagley et al., 2017)	No	Yes	Assembloid: fusion of dorsal and ventral-like aggregates
(Birey et al., 2017)	No	No	Spheroid resembling either dorsal or ventral forebrain
(Pham et al., 2018)	Yes	Yes	Day 34 organoids re-embedded into ECM with iPSC-derived endothelial cells
(Schukking et al., 2018)	Yes	No	Cortical organoids
(Xiang et al., 2019)	No	Yes	Assembloid: fusion of thalamic and cortical-like aggregates
(Miura et al., 2020)	No	Yes	Assembloid: fusion of striatal spheroids to cortical-like aggregates

2.6. Rationale

Cannabis treatments have gained tremendous traction in various types of pathologies, with further research on cannabinoids other than THC and CBD. The antiseizure, antiemetic, anti-inflammatory, and analgesic potential of CBDV without any psychoactive component has been demonstrated from *in vitro* and *in vivo* studies, warranting further research regarding its therapeutic potential. In terms of the limited PK data available, CBDV is often comparable to CBD based on their physiochemical properties, suggesting that the two cannabinoids also share similar PK parameter such as absorption, distribution, and metabolic stability. Additionally, due to its lipophilic nature, CBDV can quickly cross the BBB to interact with the ECS and act upon activated microglia, displaying neuroprotective features in response to an inflammatory stimulus. These finding suggests that its anti-inflammatory property may be beneficial to individuals with neurological disorders such as Alzheimer's disease, Parkinson's disease, and epilepsy. To improve our understanding of CBDV pharmacology, organoids can be utilized to investigate the anti-inflammatory properties of CBDV *in vitro* and *in vitro* humanized PK assays can help to understand the plasma protein binding, metabolic stability, and intestinal permeability characteristics of CBDV.

2.7. Hypothesis

In vitro models using human plasma, HLMs, Caco-2 cells, and brain organoid systems can be utilized in determining important PK parameters and PD attributes of CBDV to support the current knowledge gap of cannabinoid pharmacology.

2.8. Objectives

The objectives of this thesis are to:

1. Develop and validate a liquid chromatography-tandem mass spectrometry (LC-MS/MS) method for the quantification of CBDV.
2. Screen CBDV for its PK characteristics in established *in vitro* models of cell permeation, plasma protein binding, and metabolic stability
3. Establish a brain organoid screening system suitable for assessment of the anti-inflammatory effects of CBDV.

3. MATERIALS AND METHODS

3.1. Chemicals

Cerilliant® cannabidivarin (CBDV, #C-140), cannabidiol-D3 (CBD-D3, #C-084), formic acid (#0507), hydrochloric acid (37%, #320331), β-nicotinamide adenine dinucleotide 2'-phosphate (NADPH, #N1630), and lipopolysaccharide (1 mg/mL, #L5418) were acquired through Sigma-Aldrich Canada Ltd (Oakville, ON, CA). Magnesium chloride ($MgCl_2$, #MAG516.500) was obtained from BioShop Canada Inc (Burlington, ON, CA). Potassium phosphate dibasic (HK_2PO_4) powder was purchased from Fisher BioReagent (#BP363-500), owned by ThermoFisher Scientific (Waltham, MA, US). Human liver microsomes (#H0630) were obtained from XenoTech – Sekisui (Lenexa, KS, US). Sucrose (#B10274-34) was purchased from MilliporeSigma (Burlington, MA, US). Human pooled plasma (#HUMANPLK2-0101481) was purchased from BioIVT (Baltimore, MD, US). The reagents LC-MS/MS grade water (#W64), LC-MS/MS grade methanol (MeOH, #A4564), 2-octanol (#O269500), acetonitrile (#A9961), and isopropanol (#A461500), were acquired from Fisher Chemicals, owned by Thermo Fisher Scientific (Waltham, MA, US).

SureOne™ micropipette tips (02-707-408/411/438), disposable glass Pasteur pipettes (#13-678-20A), disposable borosilicate glass tubes, 15 mL/50 mL polypropylene centrifuge tubes (#07-200-886/05-539-13), 2 mL/5 mL/10 mL/25 mL/50 mL polystyrene disposable serological pipets (#13-678-11C/11D/11E/11/11F), 1.5 mL Protein LoBind microcentrifuge tubes (#022431081), 22-gauge 1 inch needles (#14-826B), 1 mL disposable syringes (#14-823-30), 96-well clear flat-bottom plates (#FB012931), and 96-well black/clear bottom plates (#12-566-70) were purchased from Fisher Scientific, owned by Thermo Fisher Scientific (Waltham, MA, US). High-performance liquid chromatography (HPLC) amber vials (Cat#5182-0716), vial caps (#5182-0717), 200 µL glass inserts (#5183-2090), Captiva 96-deep well collection plate (#A69600100), and Captiva EMR-Lipid 96-well plate (#5190-1001) were purchased from Agilent Technologies (Santa Clara, CA, US). CyQUANT™ LDH Cytotoxicity Assay Kit (#C20302) and Invitrogen™ PrestoBlue® Cell Viability Reagent (#A13261) were purchased from Thermo Fisher Scientific to confirm the concentration range of CBDV for each cell line.

Colorectal adenocarcinoma (Caco-2) cells were purchased from the American Type Culture Collection (ATCC, #HTB-37), isolated from colon tissue of a Caucasian male, age 72 at

time of collection (Manassas, VA, US). Dulbecco's modified Eagle medium (DMEM)/high glucose (#D6429) and lucifer yellow CH dipotassium salt (#L0144-25MG) were purchased from Sigma-Aldrich Canada Ltd (Oakville, ON, CA). Fetal bovine serum (FBS, #A3160702), N-2-hydroxyethylpiperazine-N'-2-ethanesulfonic acid (HEPES, 1M, #15630080), minimum essential medium non-essential amino acids (MEM-NEAA, 100X, #11140050), phosphate buffered saline (PBS, #70011044), trypsin (2.5%, #15-090-046), Versene (1X, #15-040-066), and trypan blue solution (0.4%, #15250061) were manufactured by Gibco™ and acquired from Thermo Fisher Scientific (Waltham, MA, US). Fisherbrand™ 24-well tissue culture plates (#FB012929) and T-75 vented flasks (#12-566-440) were also purchased from Thermo Fisher Scientific (Waltham, MA, US). Tissue Culture 24-well Plate Inserts, Polyester (PET) Membrane, pore size 0.4 µm (#76313-906) were obtained from VWR International (Mississauga, ON, CA).

The human iPSC line, UCSD087i-6-4 (#WB63448), was purchased from WiCell® (Madison, WI, US). The iPSCs, also referred to as the 87i cell line, originated from skin fibroblast of a Caucasian female, age 37 at time of collection, provided by the University of California – San Diego. The non-integrating preprogramming method used is the Sendai virus, with the factors Oct4, Klf4, Sox2, and cMyc. ROCK inhibitor (Y-27632, #72302), mTeSR™ Plus (#100-0276), STEMdiff™ Cerebral Organoid Culture Kit (#08570), and STEMdiff™ Cerebral Organoid Maintenance Kit (#08571) were obtained from STEMCELL Technologies (Vancouver, BC, CA). Costar® 6-well/24-well flat-bottom ultra-low attachment plates (#3471/3473), 96-well clear round bottom ultra-low attachment microplate (#7007), and Matrigel® hESC-qualified matrix (#354277) were purchased from Corning Inc (Corning, NY, US). Axygen™ 200 µL wide pore micropipette tips (#14-222-730), cell lifters (#08-100-240), and 25 mL single-well pipet basin (#13-681-508) were obtained from Fisher Scientific, owned by Thermo Fisher Scientific (Waltham, MA, US).

Reagents for western blotting include 30% Acrylamide/bis solution 29:1 (#1610156), tetramethylethylenediamine (TEMED, #1610800), and trisaminomethane (Tris, #1610719) purchased from Bio-Rad (Hercules, CA, US). Bovine serum albumin (BSA, #A2153), ammonium persulfate (APS, #A3678), and Polysorbate (TWEEN®) 20 solution (#P1379) were obtained from Sigma-Aldrich Canada Ltd (Oakville, ON, CA). Pierce™ Modified Lowry Protein Assay Kit (#PI23240), sodium dodecyl sulfate (SDS) micropellets (#BP8200500), and glycine (#BP381-5) were acquired from Fisher Scientific, owned by Thermo Fisher Scientific (Waltham, MA, USA).

RIPA buffer (10X, #9806) was obtained from Cell Signaling Technology (Danvers, MA, US). CB1R (# ab137410, Rabbit, 1:500) and ionized calcium binding adaptor molecule I (IBA1, # ab178846, Rabbit, 1:500) antibodies were purchased from Abcam (Boston, MA, US). Transient receptor potential vanilloid I (TRPV1, #ACC-030, Rabbit, 1:500) antibodies obtained from Alomone Labs (Jerusalem, IS) were generously donated by the Thomas Fisher Lab at the University of Saskatchewan (Saskatoon, SK, CA). Transmembrane protein 119 (TMEM119, #A16075D, Mouse, 1:500) antibodies were purchased from BioLegend (San Diego, CA, US). Inducible nitric oxide synthase (iNOS, #482728, Rabbit, 1:500) antibodies were obtained from Sigma-Aldrich Canada Ltd (Oakville, ON, CA). Secondary antibodies IRDye® 680RD (Goat anti-mouse, IgG, #926-68070, 1:20,000) and IRDye® 800CW (Goat anti-rabbit, IgG, #926-32211, 1:20,000) were acquired from LI-COR® Biosciences (Lincoln, NE, US).

3.2. Liquid Chromatography-Tandem Mass Spectrometry Method

A sensitive, accurate, and precise method was developed and validated using LC-MS/MS for the quantification of CBDV in pooled human plasma. Following this, partial method validation was conducted in the remaining two matrices: HBSS within the Caco-2 matrix and a mixture of heat inactivated pooled HLMs with K_2HPO_4 and $MgCl_2$ for the metabolic stability assay.

3.2.1. Instruments and Conditions

The LC-MS/MS system comprised of the Agilent 1290 Infinity binary pump and autosampler (Agilent Technologies, Santa Clara, CA, US) coupled with AB SCIEX 6500 Qtrap triple quadrupole (SCIEX, Framingham, MA, US) equipped with a turbo ion spray interface set to positive electrospray ionization (ESI+). Analytes were separated using an Agilent Zorbax Eclipse XDB-C18 2.1×75 mm Narrow-Bore RR analytical column and an Agilent Zorbax Eclipse XDB-C18 2.1×12.5 mm Narrow-Bore guard column. Mobile phase A consisted of liquid chromatography-mass spectrometry (LC-MS)-grade water with 0.1 mM formic acid and mobile phase B consisted of LC-MS-grade methanol with 0.1 mM formic acid. A gradient elution was used at a flow rate of 700 µL/min at 27:73 mobile phase A:B for 1.5 min, increasing mobile phase B to 80% for 3.5 min, and returning to 73% after 0.50 min, for a total run time of 6 min. Other MS conditions were: ion spray voltage, 5500 V, ion source temperature, 600°C; curtain gas, 40 psi; nebulizer gas, 70 psi; heater gas, 60 psi; declustering potential, 36 V; entrance potential, 10 V. CBDV was identified at the retention time of 1.0 min, collision energy of 29 V, and multiple

reaction monitoring with transitions of 287.108 *m/z* for the precursor ions at Q1 and 165.100 *m/z* for the product ions at Q3. All relative CBDV concentrations were expressed as peak area ratios of the analyte to internal standard (IS) and chromatographic peak integrations were conducted through Analyst Software (SCIEX, Framingham, MA, US).

3.2.2. Preparation of Working Solutions

Primary stock solutions of CBDV (1 mg/mL) and CBD-D3 (100 µg/mL) were further dissolved in LC-MS-grade methanol to produce the following working standards: lowest limit of quantification (LLOQ), 19.53; low quality control (LOQ), 28; 39.06; 78.13; 156.25; 312.5; 625; medium quality control (MQC), 1012; 1250; high quality control (HQC), 2024; 2500; and 5000 ng/mL. All standards were made to a total of 1 mL except for the 5000 ng/mL working standard, which was made to a total of 4 mL and aliquoted into three separate amber vials.

3.2.3. Preparation of Calibration Standards and Quality Control samples

Calibration standards were prepared by the addition of 10 µL of each working standard to 190 µL of matrices of human pooled plasma in Protein LoBind microcentrifuge tubes. Final concentrations were: 0.98 (LLOQ), 1.4 (LQC),1.97, 3.91, 7.81, 15.6, 31.25, 50.6 (MQC), 62.5, 101.2 (HQC), and 125 ng/mL. Protein precipitation solutions were prepared by the addition of 245.90 µL of IS, CBD-D3 (100 ng/mL), to 14.75 mL of chilled acetonitrile and vortexed for 30 seconds. Each calibration standard was spiked with 610 µL of protein precipitation solution for a final concentration of 10 ng/mL CBD-D3 and vortexed for 30 seconds and centrifuged for 10 670 × *g* for 10 minutes at 4°C (5804 R, Eppendorf, Mississauga, ON, CA). The supernatant was collected for solid phase extraction (SPE) using the Agilent Captiva EMR-Lipid filtration system (Agilent Technologies, Santa Clara, CA, US). 500 µL of each sample was collected into glass borosilicate culture tubes and solvent was evaporated from the extracted supernatant using a Thermolyne 16500 Dri Bath (Marshall Scientific) at 37°C with filtered air. Reconstitution solution was prepared by the addition of 3 mL of mobile phase A to 12 mL of mobile phase B and set aside. Calibration standards were reconstituted with 200 µL of reconstitution solution per sample, vortexed for 30 seconds, and transferred to 200 µL glass flat-bottom inserts within amber HPLC vials.

3.2.4. Cannabidivarin Method Validation

Method validation followed FDA regulations (FDA, 2018). Partial method validation was performed using human liver microsomes with K_2HPO_4 and $MgCl_2$, and HBSS. Sensitivity was established using the lowest concentration in the calibration curve which can be quantified with the most accuracy and precision (LLOQ) and the limit of detection (LOD). Linearity was assessed by a seven-point calibration curve performed over several days with a coefficient of determination (R^2) of 0.98 or greater (Nawaz, 2013). A weighting scheme of $1/y^2$ was applied in a linear least-squares regression analysis to determine slope, intercept, and R^2. Accuracy (acceptable coefficient of variation (CV): ± 20% at LLOQ; ± 15% for all other calibration standards) was calculated as the mean measured concentration of analyte divided by the nominal concentration of analyte multiplied by 100. Precision (CV: ± 20% at LLOQ; ± 15% for all other calibration standards) was calculated as the R.S.D. divided by the mean measured concentration of analyte. Intraday accuracy and precision were determined by same-day replicates of quality controls (LQC, MQC, HQC). Interday accuracy and precision were determined from replicates of each quality control over three different days.

Selectivity (CV: ± 20% at LLOQ) was determined using six replicates of blank matrix standard at the same MRM transitions as CBDV for any interferences at the retention time as the analyte (1.70 min) and IS (3.02 min). Carryover effect (<6% variability) was assessed using several injections of HQC, followed by pure methanol and a single injection of LQC. Dilution integrity (CV: ± 15%) studies were performed to target the upper end of the calibration curve using two concentration, 500 ng/mL and 1000 ng/mL, diluted by a factor of 10 using extracted blank matrix for the final concentration of 50 ng/mL and 100 ng/mL, respectively. Two types of stability (CV: ± 15%) were determined: 3-hour bench-top stability at room temperature (20°C) and 24-hour autosampler stability at 4°C. Matrix effect studies were performed using each quality control in pre-spike (before extraction), post-spike (after extraction), and pure (methanol only) samples. Extraction efficacy was calculated as the average peak area of the pre-spike samples divided by the average peak area of the pure samples multiplied by 100. Extraction recovery was calculated as the average peak area of the pre-spike samples divided by the average peak area of the post-spike samples multiplied by 100. The matrix factor was calculated as the average peak area of the post-spike samples divided by the average peak area of the pure samples.

3.3. Three-Solvent Extraction Plasma Protein Binding Method

To assess the plasma protein binding of CBDV, a previously established three-solvent extraction protocol was employed, consisting of the isooctane, 2-octanol, and acetonitrile ((Sethi et al., 2014)). Six replicates of low, medium, and high concentrations were prepared by the addition of 10 µL of working standards (500, 1000, and 10 000 ng/mL) to 190 µL of blank human pooled plasma for a total volume of 200 µL. Final concentrations were 25 ng/mL, 50 ng/mL, and 500 ng/mL, respectively. Protein LoBind microcentrifuge tubes and low retention pipette tips were utilized to avoid nonspecific binding of CBDV to plasticware. Samples were covered in aluminum foil and incubated on a Symphony™ 5000I/R orbital shaker at 37°C and 185centrifuge rpm for 24 hours (VWR, Mississauga, ON, CA). Extraction solutions were prepared by the addition of 213.2 µL of CBD-D3 (100 ng/mL) to 12.8 mL of each solvent and chilled overnight. Reconstitution solution was prepared by the addition of 3 mL of mobile phase A to 12 mL of mobile phase B (see Section 3.2.3.). Each set of samples was spiked with 610 µL of extraction solution for a final concentration of 10 ng/mL CBD-D3 and vortexed for 30 seconds and centrifuged for 10 670 × g for 10 minutes at 4°C (5804 R, Eppendorf, Mississauga, ON, CA). All samples were transferred to borosilicate glass tubes and dried using the Thermolyne 16500 Dri Bath (Marshall Scientific) at 37°C with filtered air. Due to varied solvent evaporation rates at atmospheric pressure, iso-octane and acetonitrile samples dried within an hour and 2-octanol samples were dried overnight. Dried samples were reconstituted with 200 µL of reconstitution solution per sample, vortexed for 30 seconds, and transferred to 200 µL glass flat-bottom inserts within amber HPLC vials.

3.4. Linear Extrapolation in the Stability Assay Method

Working reagents were prepared the day before each experiment. Sucrose solution (250 mM) was prepared by the addition of 0.34230 g of sucrose to 4 mL of deionized (DI) water. Magnesium chloride ($MgCl_2$) stock solution was diluted by the addition of 40 µL of stock (1 M) to 160 µL of DI water for a final concentration of 200 mM. Potassium phosphate solution (K_2HPO_4, 59 mM) was prepared by the addition of 0.20574 g of potassium phosphate dibasic (HK_2PO_4P) powder to 20 mL of DI water and adjusted with 1 M of hydrochloric acid to pH 7.4. Initiation reagent, 30 mM of β-nicotinamide adenine dinucleotide 2'-phosphate (NADPH), was prepared by weighing 0.02500 g of NADPH powder and adding 1 mL of K_2HPO_4 solution. Stock CBDV (1 mM) was prepared by the addition of 57.28 µL of 1 mg/mL of CBDV to 142.72 µL of

LC-MS-grade methanol. A secondary dilution of 60 µL of 1 mM of CBDV to 540 µL of LC-MS-grade methanol was created for a final drug concentration of 100 µM. On the day of the experiment, HLMs (20 ng/mL) were thawed from -80°C and diluted with 250 mM sucrose for the following concentrations: 1, 2, 2.5, 5, and 10 mg/mL. All reagents were vortexed for 30 seconds after being immediately prepared. All samples were added to Protein LoBind microcentrifuge tubes, referred to as reaction tubes and/or collection tubes.

The incubation mixture contained the following cofactors per reaction tube: 1270 µL of K_2HPO_4 working solution (59 mM, final: 50 mM), 15 µL of $MgCl_2$ working solution (200 mM; final: 2 mM), and 15 µL of HLMs (1, 2, 2.5, 5, or 10 mg/mL; final: 0.1, 0.2, 0.25, 0.5, 1.0 mg/mL). To prepare the collection of each sample, 1 mL of IS, CBD-D3 (100 ng/mL), was added to 60 mL of chilled LC-MS grade acetonitrile (ACN) and 610 µL of the ACN+IS mixture was added to each collection tube kept on ice. Incubation of CBDV occurred at 37°C and 5% CO_2 for 5 minutes with 15 µL of CBDV (100 µM; final: 1 µL) per reaction tube. To initiate the metabolic activity, reaction tubes were transferred to a water bath set to 37°C and 50 µL of NADPH (30 mM; final: 1 mM) was added to each tube. Samples were collected in 50 µL aliquots from each reaction tube at times 0, 2, 4, 6, 8, 10, 15, 30, and 60 minutes and immediately added to the collection tubes containing ACN+IS to stop the metabolic reaction. Collection tubes were vortexed for 30 seconds, centrifuged for 10 670 × *g* for 10 minutes at 4°C (5804 R, Eppendorf, Mississauga, ON, CA), and 200 µL of sample per tube was collected into 200 µL glass flat-bottom inserts within amber HPLC vials.

3.5. Caco-2 Cell Cytotoxicity Assay

To ensure minimal effect of CBDV on cell viability, the CyQUANT™ LDH Cytotoxicity Assay Kit (ThermoFisher, #C20302) was utilized to determine the highest allowable concentration of CBDV. Caco-2 cells were seeded at a density of 1×10^5 cells/ml per well on 24-well TC plates in 10% FBS and 1% MEM-NEAA in DMEM. The plates were be incubated at 37°C and 5% CO_2 overnight. The growth media was diluted five times, resulting in 2% FBS, and used to refresh each well after a 24-hour incubation period prior to treatment. Working concentrations of CBDV (100, 300, 500, and 1000 µM) were added as 5 µL aliquots (final: 1, 3, 5, 10 µM). Other treatments included 5 µL of methanol (1%), 55 µL of lysis buffer (10X) as a positive control for cell death, and untreated wells to represent cell viability at 0 µM of CBDV. Wells were left untouched after treatment for 24 hours at 37°C and 5% CO_2. To assess LDH activity, 50 µL of culture medium

from each well of the 24-well plate was added to an individual well of a non-sterile 96-well clear plate with pre-aliquoted wells of 50 µL substrate mix and incubated for 20 minutes at room temperature. At the end of the incubation period, 50 µL of stop solution was added to each well using a multichannel pipettor. The plate was scanned using the BioTek Synergy HTX Multi-Mode Reader at absorbance wavelengths of 490 nm and 690 nm (Agilent Technologies, Santa Clara, CA, US). Cell viability was recorded in percentage for each well.

3.6. Caco-2 Permeation Assay

Caco-2 cells were cultured in DMEM containing 10% FBS and 1% MEM-NEAA and sub-cultured using 5 mL of PBS and 3 mL of 0.25% Trypsin/EDTA. Once cells reached 70-90% confluency, a single-cell suspension was collected and counted using trypan blue solution, 0.4% and a TC20™ Automated Cell Counter (BioRad, Hercules, CA, US). Cells were diluted with the appropriate culture medium and seeded at a density of 1×10^5 cells per well on 24 Transwell® insert plates. The plates were incubated at 37°C and 5% CO_2 for 21-days with media changes the day after seeding and every second day prior to drug exposure. Solution for the transport study consisted of 10.2 mL of HEPES (1 M) to 489.8 mL of HBSS and inverted several times to mix. A mixture of 245.90 µL of IS, CBD-D3 (100 ng/mL), and 14.75 mL of chilled acetonitrile (ACN) was prepared and set aside at 4°C (see Section 3.2.3.). Additional 1 mL of ACN was set aside and added to 9 mL of LC-MS-grade water to create a lysis solution. Lucifer yellow (LY) was prepared by the addition of 1 mg lucifer yellow salt to 10 mL of HBSS+HEPES solution. Transepithelial electrical resistance (TEER) was measured using a MilliCell® ERS-2 Volt-Ohm meter (MilliporeSigma) to assess the integrity of the cell monolayer.

After 21 days, plates were refreshed with 200 µL and 600 µL of HBSS+HEPES solution in the apical (A) and basal (B) compartment of each well, respectively, and returned to the incubators for 10 minutes. After the incubation period, TEER values were recorded, and the wells were refreshed a second time with HBSS+HEPES. To determine drug transport from the apical compartment to the basal compartment (A→B), 2 µL of CBDV (100 µM) was added to each apical compartment. To determine drug transport from the basal compartment to the apical compartment (B→A), 6 µL of CBDV (100 µM) was added to each basal compartment. For sample collection at 0 minutes, media was collected from each compartment immediately after the addition of CBDV into Protein LoBind microcentrifuge tubes and wells were replaced with fresh HBSS+HEPES.

Samples at times 15, 30, 45, and 60 minutes were collected in a similar manner and stored at 4°C until the completion of LY assessment and cell lysis. After CBDV treatment, TEER values were recorded again and 200 µL of HBSS+HEPES from each apical compartments were replaced with 200 µL of LY solution. Six blank wells containing 600 µL of HBSS+HEPES were refreshed with 200 µL of LY and 400 µL of HBSS to represent complete LY transport into the basolateral side. Plates were incubated at 37°C and 5% CO_2 for one hour and each Transwell® basket was transferred to a regular 24-well plate containing 600 µL of HBSS+HEPES. LY rejection rates were determined by scanning the original Transwell® plates at excitation wavelength of 485 nm and emission wavelength of 535 nm using the BioTek Synergy HTX Multi-Mode Reader (Agilent Technologies, Santa Clara, CA, US). After the addition of LY, cell lysis was performed by the addition of 400 µL of 10% ACN per well and plates were incubated for one hour at room temperature (20°C). Lysates were collected into Protein LoBind microcentrifuge tubes.

To assess non-specific binding of CBDV to cell culture plates, Caco-2 cells were seeded at a density of 1×10^5 cells/mL per well in the appropriate culture media on 24-well TC plates and incubated at 37°C and 5% CO_2 overnight. Media was removed from each well and replaced with 600 µL of HBSS+HEPES. To mimic the permeation study, 6 µL of CBDV (100 µM) was added to each well and samples were collected at 0, 15, 30, 45, and 60 minutes into Protein LoBind microcentrifuge tubes. Wells were refreshed with 600 µL of fresh HBSS+HEPES immediately after collection and replaced with 10% ACN for one hour at room temperature to perform cell lysis. Lysates were collected into Protein LoBind microcentrifuge tubes. The assay was repeated with the same conditions in the absence of cells.

Preparation of all samples (permeation and lysate) for LC-MS/MS analysis involved aliquoting 95 µL of each sample into new Protein LoBind microcentrifuge tubes containing 305 µL of ACN+IS per tube. Tubes were vortexed for 30 seconds, centrifuged for 10 670 × *g* for 10 minutes at 4°C (5804 R, Eppendorf, Mississauga, ON, CA), 200 µL of sample per tube was collected into glass flat-bottom inserts within amber HPLC vials.

3.7. Preliminary Inflammatory Stimulus Treatment in Brain Organoids

A brain organoid system was established using a kit developed by STEMCELL™ Technologies (Vancouver, BC, CA). The STEMdiff™ Cerebral Organoid Culture Kit was adjusted with minor modifications from a previously published protocol by Lancaster et al., 2013,

such as adjusting media changes during the maturation stage. Induced pluripotent stem cell (iPSC) cultures were cultured in feeder-free conditions on six-well tissue culture plates coated with Matrigel® hESC-qualified matrix and maintained in mTeSR™ Plus medium at 37 °C in humidified 5% CO_2 and 95% air atmosphere following manufacturer's (STEMCELL Technologies) instructions. A single cell suspension from the iPSCs were seeded onto 96-well rounded-bottom ultra-low attachment microplates and underwent EB formation until Day 5. To induce neuroepithelial tissue formation, EBs were transferred to a 24-well flat-bottom ultra-low attachment plate with induction media from the kit. Each EB was transferred again to a separate well of a another 24-well flat-bottom ultra-low attachment plate with expansion media, 2% dissolved Matrigel®, for neuronal differentiation. Media conditions were switched after 48 hours to ensure maturation of EBs into brain organoids and plates were refreshed weekly, up to 90 days.

Prior to treatment, brain organoids were measured in diameter to standardize based on tissue size. CBDV and CBD treatments of 25 µM, 250 µM, and 2.5 mM were prepared in HPLC amber vials from 1 mg/mL of original stock by dilution using LC-MS-grade methanol. LPS treatment (25.5 µg/mL) was prepared by the addition of 12.5 µL of 1 mg/mL LPS to 487.5 µL of sterile DI water. Other controls included methanol as vehicle, water, lysis buffer (10X) to represent cell death, and untreated wells to represent baseline brain organoid activity. After 90 days in culture, brain organoids were treated using the following: 0.1 µM, 1 µM, and 10 µM of CBD/CBDV; 500 ng/mL of LPS (500 ng/mL); 0.1 µM, 1 µM, and 10 µM of CBD/CBDV with 500 ng/mL of LPS (500 ng/mL); sterile DI water (0.4%); LC-MS-grade methanol (0.1%); sterile DI water (0.4%) with LC-MS-grade methanol (0.1%); and lysis solution (1X). Plates were treated for 24 hours at 37°C in 5% CO_2 and due to the difficulties in organoid culturing and yield, cytotoxicity was performed after cannabinoid and LPS treatment (see Section 3.5). Organoids were collected into LoBind microcentrifuge tubes and kept at -20°C for western blotting.

The iPSC-derived brain organoids were collected and homogenized in RIPA buffer containing a protease inhibitor cocktail using 22-gauge needles and 1 mL syringe before being sonicated. Protein concentrations were quantified using the Lowry (Folin-Ciocalteu phenol reagent) assay, equalized to 250 ng/µL in 1% loading buffer (0.2 M Tris pH 6.8, 40% glycerol, 8% sodium dodecyl sulfate, 20% β-mercaptoethanol, 0.4% bromophenol blue), and heated at 100°C for 10 min. Protein (10 µg per lane) was loaded on 10% and 12% polyacrylamide gels and resolved

proteins were electroblotted onto a nitrocellulose membrane. After blocking in 5% w/v skim milk powder in TRIS-buffered saline (TBS: 250 mM Tris pH 7.4, 1.37 M NaCl) for one hour, membranes were incubated with primary antibodies diluted in 5% w/v skim milk powder in TBS-T (TBS with 0.1% Tween®20) at 4°C overnight. Membranes were washed three times in 30-minute periods with TBS-T and secondary fluorescently labelled antibodies were added for one h, followed by three washes of the same time increment and TBS-T solution (see **Table 3.1** for the list of primary antibodies and the respective secondary antibodies). Proteins were visualized with a LI-COR Odyssey® Imager and manufacturer's software (Image Studio 5.3.5, LI-COR Biosciences, Lincoln, NE, USA).

Table 3.1. Antibodies used for immunostaining of primary murine astrocytes and human iPSC-derived cells and brain organoids.

Primary Antibodies			**Secondary Antibodies**		
Target	Catalogue number	Immunoblotting	Target	Catalogue number	Immunoblotting
Mouse anti-TMEM119	BioLegend (Cat#A16075D)	1:500	IRDye® 680RD Goat anti-mouse IgG	LI-COR® Biosciences (Cat#926-68070)	1:20,000
Rabbit anti-CB1R	Abcam (Cat#ab137410)	1:500	IRDye® 800CW Goat anti-rabbit IgG	LI-COR® Biosciences (Cat#926-32211)	1:20,000
Rabbit anti-IBA1	Abcam (Cat#ab178846)	1:500	IRDye® 800CW Goat anti-rabbit IgG	LI-COR® Biosciences (Cat#926-32211)	1:20,000
Rabbit anti-iNOS	Abcam (Cat#ab178945)	1:500	IRDye® 800CW Goat anti-rabbit IgG	LI-COR® Biosciences (Cat#926-32211)	1:20,000
Rabbit anti-TRPV1	Alomone labs (Cat#ACC-030)	1:500	IRDye® 800CW Goat anti-rabbit IgG	LI-COR® Biosciences (Cat#926-32211)	1:20,000

3.8. Data Analysis and Statistics

Accuracy and precision of quality control (QC) standards during LC-MS/MS method validation were calculated using the following equations (eq):

$$\text{Accuracy} = \frac{100 \times [\text{Analyte}]_{\text{measured}}}{[\text{Analyte}]_{\text{nominal}}} \quad \text{(Eq 3.1)}$$

$$\text{Precision} = \frac{100 \times \text{S.D.}}{[\text{Analyte}]_{\text{measured,average}}} \quad \text{(Eq 3.2)}$$

where $[\text{Analyte}]_{\text{nominal}}$ is the theoretical concentration, $[\text{Analyte}]_{\text{measured}}$ is the actual concentration, $[\text{Analyte}]_{\text{measured,average}}$ is the average of actual concentrations, and S.D. is the standard deviation of the average of actual concentrations.

Additional parameters such as extraction efficacy, recovery, and matrix effect were also assessed in method validation using the total peak area of samples spiked with CBDV prior to methanol extraction ($\text{Area}_{\text{pre-spike}}$), samples spiked with CBDV after methanol extraction ($\text{Area}_{\text{post-spike}}$), and samples created in the absence of matrix ($\text{Area}_{\text{pure}}$):

$$\text{Extraction efficacy} = \frac{Area_{\text{pre-spike}}}{Area_{\text{pure}}} \times 100 \quad \text{(Eq 3.3)}$$

$$\text{Extraction recovery} = \frac{Area_{\text{pre-spike}}}{Area_{\text{post-spike}}} \times 100 \quad \text{(Eq 3.4)}$$

$$\text{Matrix effect} = \frac{Area_{\text{post-spike}}}{Area_{\text{pure}}} \quad \text{(Eq 3.5)}$$

The plasma protein binding assay estimated the albumin-bound, lipoprotein-bound, and unbound (f_u) fractions of CBDV concentrations varying from low, medium, and high. Percentages were determined by dividing the concentration of the fraction of interest divided by the sum of the

concentrations for all fractions. Multiple comparison between each concentration of CBDV were performed on Prism 9.1.1. (GraphPad Prism, San Diego, CA, US) using One-way ANOVA.

Metabolic stability assays using HLMs estimated the substrate depletion rate constant (k_{dep}) and the intrinsic clearance (Cl_{int}) of CBDV (Obach and Reed-Hangen), while the linear extraction in the stability assay (LESA) was performed to allow for direct calculation of the unbound intrinsic clearance ($Cl_{int,u}$), as proposed by Giuliano et al., 2005. The methodology was first adopted by a previous lab member, Chaojie Lin, and was later revised by another lab member, Jim He, who incorporated specificity towards cannabinoids. The peak area of CBDV/IS (CBD-D3) was standardized to time, t=0, to represent total CBDV present at the beginning of the experiment (100%) and subsequent depletion of drug over time. A graph of natural log percent of remaining CBDV (1 µM) was plotted against time to estimate the depletion rate constant (k_{dep}), following first-order kinetics, which is determined as the slope of linear regression at each CBDV concentration. The Michaelis-Menten constant, K_m, and theoretical maximum depletion rate constant at indiscernibly low substrate concentrations, $k_{dep([S]\rightarrow 0)}$, were calculated by plotting k_{dep} against initial CBDV concentrations through nonlinear least squares regression using Prism 9.1.1. (GraphPad Prism, San Diego, CA, US) with Eq 3.6:

$$k_{dep} = k_{dep([S]\rightarrow 0)} \times \left(1 - \frac{[S]}{[S] + K_m}\right)$$

(Eq 3.6)

The value of Cl_{int}, measured as µL/min/mg microsomal protein, was calculated using the following equation:

$$Cl_{int} = \frac{Dose}{AUC_{\infty}}$$

(Eq 3.7)

where ‘Dose’ is the initial amount of CBDV in the microsomal mixture (mol/mg microsomal protein) and ‘AUC’ is the area under the curve in the concentration versus time profile(s), extrapolated to infinity ((mol/L)·h). Due to the correlation between the inverse of the intrinsic clearances (min·mg microsomal protein/µL) and the respective HLM concentrations, the y-axis

intercept of the linear regression corresponds to the inverse of the intrinsic clearance of CBDV in the absence of microsomal protein ($1/Cl_{int,u}$).

For the Caco-2 permeability assays, the apparent permeability coefficient (P_{app}) and efflux ratio (ER) were calculated using the following equations:

$$P_{app}(cm/sec) = \frac{dQ}{dt} \times \frac{1}{C_{initial\ donor} \times A}$$

(Eq 3.8)

$$ER = \frac{P_{app(B \rightarrow A)}}{P_{app(A \rightarrow B)}}$$

(Eq 3.9)

where 'dQ/dt' is the apparent steady-state permeation rate (μM/sec) in the basal chamber as determined in the drug permeation versus time profile, 'A' is the surface area of the Transwell® inserts (cm^2), and '$C_{initial\ donor}$' is the initial concentration (μM) of drug in the donor chamber. To determine ER, P_{app} coefficients in both directions are required where 'B→A' is the basolateral to apical transport of drug and 'A→B' is the apical to basolateral transport of drug.

The lucifer yellow (LY) rejection percentages were calculated using the following equation:

$$LY\ rejection\ (\%) = \left(1 - \frac{x - Mean_{blank}}{Mean_{LY} - Mean_{blank}}\right) \times 100$$

(Eq 3.10)

where 'x' is the individual sample, '$mean_{blank}$' is the mean of samples containing HBSS+HEPES only, and '$mean_{LY}$' is the mean of all sample containing 200 μL of LY and 400 μL of HBSS+HEPES to represent complete LY transport from apical to basolateral. To calculate for the remaining CBDV in Caco-2 cells during the nonspecific binding to plasticware assay, the peak areas of CBDV/IS (CBD-D3) was normalized to the amount of CBDV (3 μM) present in lysates at time, t = 0, and each concentration was subtracted by the concentration at its previous time point. Mass balance data are expressed as percentage of total mass quantified in cell media and lysate

4. RESULTS

4.1. Liquid Chromatography Tandem Mass Spectrometry Method Validation for Cannabidivarin

A LC-MS/MS method was developed and validated for the quantification of CBDV in human pooled plasma for specific, accurate, and precise determination and detection. **Figure 4.1.** represents the LC-MS/MS chromatogram of CBDV incubated in plasma at 37°C for 24 hours and shows that retention time of CBDV and CBD-D3 were 1.70 min and 3.02 min, respectively. **Table 4.1** summarizes the matrix effect, as well as the extraction efficacy and recovery, of three quality control (QC) levels of CBDV incubated in plasma, human liver microsomes (HLMs) mixed with $MgCl_2$ and K_2HPO_4, and Hank's balanced salt solution (HBSS). In plasma, the matrix effect ranged from 1.3 to 1.5, extraction efficacy ranged from 110.9% to 113.0%, and extraction recovery ranged from 74.1% to 84.0%. In the HLM mixture, the matrix effect ranged from 3.1 to 3.5, extraction efficacy ranged from 80.3% to 87.7%, and extraction recovery ranged from 24.4% to 26.8%. In HBSS, the matrix effect ranged from 3.6 to 3.9, extraction efficacy ranged from 88.9% to 94.5%, and extraction recovery ranged from 24.2% to 26.2%.

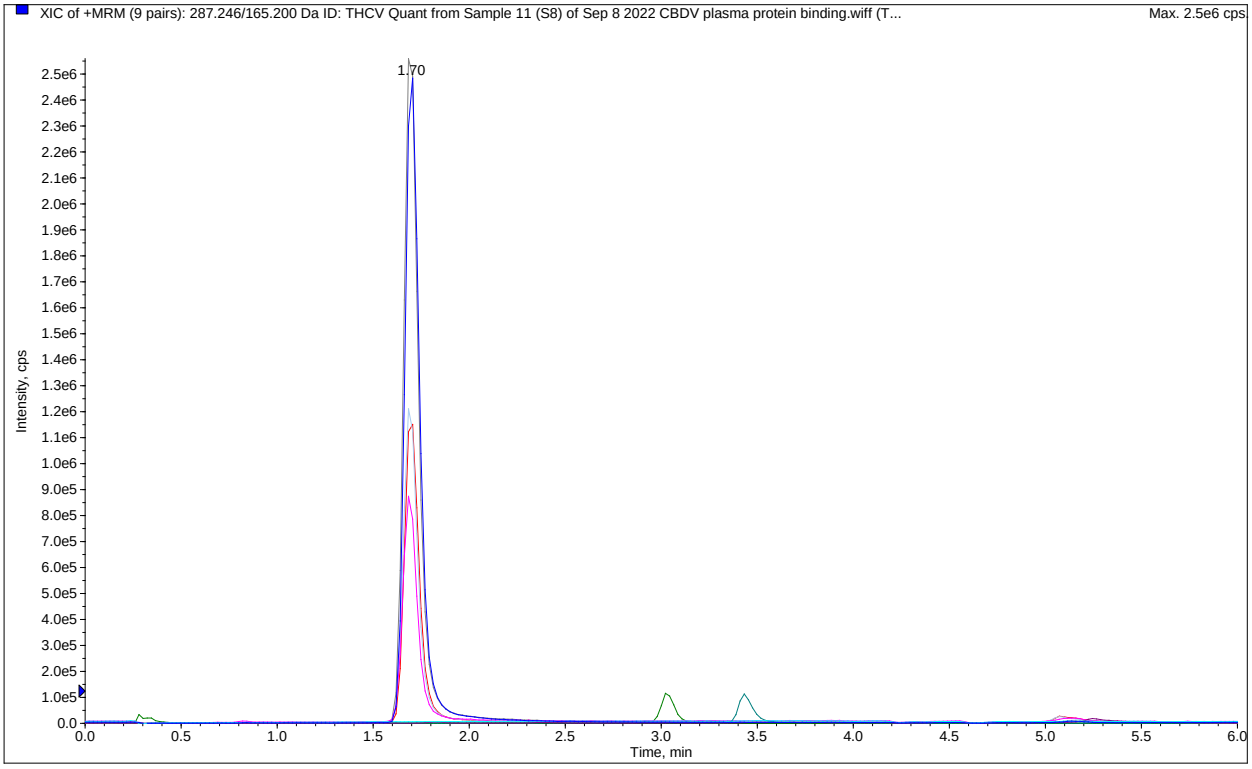

Figure 4.1. Representative LC-MS/MS chromatogram of plasma spiked with internal standard, IS (CBD-D3, 100 ng/mL, 3.02 min) and CBDV (125 ng/mL, 1.70 min). Conditions: Agilent 1290 Infinity binary pump coupled with AB Sciex 6500 Qtrap triple quadrupole; Agilent Zorbax Eclipse XDB-C18 analytical column (4.6×150 mm, 5 µm); mobile phase A: LC-MS-grade water with 0.1% formic acid, mobile phase B: LC-MS-grade water with 0.1% formic acid.

Table 4.1. Matrix effect of CBDV in pooled human plasma (n=6), human liver microsome (n=3), and Hank's balanced salt solution (HBSS) (n=3).

QC levels*	Extraction efficacy (%)	Extraction recovery (%)	Matrix factor
LQC			
Plasma	113.0	84.0	1.3
Liver microsome	83.4	26.8	3.1
HBSS	94.5	26.2	3.6
MQC			
Plasma	111.3	77.8	1.4
Liver microsome	80.3	24.4	3.3
HBSS	88.9	24.8	3.6
HQC			
Plasma	110.9	74.1	1.5
Liver microsome	87.7	24.8	3.5
HBSS	94.0	24.2	3.9

* LQC for CBDV is 1.4 ng/mL; MQC is 50.6 ng/mL; and HQC is 101.2 ng/mL.

4.1.1. Linearity of Calibration Curve and Accuracy and Precision of Quality Control Standards in Pooled Human Plasma

The LC-MS/MS method validation included intraday and interday accuracy and precision for QC levels and lowest limit of quantification (LLOQ) of CBDV in human pooled plasma, as summarized in **Table 4.2** and **Table 4.3**, respectively. The intraday accuracy for all QC levels (LLOQ, LQC, MQC, and HQC) was < 10%, ranging from 91.7% to 105.4%. The intraday precision for all QC levels was < 10%, ranging from 1.4% to 6.9%. The interday accuracy for all QC levels was < 10%, ranging from 94.5% to 104.6%. The interday precision for all QC levels was < 10%, ranging from 2.7% to 5.1%. **Figure 4.2** shows the standard curves of CBDV ranging from 0.98 ng/mL to 125 ng/mL, weighted $1/y^2$ with an average coefficient of determination (R^2) of 0.9962, during three days of plasma protein binding experiments.

Table 4.2. Intraday accuracy and precision for CBDV determination by LC-MS/MS detection in human plasma (n = 6).

QC levels*	Accuracy (%)	Precision (%)
LLOQ		
Day 1	91.7	2.9
Day 2	93.3	5.1
Day 3	98.2	4.5
LQC		
Day 1	101.1	1.4
Day 2	96.0	6.9
Day 3	101.2	4.7
MQC		
Day 1	104.1	3.6
Day 2	105.4	2.6
Day 3	104.2	1.7
HQC		
Day 1	98.6	4.2
Day 2	97.9	3.2
Day 3	96.0	1.8

Table 4.3. Interday accuracy and precision for CBDV determination by LC-MS/MS detection in human plasma (n = 18).

QC levels*	Accuracy (%)	Precision (%)
LLOQ	94.5	5.0
LQC	99.5	5.1
MQC	104.6	2.7
HQC	97.5	3.3

* LLOQ for CBDV is 0.98 ng/mL; LQC for CBDV is 1.4 ng/mL; MQC is 50.6 ng/mL; and HQC is 101.2 ng/mL.

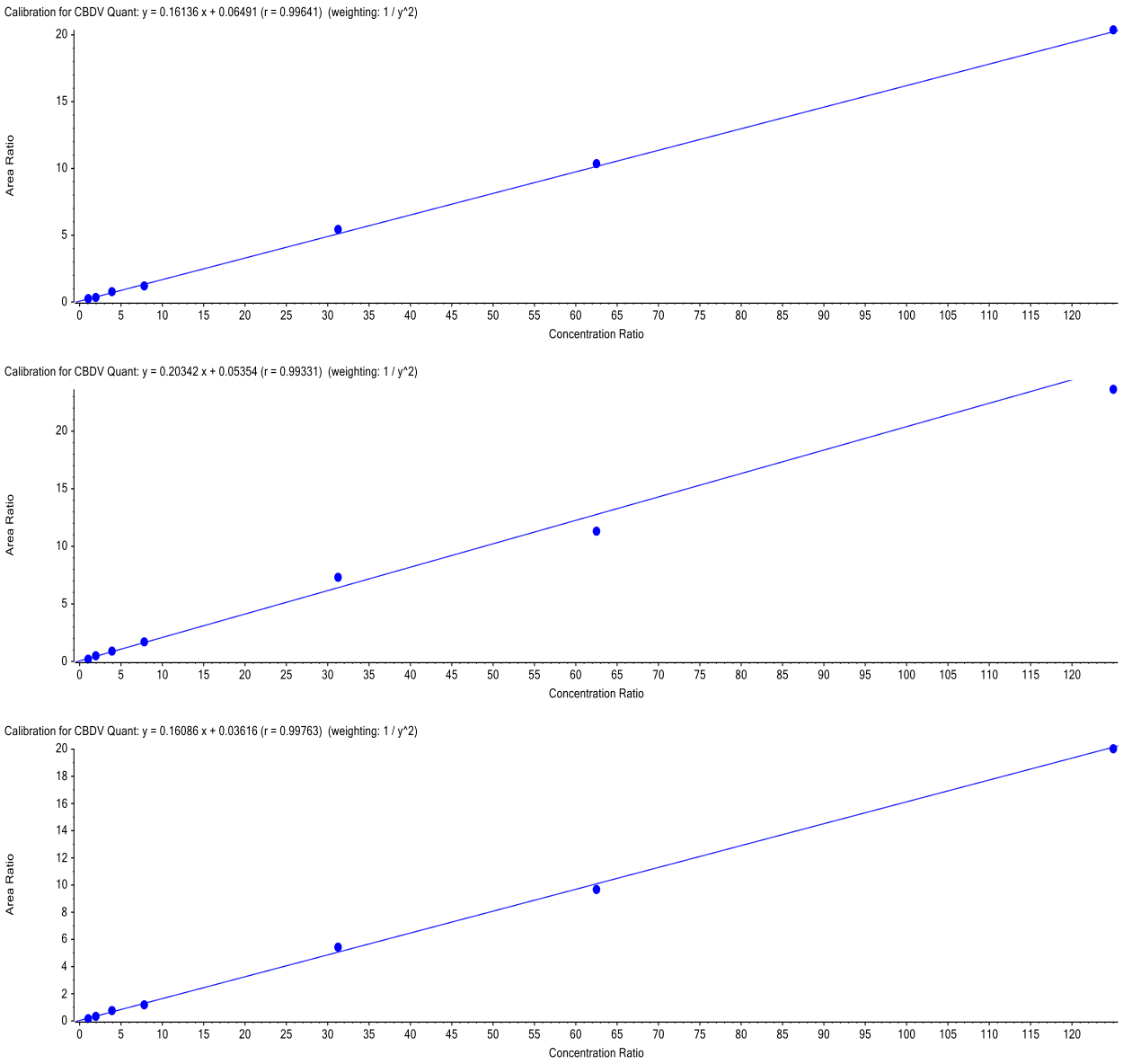

Figure 4.2. Standard curves of CBDV during three days of plasma protein binding experiments involving the three-solvent extraction method in pooled human plasma, showing linearity with R^2 values > 0.99. The standard curve for CBDV has seven concentrations, ranging from 0.98-125 ng/mL. Standard curves were weighted $1/y^2$ to improve the regression fit for low standard concentrations. * Plots were generated and modified in MultiQuant™ software.

4.1.2. Linearity of Calibration Curve and Accuracy and Precision of Quality Control Standards in Human Liver Microsomes

The LC-MS/MS method validation included intraday and interday accuracy and precision for QC levels and LLOQ of CBDV in human liver microsome (HLM) mixed with $MgCl_2$ and K_2HPO_4, as summarized in **Table 4.4** and **Table 4.5**, respectively. The intraday accuracy for all QC levels (LLOQ, LQC, MQC, and HQC) was < 10%, ranging from 94.2% to 108.4%. The intraday precision for all QC levels was < 10%, ranging from 0.6% to 7.7%. The interday accuracy for all QC levels was < 10%, ranging from 95.8% to 106.5%. The interday precision for all QC levels was < 10%, ranging from 3.9% to 5.6%. **Figure 4.3** shows the standard curves of CBDV ranging from 0.98 ng/mL to 125 ng/mL, weighted $1/y^2$ with an average coefficient of determination (R^2) of 0.9949, during three days of metabolic stability assays using HLMs.

Table 4.4. Intraday accuracy and precision for CBDV determination by LC-MS/MS detection in human liver microsome (n = 3).

QC levels*	Accuracy (%)	Precision (%)
LLOQ		
Day 1	107.2	5.3
Day 2	108.4	5.0
Day 3	103.8	7.7
LQC		
Day 1	95.6	3.5
Day 2	100.5	7.0
Day 3	94.2	2.7
MQC		
Day 1	94.6	2.3
Day 2	103.5	2.1
Day 3	92.3	1.3
HQC		
Day 1	99.9	1.1
Day 2	105.4	2.6
Day 3	97.1	0.6

Table 4.5. Interday accuracy and precision for CBDV determination by LC-MS/MS detection in human liver microsome (n = 9).

QC levels*	Accuracy (%)	Precision (%)
LLOQ	106.5	5.6
LQC	97.1	5.3
MQC	95.8	5.6
HQC	100.8	3.9

* LLOQ for CBDV is 0.98 ng/mL; LQC for CBDV is 1.4 ng/mL; MQC is 50.6 ng/mL; and HQC is 101.2 ng/mL.

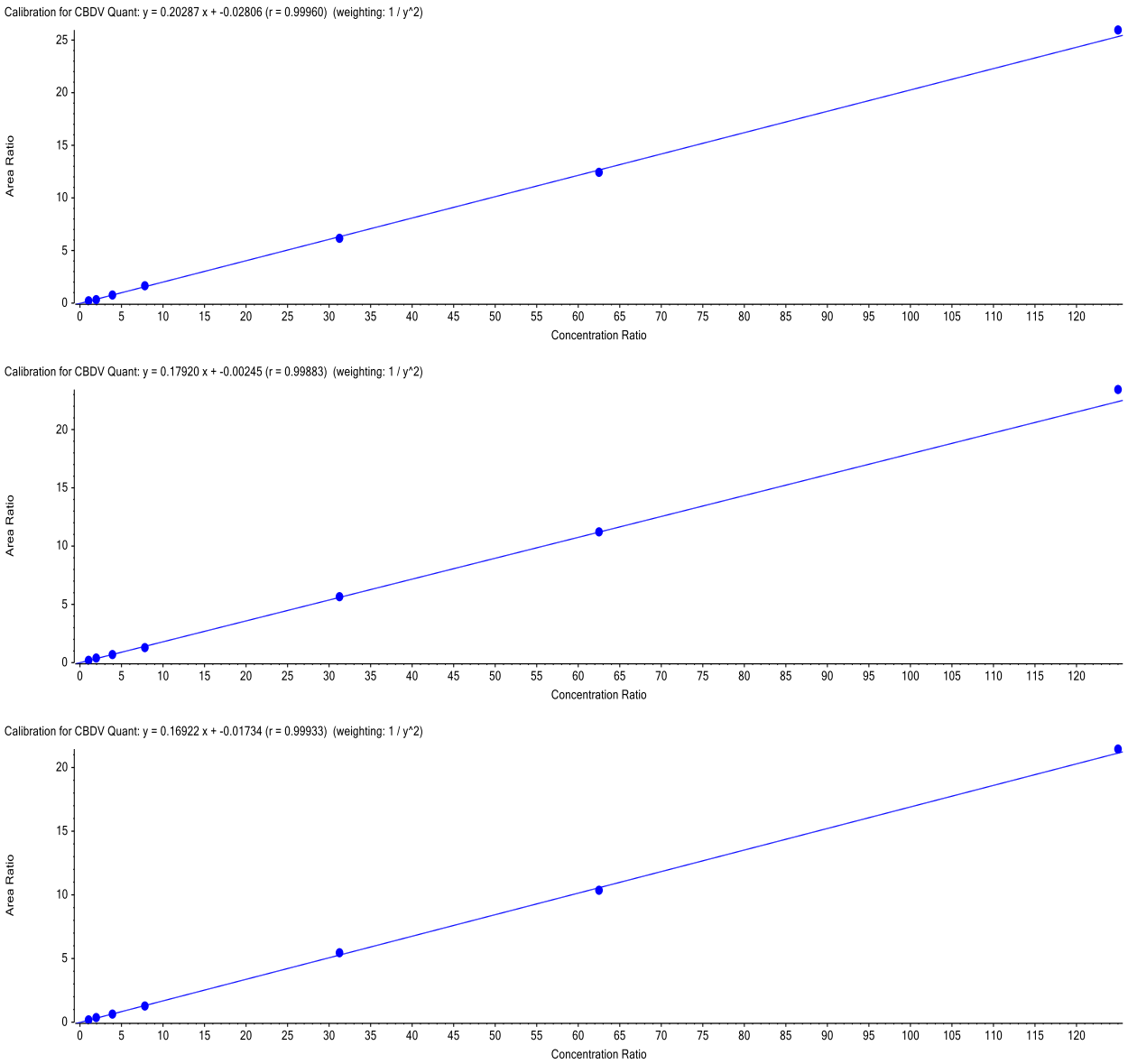

Figure 4.3. Standard curves of CBDV during three days of metabolic stability experiments involving the linear extrapolation in the stability assay (LESA) method in pooled human liver tissue, showing linearity with R^2 values > 0.98. The standard curve for CBDV has seven concentrations, ranging from 0.98-125 ng/mL. Standard curves were weighted $1/y^2$ to improve the regression fit for low stand11ard concentrations. * Plots were generated and modified in MultiQuant™ software.

4.1.3. Linearity of Calibration Curve and Accuracy and Precision of Quality Control Standards in Hank's Balanced Salt Solution

The LC-MS/MS method validation included intraday and interday accuracy and precision for QC levels and LLOQ of CBDV in Hank's balance salt solution (HBSS), as summarized in **Table 4.6** and **Table 4.7**, respectively. The intraday accuracy for all QC levels (LLOQ, LQC, MQC, and HQC) was < 10%, ranging from 93.8% to 107.2%. The intraday precision for all QC levels except for LLOQ (Day 1: 10.0%) was < 10%, ranging from 2.2% to 10.0%. The interday accuracy for all QC levels was < 10%, ranging from 95.8% to 106.5%. The interday precision for all QC levels were < 10%, ranging from 3.9% to 5.6%. **Figure 4.4** shows the standard curves of CBDV ranging from 0.98 ng/mL to 125 ng/mL, weighted $1/y^2$ with an average coefficient of determination (R^2) of 0.9960, during three days of Caco-2 drug permeability assays in HBSS.

Table 4.6. Intraday accuracy and precision for CBDV determination by LC-MS/MS detection in Hank's balanced salt solution (n = 3).

QC levels*	Accuracy (%)	Precision (%)
LLOQ		
Day 1	101.8	6.6
Day 2	99.4	10.0
Day 3	107.2	6.0
LQC		
Day 1	93.8	3.7
Day 2	101.3	5.1
Day 3	104.8	2.2
MQC		
Day 1	95.1	2.3
Day 2	100.4	2.2
Day 3	98.3	3.2
HQC		
Day 1	101.3	3.1
Day 2	103.3	3.4
Day 3	102.6	2.4

Table 4.7. Interday accuracy and precision for CBDV determination by LC-MS/MS detection in Hank's balanced salt solution (n = 9).

QC levels*	Accuracy (%)	Precision (%)
LLOQ	102.8	7.4
LQC	100.0	5.9
MQC	97.9	3.3
HQC	102.4	2.7

* LLOQ for CBDV is 0.98 ng/mL; LQC for CBDV is 1.4 ng/mL; MQC is 50.6 ng/mL; and HQC is 101.2 ng/mL.

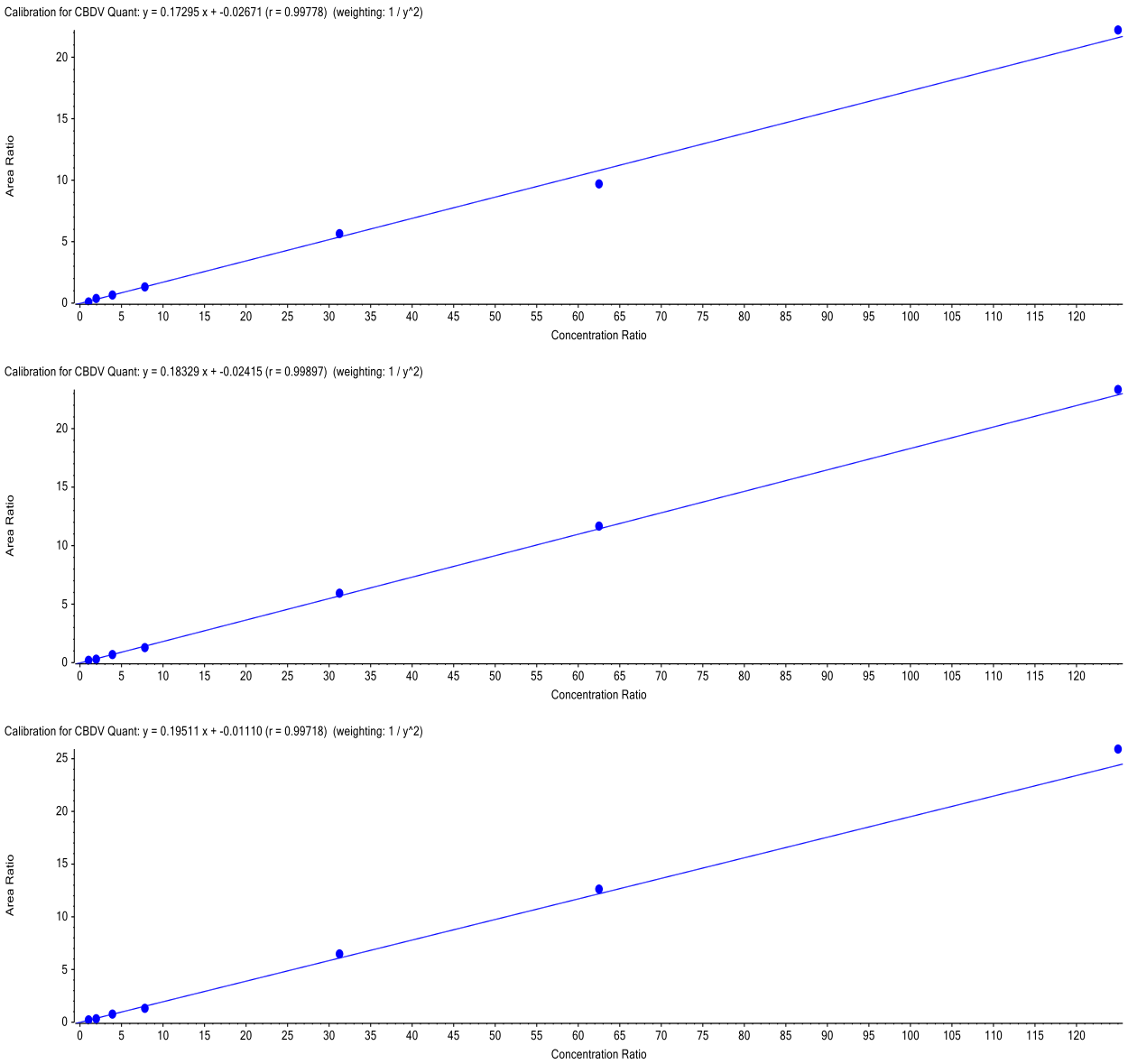

Figure 4.4. Standard curves of CBDV during three days of nonspecific binding experiments in Hank's balanced salt solution (HBSS), showing linearity with R^2 values > 0.99. The standard curve for CBDV has seven concentrations, ranging from 0.98-125 ng/mL. Standard curves were weighted $1/y^2$ to improve the regression fit for low standard concentrations. * Plots were generated and modified in MultiQuant™ software.

4.2. Determination of the Unbound Fraction of Cannabidivarin in Human Plasma

The three-solvent extraction method utilizes iso-octane, acetonitrile, and 2-octanol to approximate the unbound, protein albumin and/or α_1-acid-glycoprotein bound (denoted as "protein bound"), and lipoprotein bound fractions, respectively. The method was repeated on three separate days in replicates of six at 25, 50, and 500 ng/mL of CBDV to ensure the reproducibility of the results. The relative binding of CBDV to lipoprotein and protein albumin, as well as the unbound fraction, is reported in **Table 4.8** and **Table 4.9** for intraday and interday recovery and precision, respectively, and One-way ANOVA analysis was performed. **Figure 4.5** summarizes total CBDV binding to the components in human plasma.

At 25 ng/mL of CBDV, the intraday recovery for the unbound, protein albumin, and lipoprotein bound fractions are 24.8%, 59.1%, and 16.1%, respectively. At 50 ng/mL of CBDV, the intraday recovery for the unbound, protein bound, and lipoprotein bound fractions are 24.5%, 60.0%, and 15.5%, respectively. At 500 ng/mL of CBDV, the intraday recovery for the unbound, protein albumin, and lipoprotein bound fractions are 23.3%, 58.2%, and 18.5%, respectively. The intraday precision, also referred to as the relative standard deviation (R.S.D.), for all concentrations in each fraction was < 10%. Tukey's multiple comparisons ($\alpha = 0.05$) test also showed that the difference between 25 ng/mL and 500 ng/mL of intraday CBDV binding to lipoprotein are statistically significant ($p < 0.05$), as well as between 50 ng/mL and 500 ng/mL ($p < 0.01$). At 25 ng/mL of CBDV, the interday recovery for the unbound, protein bound, and lipoprotein bound fractions is 23.2%, 59.3%, and 17.5%, respectively. Of note, the interday precisions associated with 50 ng/mL and 500 ng/mL CBDV shared the same percentages of unbound (22.9%), protein-bound (60.6%), and lipoprotein-bound (16.5%) fractions. The interday precision for all concentrations in each fraction except for the lipoprotein fraction (25 ng/mL: 17.3%; 50 ng/mL: 11.1%; 500 ng/mL: 10.5%) were < 10%. No statistically significant differences were seen with increasing concentration of CBDV among any fractions of interday recovery.

Table 4.8. Intraday precision (relative standard deviation, R.S.D.) of CBDV binding to human plasma components (n = 6).

Theoretical Concentration of CBDV (ng/mL)	Unbound fraction (%)	Precision (%)	Protein-bound fraction (%)	Precision (%)	Lipoprotein-bound fraction (%)	Precision (%)
	(Mean ± S.D.)	(R.S.D.)	(Mean ± S.D.)	(R.S.D.)	(Mean ± S.D.)	(R.S.D.)
25	24.8 ± 1.8	7.0	59.1 ± 3.0	5.1	16.1 ± 1.6	9.8
50	24.5 ± 1.2	4.9	60.0 ± 1.2	2.0	15.5 ± 1.0	6.6
500	23.3 ± 1.1	4.6	58.2 ± 1.7	2.9	18.5 ± 1.4	7.8

Table 4.9. Interday precision (relative standard deviation, R.S.D.) of CBDV binding to human plasma components (n = 18).

Theoretical Concentration of CBDV (ng/mL)	Unbound fraction (%)	Precision (%)	Protein-bound fraction (%)	Precision (%)	Lipoprotein-bound fraction (%)	Precision (%)
	(Mean ± S.D.)	(R.S.D.)	(Mean ± S.D.)	(R.S.D.)	(Mean ± S.D.)	(R.S.D.)
25	23.2 ± 1.6	6.8	59.3 ± 2.0	3.3	17.5 ± 3.0	17.3
50	23.0 ± 1.7	7.2	60.5 ± 0.8	1.2	16.5 ± 1.8	11.1
500	22.9 ± 1.5	6.7	60.6 ± 2.4	4.0	16.5 ± 1.7	10.5

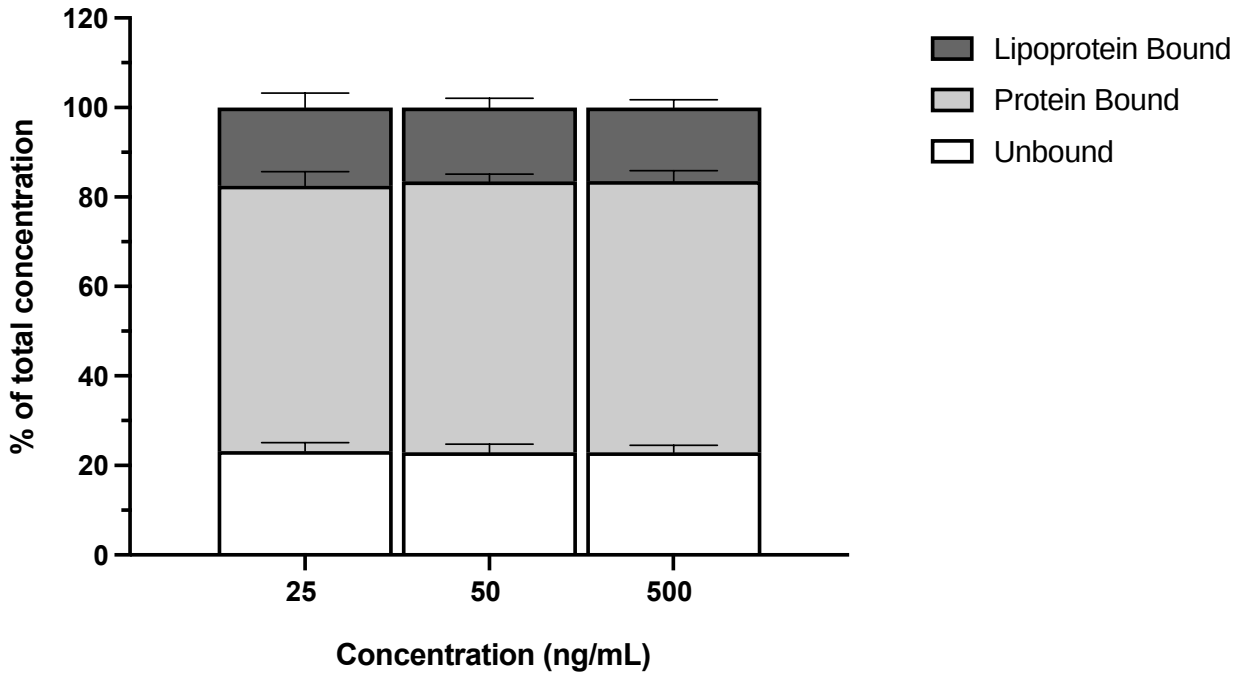

Figure 4.5. Comparison of total percent binding of CBDV to human plasma components ("Lipoprotein Bound", "Protein. Bound", and "Unbound") based on drug concentrations (*n* = 18).

4.3. *In Vitro* Hepatic Intrinsic Clearance of Cannabidivarin

The LESA method using HLMs was employed to determine the hepatic intrinsic clearance of CBDV, bound and unbound. Increasing concentrations of HLMs (0.1, 0.2, 0.25, 0.5, and 1.0 mg/mL) were incubated with the same CBDV concentration in the presence of NADPH. **Figure 4.6** represents a) percent substrate depletion of CBDV over time (t = 60 min), and b) the natural log percent remaining of CBDV until 30 min whereby linear regression was performed for each treatment group (R^2: 0.95-0.99), as seen in **Table 4.10**.

To calculate the *in vitro* intrinsic clearance (Cl_{int}) for each treatment group, the peak area of CBDV/IS were standardized to time, t = 0, equaling to 100% and utilized to plot the area under the curve (AUC). The tail end of the AUC was calculated by dividing the last concentration at time, t = 60, by the slope (k_{dep}) and added to determine the area under the curve extrapolated to infinity (AUC_{∞}). The final units of AUC were transformed from min/ng/mL to L/h/mol and dose was calculated as molar amount CBDV (mol) multiplied by the microsomal concentration (mg/mL) to calculate Cl_{int} using Eq 3.2. The calculated Cl_{int} results in units of mL/h/mg and must be divided by 1000 to convert mL to µL and multiplied by 60 to convert hours to minutes for the final unit of µL/min/mg. The inverse of each Cl_{int} was then plotted against the amount of microsomal protein, depicting a linear correlation that, when extrapolated to the y-intercept, represents the unbound intrinsic clearance ($Cl_{int,u}$). This is presented in **Figure 4.7** where the relationship between $1/Cl_{int}$ and the concentration of HLM yield a coefficient of determination (R^2) of 0.9685. Using the equation given from the linear regression, $1/Cl_{int,u}$ was calculated, and the inversion resulted in the $Cl_{int,u}$ as 128.1 µL/min/mg.

a)

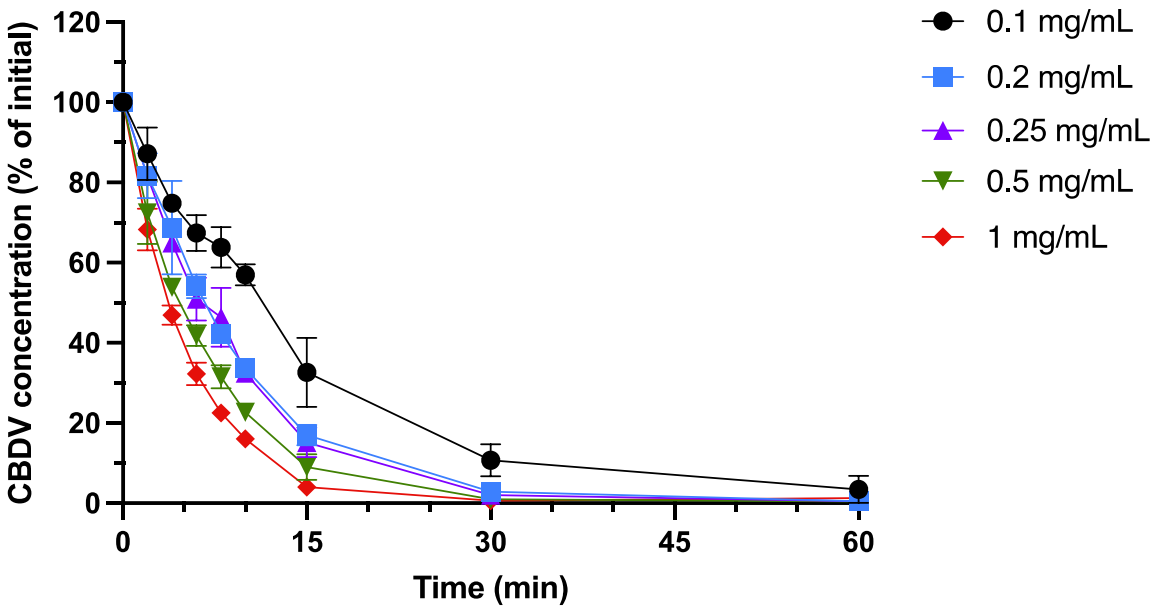

b)

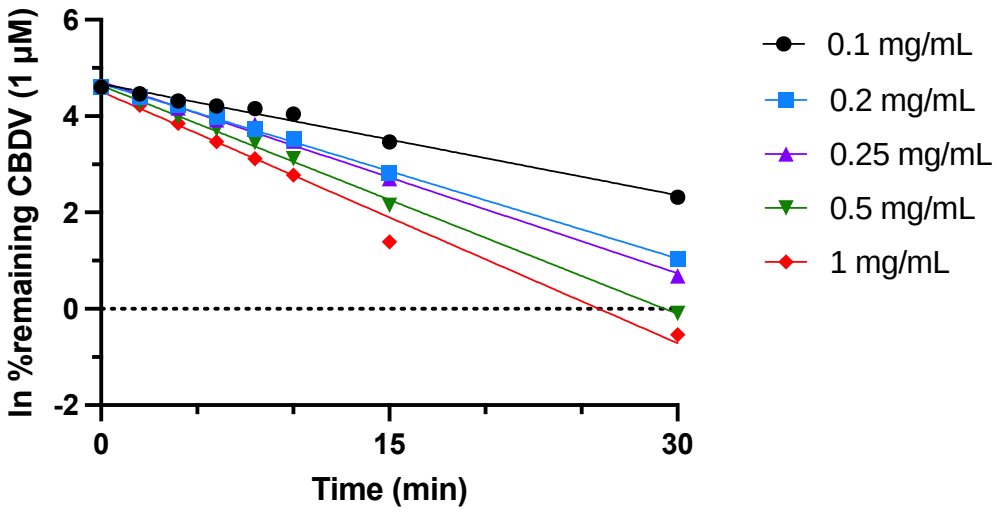

Figure 4.6. a) Time-drug depletion profile of CBDV (1 µM) in pooled human liver microsomes (HLMs). The drug was incubated in indicated concentrations of HLMs for five minutes in 37°C and 5% CO_2 before addition of NADPH to initiate each assay. Each point represents the mean of detected CBDV concentration (n = 4). B) Natural log percent remaining of CBDV (1 µM) plotted against time (t) after 30 minutes of hepatic microsomal metabolism in 0.1, 0.2, 0.25, 0.5, and 1.0 mg/mL of HLMs (n = 2).

Table 4.10. Linear regression analysis of CBDV (1 µM) after 30 minutes (data represented in **Figure 4.6**) of hepatic microsomal metabolism in 0.1, 0.2, 0.25, 0.5, and 1.0 mg/mL of HLMs (*n* = 2).

Microsomal protein (mg/mL)	**Linear regression parameters**		
	Equation	k_{dep}	R^2
0.1	$y = -0.07710x + 4.671$	-0.07710	0.9462
0.2	$y = -0.1209x + 4.672$	-0.1209	0.9866
0.25	$y = -0.1326x + 4.718$	-0.1326	0.9846
0.5	$y = -0.1580x + 4.634$	-0.1580	0.9806
1.0	$y = -0.1741x + 4.509$	-0.1741	0.9688

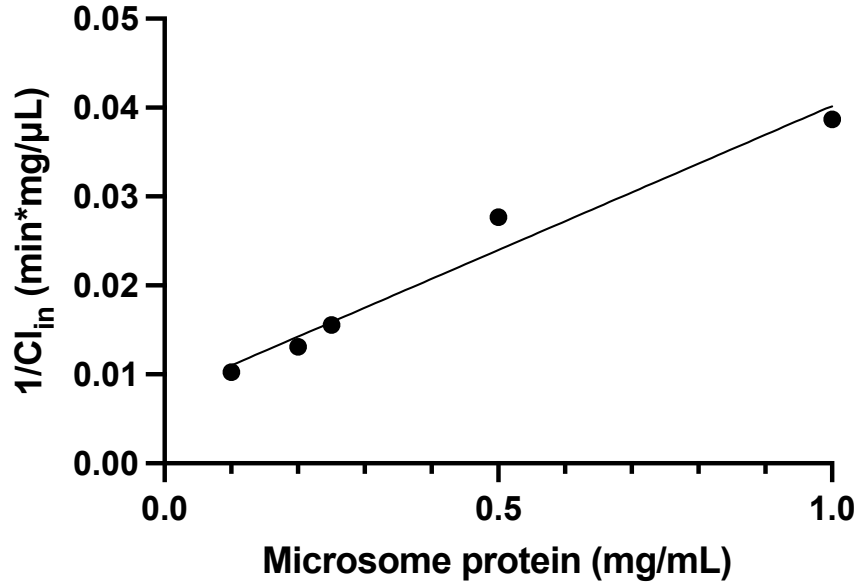

Figure 4.7. Linear correlation between the inverse of the intrinsic clearance ($1/Cl_{int}$) and HLM concentrations for CBDV (1 µM). Data fitted by linear regression ($y = 0.03232\chi + 0.007808$, $R^2 = 0.9685$) and the y-axis intercept corresponds to the inverse of the intrinsic clearance of the unbound fraction ($1/Cl_{int,u}$).Treatments were conducted in duplicates on two independent days (*n* = 4) and each point represents the average.

4.4. Cannabidivarin Cytotoxicity in Caco-2 Monolayer

To optimize the concentration of CBDV used to assess the *in vitro* intestinal permeation, the cytotoxicity of CBDV was assessed in Caco-2 monolayers at four concentrations (1, 3, 5, and 10 µM) with 1% methanol as a vehicle control and a nontreated control (0 µM CBDV) to represent 100% cell viability. Percent viability at all concentrations were > 98% (1 µM: 98.1% ± 0.5; 3 µM: 98.2% ± 2.0; 5 µM: 98.0% ± 0.8; 10 µM: 98.0% ± 1.4) with no statistically significant differences to the nontreated group. High cell viability among the CBDV concentrations is also depicted in **Figure 4.8**.

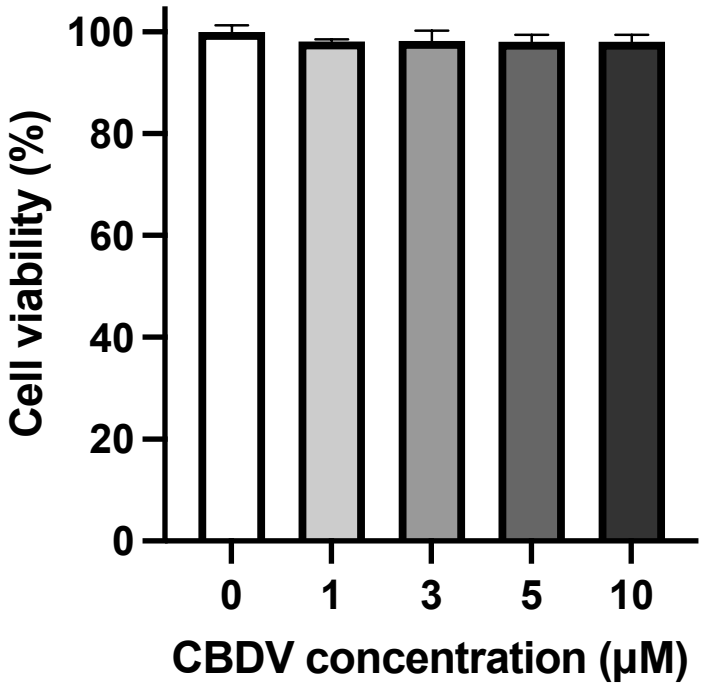

Figure 4.8. CyQUANT™ LDH Cytotoxicity Assay (ThermoFisher, Eugene, OR, USA) in Caco-2 cell cultures treated with 0, 1, 3, 5, and 10 µM CBDV for 24 h. Data are presented as mean ± S.D. of triplicate determinations. Differences in sample means were compared using One-way ANOVA ($F_{4,10} = 1.144$, $p > 0.05$).

4.5. *In Vitro* Permeation Assessment of Cannabidivarin in Caco-2 Monolayer

It was confirmed that little to no CBDV could be detected in the receiver compartments from LC-MS/MS analysis. It was predicted that nonspecific binding could have been a confounding factor in the assessment of intestinal permeation of drug and was therefore assessed in regular 24-well plates.

Treatment of CBDV (3 μM) in HBSS was performed in the presence and absence of Caco-2 cells, as well as lysis of cell samples, and were collected at the same time points in the permeability assay (t = 0, 15, 30, 45, 65 min), as seen in **Figure 4.9**. Concentrations of CBDV across all treatments and time points were lower than the theoretical initial concentration (859.2 ng/mL), with concentration in the HBSS ($p < 0.01$) and lysate ($p < 0.0001$) groups being significantly lower than in the absence of cells. Multiple comparisons of CBDV at the final time collection point, t = 60, was conducted using Dunnett's test and revealed that the combined concentration of CBDV of cell and lysed samples (464.4 ng/mL ± 19.9) compared to the absence of cells (563.1 ng/mL ± 14.1) were significantly lower ($p < 0.0001$). Peak area of CBDV/IS for cell samples and cell lysate samples were standardized to time, t = 0, representing 100% as seen in **Figure 4.10**, and the mass balance data expressed as percentage of total mass quantified in HBSS and lysate is summarized in **Table 4.11**. Percent remaining of total CBDV at 30, 45, and 60 min were significantly decreased from time, t = 0, to 90.7% ± 5.7, 88.7% ± 11.03, and 88.9% ± 7.8, respectively ($\alpha = 0.05$).

To calculate for cellular accumulation of CBDV, the peak areas of CBDV/IS (CBD-D3) of lysed samples were normalized to the amount of CBDV (3 μM) present at time, t = 0, and each concentration was subtracted by the concentration at its previous time point (**Figure 4.11**). The greatest amount of CBDV was 90.8 ng/mL ± 15.4 at the last collection time point, t = 60.

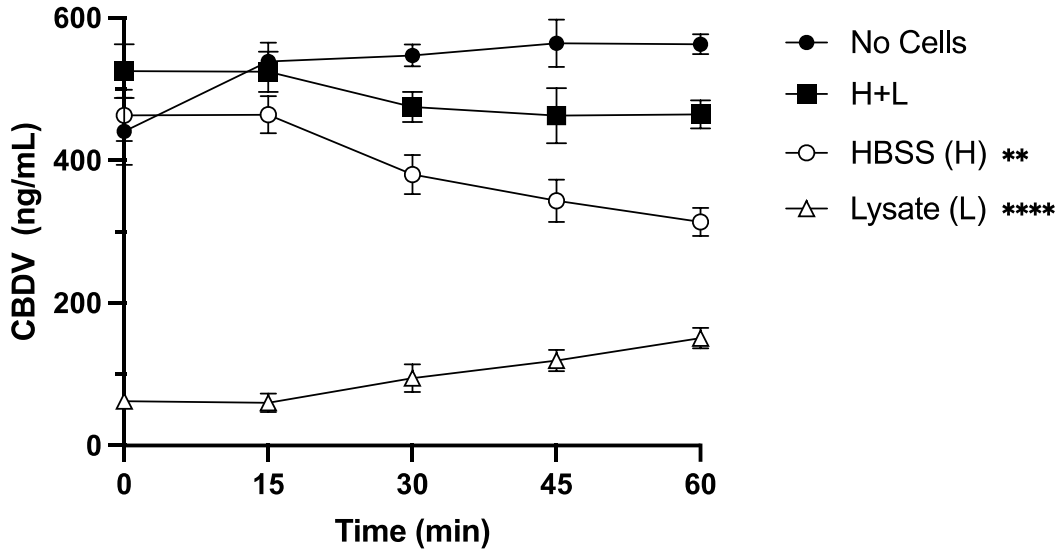

Figure 4.9. Plot of remaining CBDV (3 μM) in Hank's balanced buffered salt solution (HBSS) collected at 0, 15, 30, 45, and 60 minutes in the presence or absence of Caco-2 cells ("No Cells"). The sum of concentrations from HBSS ("H") in the presence of cells and corresponding lysates ("L") are also included ("H+L"). Each point represents the mean ± S.D. of triplicate determinations. Differences in CBDV concentrations in the absence of cells compared to the HBSS and lysate groups in the presence of Caco-2 cells were analyzed using One-way ANOVA ($F_{3,32} = 77.64$, $p < 0.0001$), and post hoc comparisons were conducted using Šidák's test (** = $p < 0.01$,**** = $p < 0.0001$).

Table 4.11. Mass balance of CBDV (3 µM) in 24-well plates containing Caco-2 cells (*n* = 9). Mass balance data expressed as percentage of total mass quantified in HBSS and lysate.

Time (min)	Mean ± S.D. Mass Balance of CBDV (%)	
	HBSS	Lysate
0	88.1 ± 1.6	11.9 ± 1.6
15	88.7 ± 7.0	11.5 ± 2.5
30	72.7 ± 6.7	18.0 ± 3.5
45	65.8 ± 8.0	22.9 ± 3.8
60	60.0 ± 6.0	28.9 ± 3.5

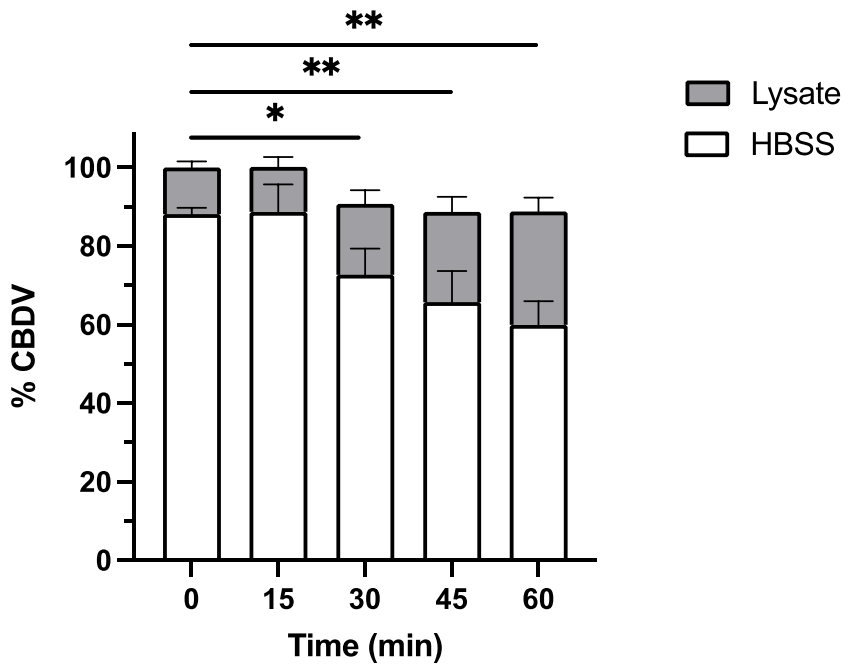

Figure 4.10. Mass balance of CBDV (3 µM) in 24-well plates containing Caco-2 cells (*n* = 9). Mass balance data are expressed as percentage of total mass quantified in HBSS ("HBSS") in the presence of cells and the corresponding lysates ("Lysate"). Differences in sample means were compared using One-way ANOVA ($F_{4,40} = 5.688$, $p = 0.001$), and post hoc comparisons of total percent CBDV were conducted using Dunnett's test (* = $p < 0.05$, ** = $p < 0.01$).

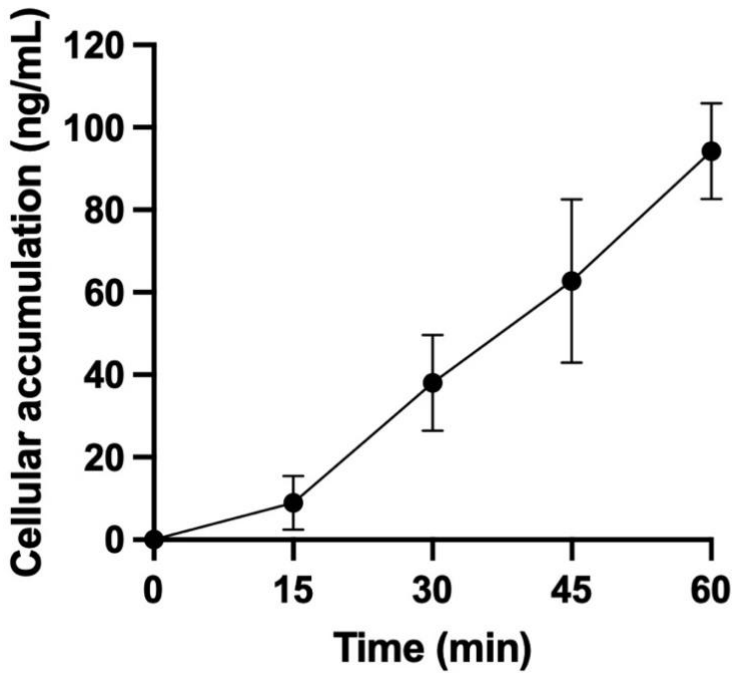

Figure 4.11. Cellular accumulation of CBDV in Caco-2 cells over time (t) normalized to the amount of CBDV (3 μM) present in lysates at t = 0. Each point represents the mean ± S.D. of triplicate determinations.

4.6. Brain Organoid Establishment

The human iPSC line, UCSD087i-6-4, also referred to as the 87i cell line, was maintained on culture plates coated in Matrigel® hESC-qualified matrix and mTeSR™ Plus media prior to use in brain organoid development (see **Figure 4.12**). All plates were maintained at 37°C and 5% CO_2 with minor modifications in the commercial kit due to unmentioned and/or unforeseen difficulties, including: low yield of embryoid bodies (EBs) due to size issues (< 300 µM in diameter); outgrowth of neuroepithelial buds and non-neuroepithelial cells from EBs; embedding of EBs into temperature-specific Matrigel® droplets, often resulting in ruptured matrices; fusion of multiple EBs per well; inconsistent EB sizes due to exceedingly large EBs; and fungal infections. Due to difficulties in culturing, only a small sample size of 90-day brain organoids, also referred to as mature brain organoids, could be established.

The cytotoxicity of CBDV and CBD were assessed in brain organoids at three concentrations (0.1, 1, and 10 µM) in the absence and presence of 500 ng/mL lipopolysaccharide (LPS). Control wells included 0.4% methanol as a vehicle, 2% water, LPS (500 ng/mL) and 0.4% methanol, lysis (1X) to represent cell death, and a nontreated control (0 µM CBDV) to represent 100% cell viability. Percent viability of CBD in the absence and presence of LPS concentrations were > 98%, ranging from 98.9% to 100.1% and 97.9% to 101.5%, respectfully. Percent viability of CBDV in the absence and presence of LPS concentrations were also > 98%, ranging from 98.8% to 100.1% and 98.6% to 101.2%, respectfully. High cell viability among the CBD and CBDV concentrations are depicted in **Figure 4.13**.

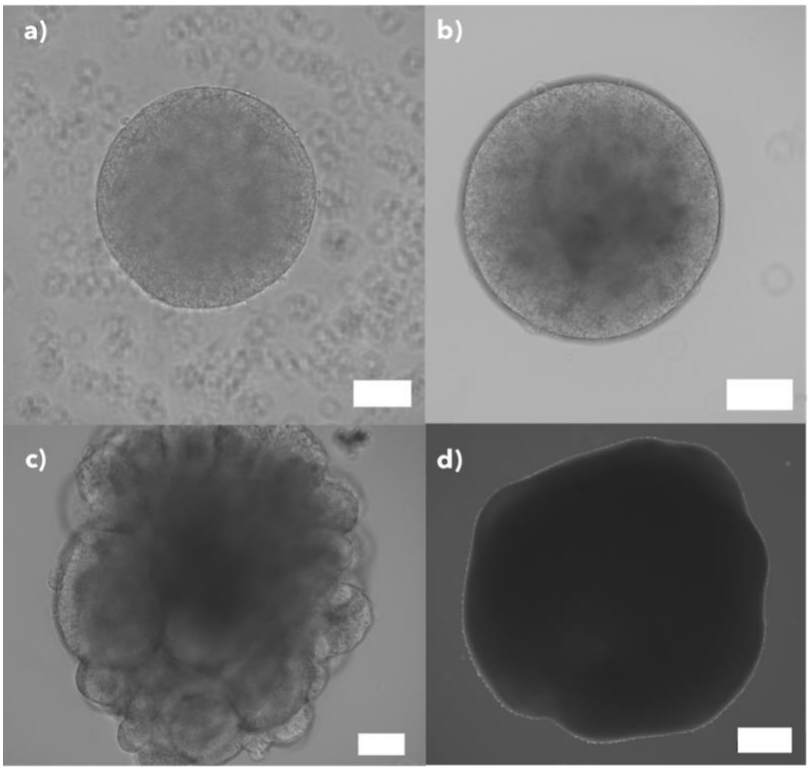

Figure 4.12. Development of brain organoid cultures using the STEMdiff™ Cerebral Organoid Kit with minor modifications. Brain organoids displayed formation of an embryoid body (EB) (a), EB expansion (b), neural folding during differentiation (c), and characteristics of maturation by day 90 (d). Scale bars represent 100 µm (a-c) and 500 µm (d).

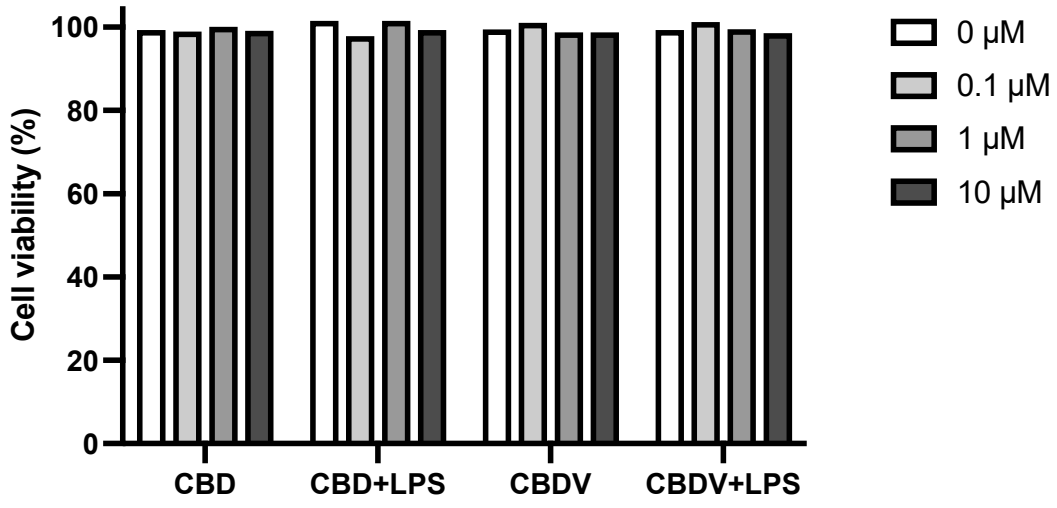

Figure 4.13. CyQUANT™ LDH Cytotoxicity Assay (ThermoFisher, Eugene, OR, USA) in brain organoid cultures treated with 0, 0.1, 1, and 10 µM CBD or CBDV for 24 h in the absence and presence of LPS (500 ng/mL) (n = 1).

4.7. Preliminary Inflammatory Stimulus Treatment of Lipopolysaccharide in Brain Organoids

After 90 days in culture, plates were treated with CBD or CBDV in the presence or absence of LPS for 24 hours at 37°C in 5% CO_2 (see Section 3.5). Organoids were collected into LoBind microcentrifuge tubes and kept at -20°C until western blotting. Lysed brain organoids underwent protein quantification and normalization prior to loading (10 µg per lane) onto 10% and 12% polyacrylamide gels. Proteins were transferred from the electrophoretic gels onto nitrocellulose membranes and incubated with primary antibodies and secondary fluorescently labelled antibodies (see **Table 3.1** for the list of primary antibodies and the respective secondary antibodies). **Figure 4.14** represents the western blot analysis as protein expression in brain organoids were visualized with a LI-COR Odyssey® Imager and manufacturer's software (Image Studio™ 5.3.5, LI-COR® Biosciences, Lincoln, NE, USA). Densitometry data for transient receptor potential vanilloid 1 (TRPV1) (**Figure 4.15**), cannabinoid receptor 1 (CB1R) (**Figure 4.16**), ionized calcium binding adaptor molecule 1 (IBA1) (**Figure 4.17**), inducible nitric oxide synthase (iNOS) (**Figure 4.18**), and transmembrane protein 119 (TMEM119) (**Figure 4.19**) expression were created by normalization of the band area of the protein of interest to total lane expression from western blots depicted in **Figure 4.14**.

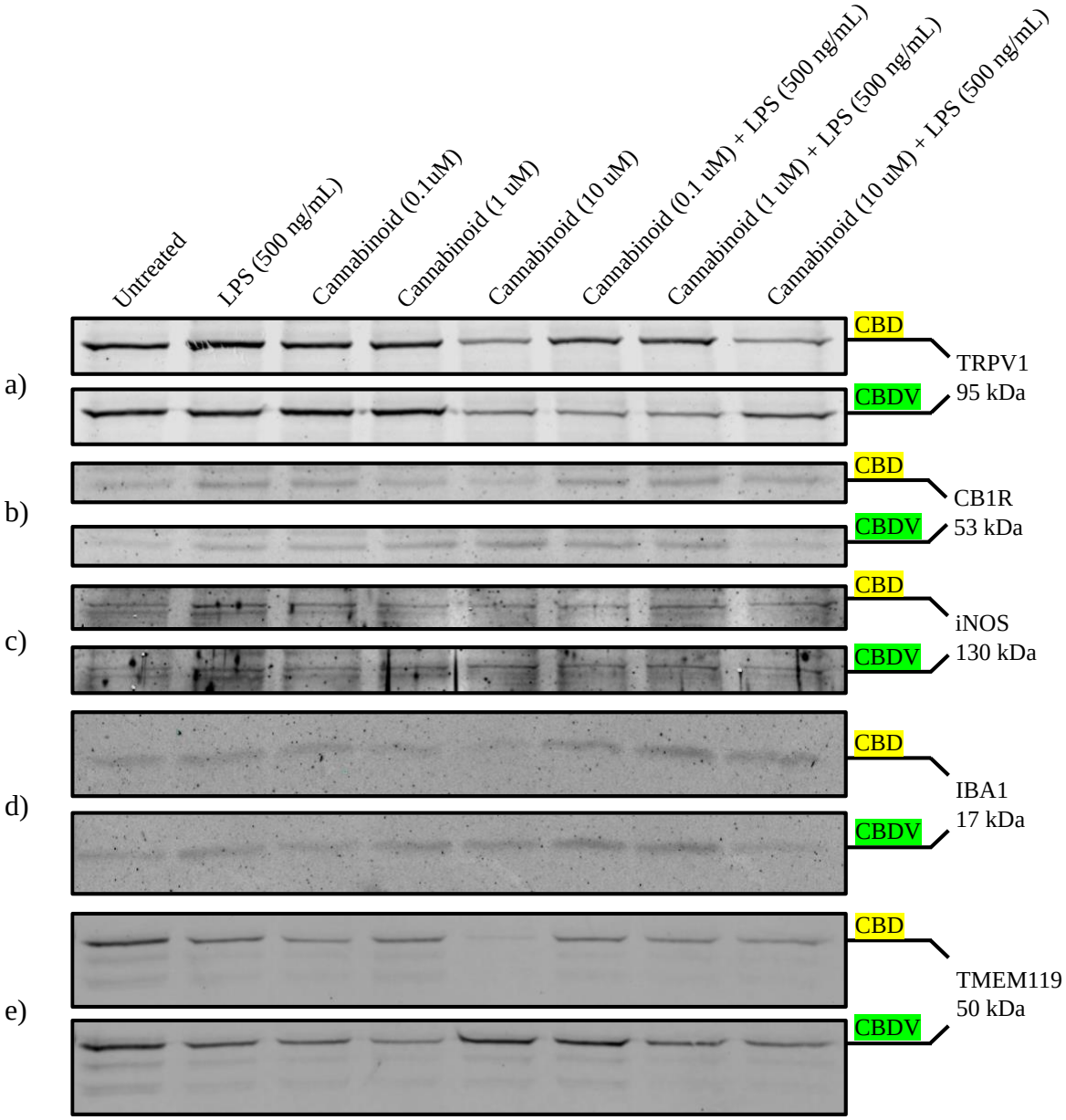

Figure 4.14. Western blot analysis of a) transient receptor potential vanilloid 1 (TRPV1) (1:500), b) cannabinoid receptor 1 (CB1R) (1:500), c) ionized calcium binding adaptor molecule 1 (IBA1) (1:500), d) inducible nitric oxide synthase (iNOS) (1:500), and e) transmembrane protein 119 (TMEM119) expression in brain organoids treated with 0.1, 1, and 10 µM CBD (top, yellow) or CBDV (bottom, green) with/without LPS treatment (500 ng/mL) (n = 1). *Treatments were added for total duration of 24 h.

Figures 4.15 and **4.16** depict the densitometry values of TRPV1 and CB1R protein expression, respectively, in brain organoids. The presence of LPS causes a two-fold increase of CB1R expression but does not influence TRPV1 compared to the untreated organoid. Treatment with CBD causes a trend of desensitization of TRPV1 in the presence and absence of LPS, as well upregulation of CB1R. Treatment with CBDV also displays desensitization of TRPV1, with a trend of increasing expression in the presence of LPS with the increase of CBDV. The CB1R expression is lower in the absence of LPS at 0.1 and 1 μM CBDV compared to CBDV+LPS yet CBDV at 10 μM displays increased expression five times greater than CBDV+LPS which has substantially decreased back to baseline levels.

Figures 4.17-4.19 depict the densitometry values of iNOS, IBA1, and TMEM119 protein expression, respectively, in brain organoids. The presence of LPS causes a substantial increase of iNOS and IBA1, and a decrease in TMEM119 compared to the untreated organoid. No trends can be seen in iNOS expression between the CBD and CBDV treatments, as well as between cannabinoid-treated and untreated organoids. Both CBD and CBDV downregulate iNOS in the presence of LPS at 0.1 and 1 μM but have no effect at 10 μM. The IBA1 expression of brain organoid treated with LPS is upregulated and further increased upon CBD treatment. Meanwhile, CBDV appears to decrease IBA1 in the presence of LPS as the cannabinoid concentration increases. Expression of TMEM119 of the untreated organoid is much higher than in the cannabinoid-treated organoid, regardless of LPS, with the lowest expression seen at 1 μM CBDV and 10 μM CBD. Interestingly, no differences in TMEM119 are seen between the LPS-treated organoid and the cannabinoid+LPS organoid except at 1 μM, which displays slightly lower expression.

a)

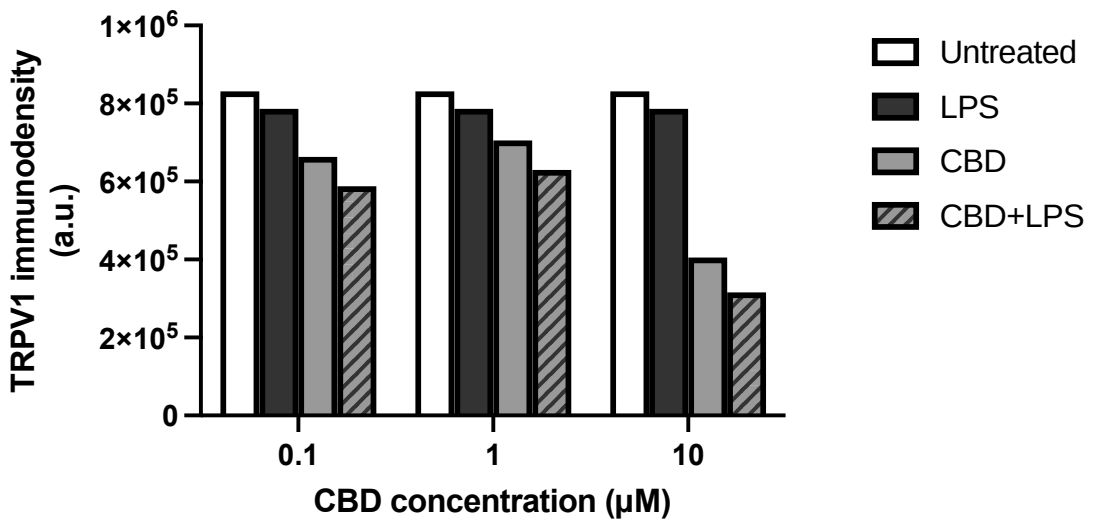

b)

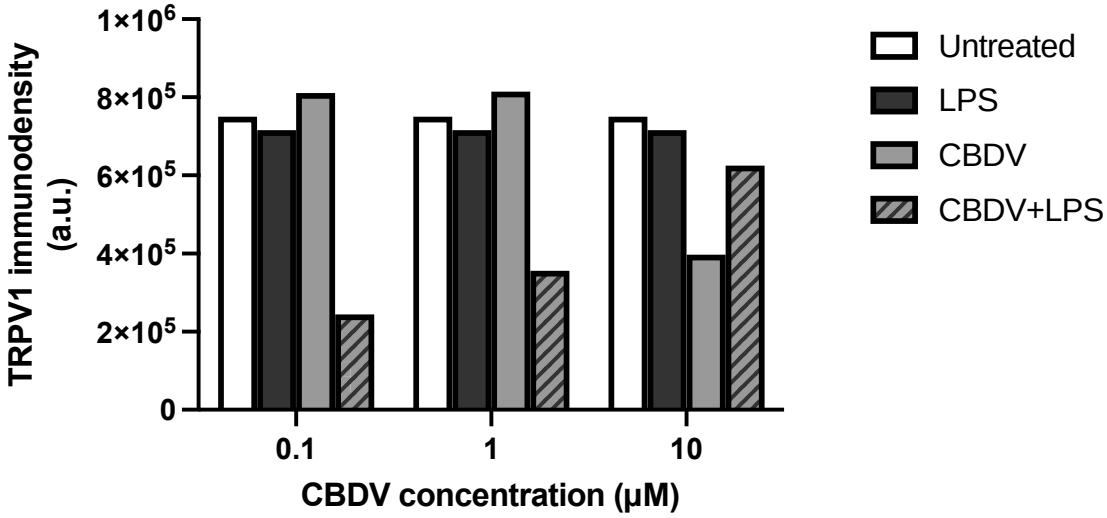

Figure 4.15. Densitometry values of TRPV1 protein expression in brain organoids treated with CBD (a) or CBDV (b) in the presence or absence of LPS (500 ng/mL), including baseline expression ("Untreated") and normal inflammatory response ("LPS") for comparison (see **Figure 4.14**). Values presented as arbitrary units (a.u.) (n = 1).

a)

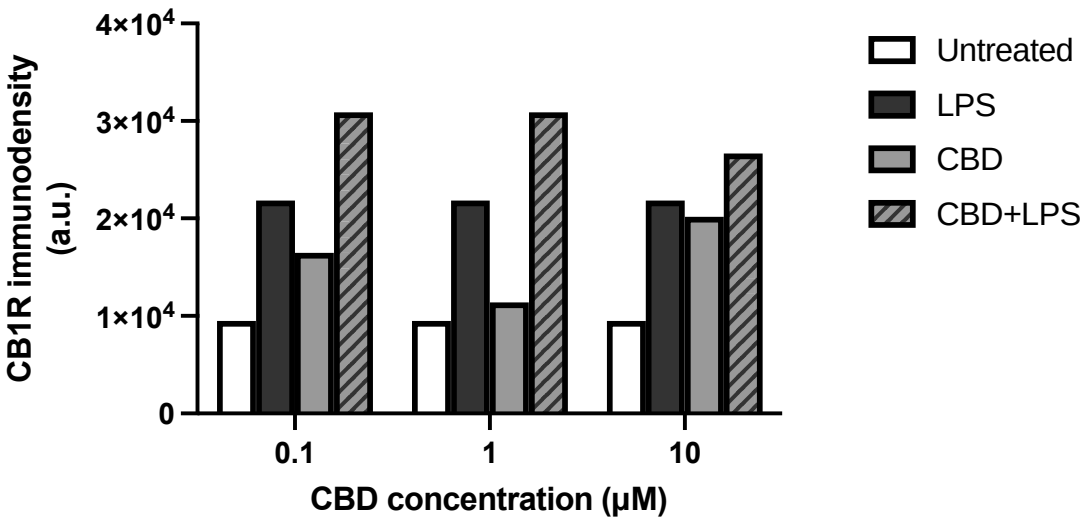

b)

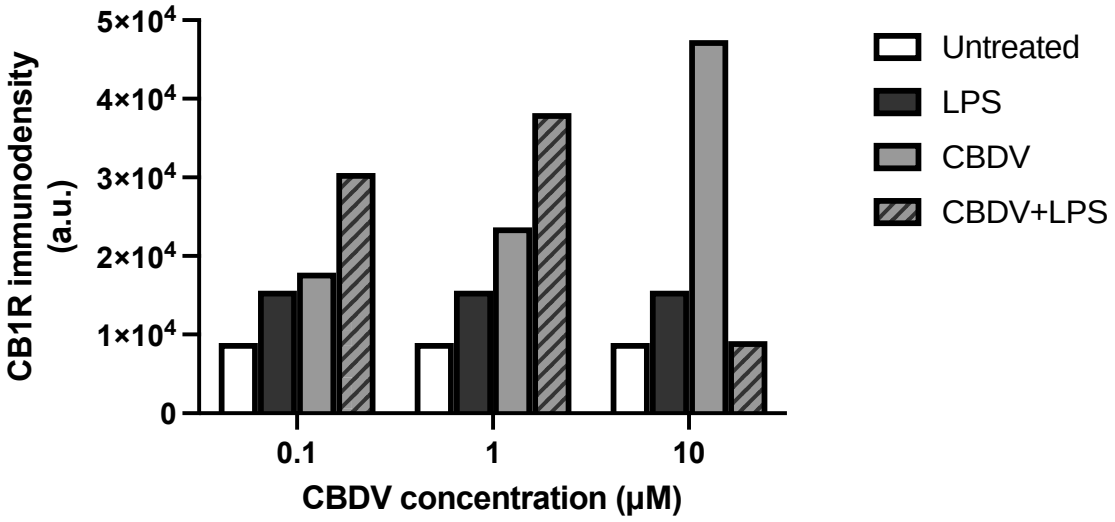

Figure 4.16. Densitometry values of CB1R protein expression in brain organoids treated with CBD (a) or CBDV (b) in the presence or absence of LPS (500 ng/mL), including baseline expression ("Untreated") and normal inflammatory response ("LPS") for comparison (see Fig 4.14). Values presented as arbitrary units (a.u.) (n = 1).

a)

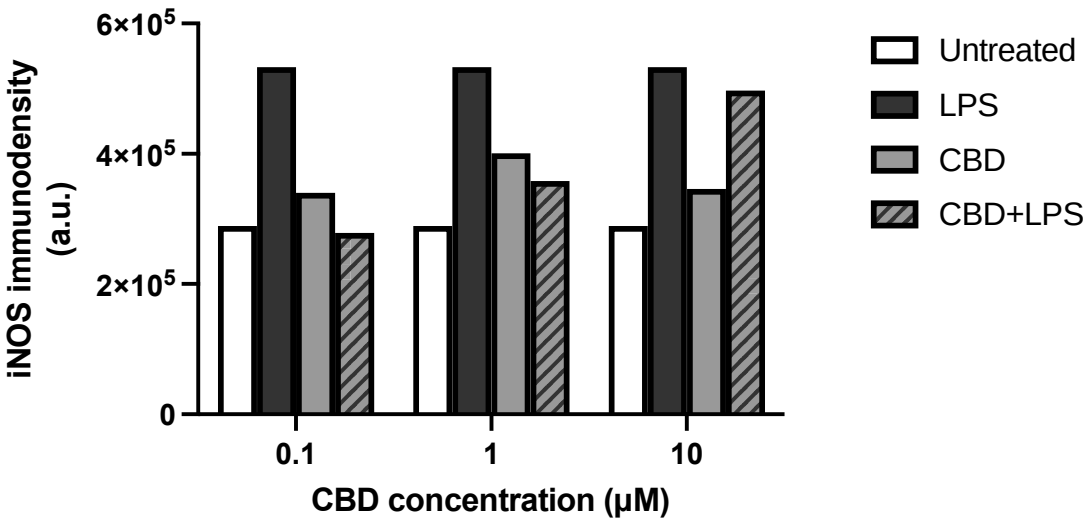

b)

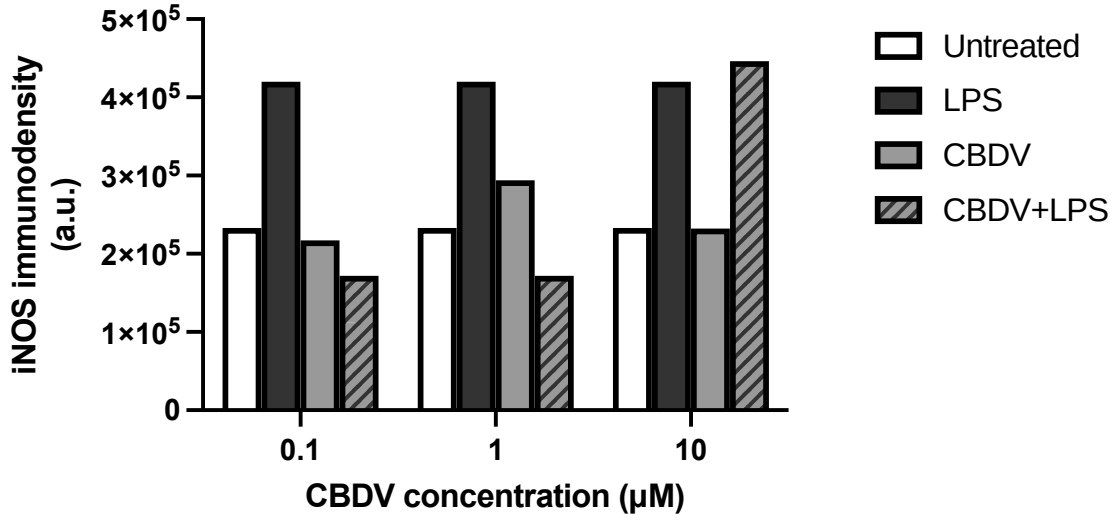

Figure 4.17. Densitometry values of iNOS protein expression in brain organoids treated with CBD (a) or CBDV (b) in the presence or absence of LPS (500 ng/mL), including baseline expression ("Untreated") and normal inflammatory response ("LPS") for comparison (see **Figure 4.14**). Values presented as arbitrary units (a.u.) (n = 1).

a)

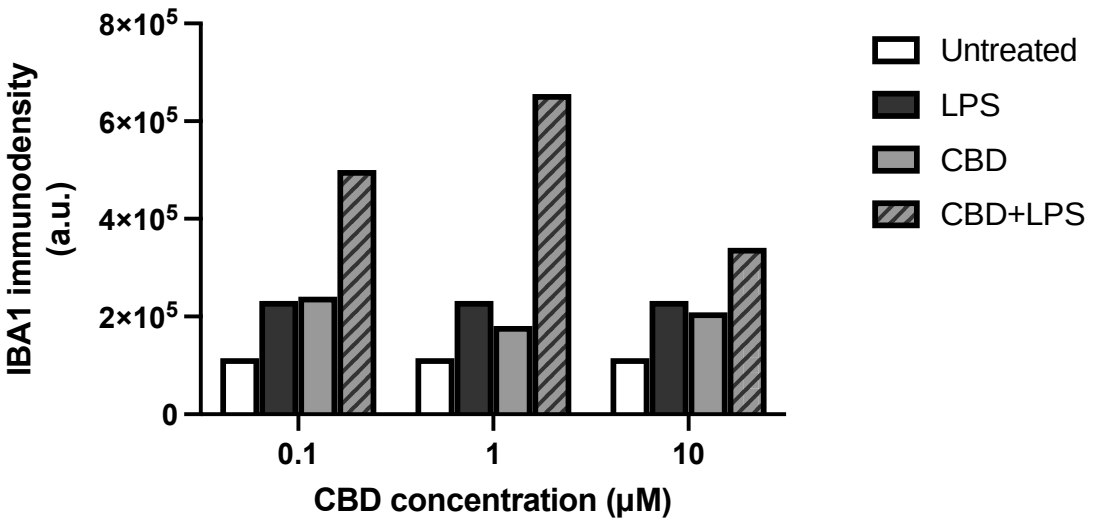

b)

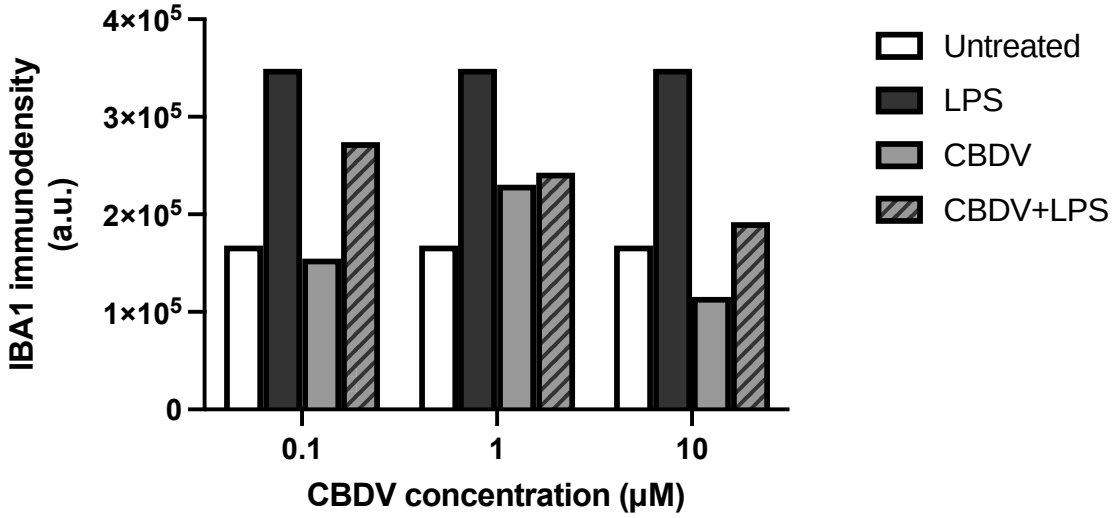

Figure 4.18. Densitometry values of IBA1 protein expression in brain organoids treated with CBD (a) or CBDV (b) in the presence or absence of LPS (500 ng/mL), including baseline expression ("Untreated") and normal inflammatory response ("LPS") for comparison (see **Figure 4.14**). Values presented as arbitrary units (a.u.) (n = 1).

a)

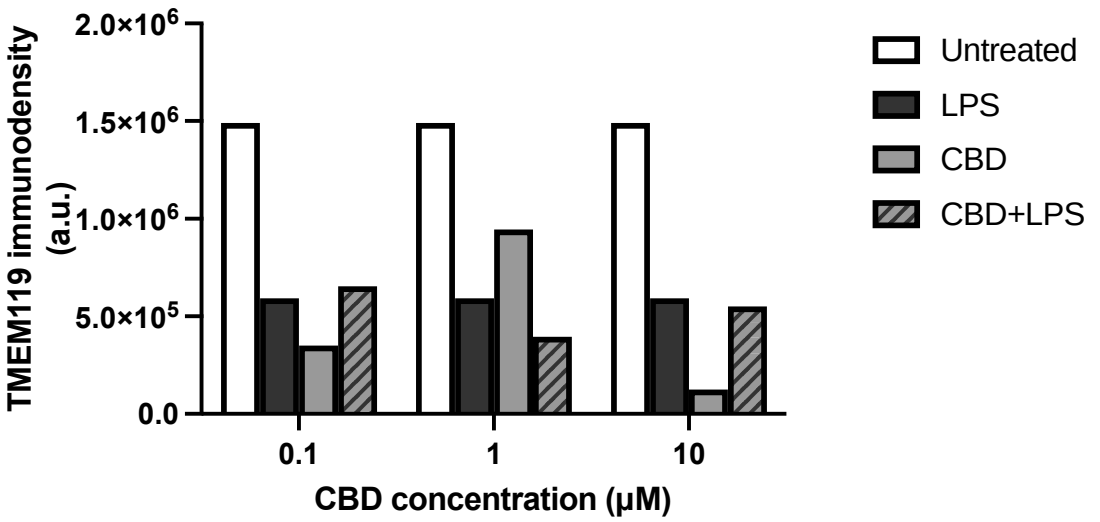

b)

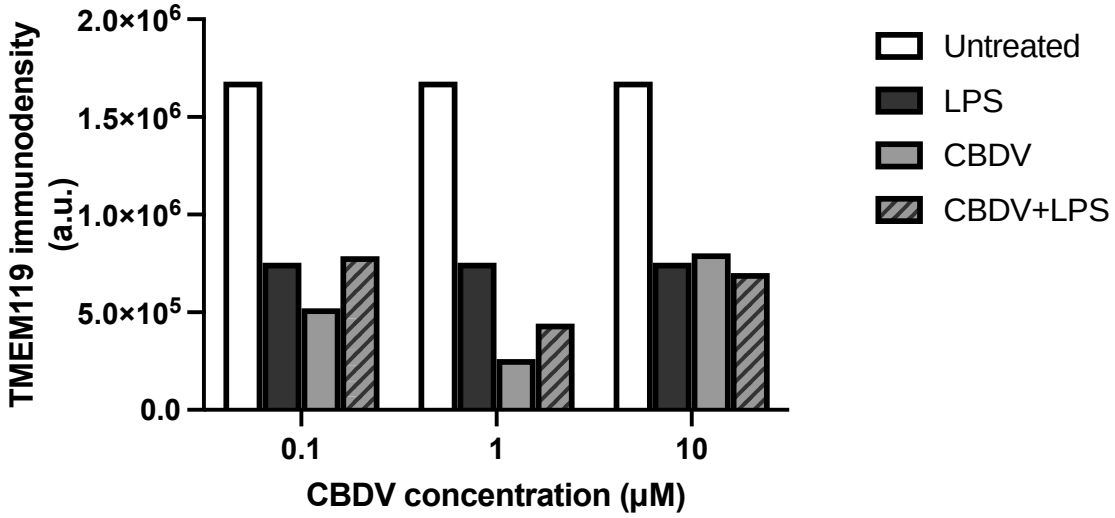

Figure 4.19. Densitometry values of TMEM119 protein expression in brain organoids treated with CBD (a) or CBDV (b) in the presence or absence of LPS (500 ng/mL) (see **Figure 4.14**). Values presented as arbitrary units (a.u.), including baseline expression ("Untreated") and normal inflammatory response ("LPS") for comparison (n = 1).

5. DISCUSSION

5.1. *In Vitro* Pharmacokinetic Assessment of Cannabidivarin

A knowledge gap exists in the pharmacokinetics of cannabinoids, especially regarding lesser-known cannabinoids that are not THC or CBD. In literature searches, CBDV is often used as a secondary cannabinoid in the study of CBD, as the chemical structure of each compound are highly similar. While CBDV has been implicated in treatment for neurological disorders and neurodegeneration, this lack of pharmacologically relevant data makes it difficult to determine safe consumption under medicinal or non-medicinal usage. We investigated the plasma protein binding (PPB), metabolic stability, and intestinal permeability of CBDV with *in vitro* methods to supplement for the lack of PK data, utilizing the three-solvent extraction technique, substrate depletion and linear extraction in the stability assay, and 21-day human colorectal adenocarcinoma cell line (Caco-2) Transwell® system, respectively.

5.1.1. Three-Solvent Extraction Plasma Protein Binding Method

One of the main determinants of distribution is the unbound fraction (f_u) in blood, which represents the amount of free drug available to partition between blood and tissue. Inadvertently, f_u can indicate the total plasma protein-bound concentration, including components such as albumin, α-1-acid-glycoprotein (AAG), and lipoprotein. Of note, CBD is known to primarily bind to albumin and has an unbound fraction of 6.98% under normal physiologically conditions, ranging from 4.88-11.69% for individuals with mild to severe hepatic impairment (Taylor, Crockett, Tayo, & Morrison, 2019). Since CBD was ≥ 88% bound to plasma proteins in all groups, no distinct trends for volume of distribution (V_d) were found. Interestingly, THC is 95-99% bound to plasma proteins, primarily bound to lipoprotein (Huestis, 2007). This suggests that CBDV may also be highly bound to plasma proteins with low free concentrations, which is often seen with lipophilic compounds such as cannabinoids.

Ultrafiltration, ultracentrifugation, and equilibrium dialysis are the three most common techniques to determining f_u; however, the issue of nonspecific binding (NSB) of drug to lab equipment such as glass, plastic, and dialysis membrane filters is disadvantageous. Other limitations include volume shifts due to colloidal osmotic pressure, the Gibbs-Donnan effects (uneven distribution of charged particles on both sides of the membrane), and protein leakage

across compromised membranes (Bowman & Benet, 2018). The three-solvent extraction technique was first introduced to the lipophilic compounds, pyrethroids, and we further extended its applicability to cannabinoids such as CBDV (Sethi et al., 2014).

The sum of the cannabinoid concentration extracted from all three solvents were equivalent to the total theoretical CBDV concentration, displaying minimal NSB and high recovery. Additionally, this technique provided not only the unbound fraction from iso-octane, but also the lipoprotein- and albumin-bound fraction of CBDV using 2-octanol and acetonitrile, respectively, in human plasma. This is significant due to the fact that other techniques only differentiate between the unbound concentration and the total bound concentration during PPB assessment, thus requiring more experiments to specify drug binding to individual protein(s).

At 25, 50, and 500 ng/mL of CBDV, the unbound fraction was reported as 23.2, 23.0, and 22.9%, respectively. These fractions are not usually considered clinically significant, and the unbound fraction contrasts to CBD whose reported value is ~ 7% (Taylor et al., 2019). The lipoprotein-bound fraction was reported as 17.5, 16.5, and 16.5%, respectfully, resulting in the albumin-bound fraction as 59.3% at 25 ng/mL, 60.5% at 50 ng/mL, and 60.6% at 500 ng/mL of CBDV. This suggests that no saturable binding to albumin was observed at the higher concentration. Additionally, the largest fraction for all three CBDV concentrations was albumin, indicating some similarity to CBD whose albumin-binding is exceptionally higher (≥ 88%). It should be of note that while the drying of isooctane and acetonitrile were rather quick, between 15-40 minutes, 2-octanol samples had to be dried for over 12 hours at 37ºC due to its high viscosity. This extended drying period could lead to degradation of CBDV and affect the true f_u. Additionally, the lipoprotein fractions showed greater relative standard deviation (R.S.D.) compared to the protein-bound and unbound fractions, ranging from 10.5-17.5%. However, in the case of CBDV where all 2-octanol samples were subjected to the same conditions and drying period, greater variation of lipoprotein fractions would have been displayed between the concentrations if sample degradation was a concern.

5.1.2. Linear Extrapolation in the Stability Assay

Microsomal stability assays using human liver microsomes (HLMs) is one of the most well characterized models in drug metabolism, known for categorizing compounds based on their metabolic stability. The intrinsic clearance (Cl_{int}) is a PK parameter that directly measures the

ability of an organ, more specifically the liver, to metabolize a drug in the absence of plasma protein and hepatic blood flow restrictions and can be used to identify the clearance of a compound as either high, intermediate, or low. While many experiments to determine Cl_{int} require the determination of the unbound fraction, the techniques are highly limited due to the issue of NSB which can prove to be challenging for lipophilic compounds such as cannabinoids that often bind to plasticware, as well as the lipid-protein matrix of the microsomal membrane (Giuliano et al., 2005). Such NSB results in a reduction of free CBDV and decreased interaction between CBDV and metabolizing enzymes, and the "true" intrinsic clearance ($Cl_{int,u}$) in the absence of NSB cannot be extrapolated from these experiments alone. Utilizing the substrate depletion approach, the depletion of CBDV using five various concentrations of liver microsomes was monitored over time and due to the simplicity of the model, no additional method validation of LC-MS/MS was required. **Figure 4.4** depicts the natural log percentage remaining of CBDV (1 µM) following the addition of NADPH to initiate the metabolic activity. Rapid depletion of CBDV was observed across all HLM concentrations, indicating that the low cannabinoid concentration was unlikely to cause saturable binding in this stability assay. Further, the limitation of the substrate depletion approach, whereby at least 20% of the initial compound must be consumed, was not a concern with CBDV.

Cl_{int} of CBDV was directly evaluated, and the calculation of $Cl_{int,u}$ without need for the determination of the unbound fraction (f_u) was achieved using the linear extrapolation in the stability assay (LESA). Ultrafiltration, ultracentrifugation, and equilibrium dialysis are the three most common techniques to determining f_u, consequently allowing for the determining of Cl_{int}, with limitations that are highly likely to affect the true parameter values. This is due to the lipophilic nature of the drug in combination with the high NSB to plasticware, leading to a decrease in available drug for metabolic interaction. Therefore, the LESA method was considered more favourable as it utilizes simple and specialized experimental and collection apparatus with minimal sample-to-surface binding. It was determined that $Cl_{int,u}$ was 128.1 µL/min/mg and in the context of the well-stirred model of hepatic clearance, any compound possessing an *in vitro* $Cl_{int} \geq 100.0$ µL/min/mg is perceived as a high clearance drug (Brian Houston, 1994). Cl_{int} of CBD was also investigated in a different study of HLMs, which was reported at 460.06 µL/min/mg (Beers, Fu, & Jackson, 2021). However, the equation used in that study, $Cl_{int} = k_{dep}$ x (µL of incubation)/(mg protein), likely lead to an exaggerated overestimation of the actual value (Zientek et al., 2016).

Overall, the LESA method directly calculated for $Cl_{int,u}$ in the absence of f_u due to the linear correlation between the Cl_{int} values and various microsomal concentrations for CBDV.

5.1.3. Permeation Assessment of Cannabidivarin in Caco-2 Monolayer

To ensure a nontoxic concentration of CBDV for the Caco-2 permeation assay, a single study assessed the cytotoxicity effects of both CBD and CBDV in Caco-2 cells using the colorimetric cell viability (MTT) assay with concentrations from 0-30 µM in 1% FBS for 24 h (Borrelli et al., 2014). At a density of $1x10^4$ cells per well, the inhibitory concentration at half the cell population (IC_{50}) of CBD and CBDV was determined as 3.73 ± 2.3 µM and 10.09 ± 1.32 µM, respectively. This suggests that CBDV is likely to have less cytotoxic effects in the intestinal epithelium than CBD at the same concentration(s). However, the primary aim of this study was to assess the effects of cannabigerol (CBG), another lesser-known phytocannabinoid, on cell growth in colorectal cancer cells with a secondary focus on other cannabinoids and other cancerous cell lines. The cell density was also much lower than what is proposed for in the Transwell® system (approx. $1–3×10^5$ cells per well) (Alhamoruni et al., 2010; Hu et al., 2004; Rourke, 2019). Our results confirmed this as cell viability was ≥ 96% for 0-10 µM of CBDV, displaying no statistical difference between the vehicle and CBDV concentrations that would suggest a trend.

Drug permeability is one of the key determinants of drug absorption, specifically at the intestinal epithelium during oral administration. An *in vitro* method using Caco-2 cells, recognized by the Food and Drug Administration (FDA) in the Biopharmaceutics Classification System, has been utilized for decades to assess absorption of drug candidates (Hu et al., 2004). Caco-2 cells were seeded onto a semi-permeable membrane in Transwell® inserts and cultured up to 21-day to exhibit *in vivo*-like characteristics of intestinal permeability. Prior to experiments, the transepithelial electrical resistance (TEER, $Ω×cm^2$) values were recorded multiple times up to and including the day of experimentation with the expectation of values ≥ 420 $Ω×cm^2$. However, during the LC-MS/MS analysis of CBDV (3 µM) in each compartment of the Transwell® system, minimal to no CBDV could be detected in the receiver compartment (< 1%), regardless of whether drug was added to the apical or basal compartment.

Given the lipophilic nature of cannabinoids, NSB of drug to the walls of the insert or the polycarbonate membrane may, in part, have explained the absence of quantifiable CBDV levels in

the Transwell® receiver compartment. However, this could not have been the only limitation that would have led to these results. In one Transwell® study utilizing Mandin-Darby canine kidney (MDCKII) cells, another model used to assess intestinal permeation, it was determined that 80-100% of THC (5 µM) accumulated within the cells after two hours. The significant intracellular accumulation could also be implicated in the Caco-2 Transwell® study as the mass balance study showed significant decreases of CBDV in both HBSS and lysate samples after 30 minutes, resulting in 90.8 ng/mL of CBDV to accumulate within the cells. Additionally, it was calculated that 61.8 ± 6.0% of CBDV (3 µM) was detected in the absence of Caco-2 cells, further suggesting that NSB is a limiting factor. Therefore, the intracellular accumulation and NSB further complicate the study of cannabinoids utilizing the Caco-2 permeability method.

5.2. *In Vitro* Pharmacodynamic Assessment of Cannabidivarin

Another crucial aim in this thesis was to provide potential PD characteristics of CBDV in brain models. While *in vivo* animal testing is considered the "gold-standard" to inform future human clinical trials, it is often time-consuming, costly, and can pose issues in extrapolation due to interspecies differences. Human brain organoids were established in our lab and treated with an inflammatory stimulus, lipopolysaccharide (LPS), to characterize the effects of CBDV during inflammation.

5.2.1. Complications in Brain Organoid Establishment

Several complications arose during the establishment of the human brain organoid system. The commercialized kit utilized in establishing the 3D brain organoids is rated for 50-60% success in cultures (approx. 48-57 organoids) per kits. However, in our hands and despite multiple attempts, less than 10% of viable brain organoids were created using this kit. Various issue arose that required modification to the existing protocol at each stage of organoid development (Lancaster & Knoblich, 2014a).

One such modification involved the induction of embryoid bodies (EBs). The EBs consistently failed to grow larger than 300 µM (e.g., 2/96 viable EBs), making them unacceptable for the induction into neural stem cells. It was theorized that two factors were involved in the failure of EB growth: lack of single cell suspension and unequal distribution of stem cells per well. Time of stem cell incubation with passaging reagent was increased (> 10 min) to form single cell

suspension and pipetting technique was adjusted, as well as the inclusion of reverse pipetting, to ensure equal cell distribution at the bottom of the well. During the neural induction stage, it was shown that EBs had outgrowth of neuroepithelial buds and non-neuroepithelial cells from the main body, likely because of carryover EB formation media due to the outlined technique of transferring EBs into induction media. Pipetting technique/EB handling was also adjusted from the original protocol to ensure minimal carryover of media. Additionally, Matrigel® is a temperature-specific extracellular matrix that thaws at 4ºC and solidifies quickly at 20ºC, complicating the embedding of EBs into the Matrigel® droplet required for the differentiation stage. Ruptured matrices often occur during this step due to handling and collision/attachment of EBs to the side of the wells. In contrast, the free-floating nature of the droplets often led to fusions of multiple EBs. Instead of Matrigel® embedding, one study suggested that Matrigel® could be dissolved at 2% v/v in the cell culture medium and still cause organoid differentiation and maturation seen with droplets (Hocevar, Liuc, & Duncan, 2021). This adaptation bypassed difficulties of temperature-specificity, resulting in decreased organoid-plasticware attachment and matrix/tissue ruptures. However, ruptures caused by handling was theorized to "heal" into fluid filled cavities, resulting in exceedingly large EBs and inconsistent EB sizes. The fluid filled cavities resemble the CSF-producing organoids; however, Lancaster & Knoblich (2014a) agreed that this phenotype was often characterized by mechanically injured brain organoids if no additional co-factors or genetic modifications were present. Additionally, plates were susceptible to fungal infection as certain wells display yellow discoloration and cloudiness. This suggests that although media formulation is not disclosed in the commercialized kits, they do not include antibiotics and antimycotics.

Due to the costliness of the commercialized kits and the time-consuming nature of the differentiation and maturation process (maturation at 30-90 days), brain organoids are difficult to establish. The additional limitations and issues with the kits that could not be addressed in previous protocols further complicated and reduced brain organoid turnover. Therefore, only a low sample size could be procured. It should be noted that all solutions and modifications were proposed by Dr. Tyler J. Wenzel.

5.2.2. Pilot Brain Organoid Assays Evaluating the Anti-Inflammatory Potential of Cannabidivarin

In the utilization of brain organoids for PD assessments, an important concern is the ability of compounds to fully penetrate the organoid. Brain organoids lack a vasculature to support transport of cannabinoids and other compounds further into the organoid, as well as lack of brain endothelial cells (BMECs) to mimic the BBB, making this model unsuitable for the purpose of drug transport. Further, it has been theorized that tissue death can occur at the centre of organoids, creating the appearance of a dark, necrotic core (Lancaster & Knoblich, 2014a). It should be noted, however, that confocal microscopes are only able to penetrate a thickness of < 100 μm and the appearance of the necrotic core is potentially the inability of light to penetrate brain organoids of a larger diameter (Graf & Boppart, 2010). Therefore, dark shadows casted at the centre of larger organoids may still be viable tissue. During the brain organoid cytotoxicity assessment of CBD and CBDV (0.1, 1, and 10 μM), high cell viability was shown, 98.8% to 100.1% and 98.6% to 101.2%, respectfully (see **Figure 4.8**). With such limitations in mind, we evaluated whether 1) the expression of certain genes in brain organoids would change in response to an inflammatory stimulus lipopolysaccharide (LPS, 500 ng/mL), and 2) the anti-inflammatory properties of CBD and CBDV in response to LPS.

Brain organoids cultured to day 90 were treated with LPS, CBD, CBDV, CBD+LPS, and CBDV+LPS at 37 °C and 5% CO_2 for 24 h. Samples were then lysed and analyzed western blotting to determine protein expression. The presence of LPS caused a substantial increase of CB1R, iNOS, and IBA1, as well as a decrease in TMEM119 compared to the untreated organoid. In the presence of LPS, CB1R expression was further increased in CBDV and CBD-treated organoids, except at 10 μM CBDV, which returned to baseline levels. Interestingly, a five-fold increase of CB1R with seen in CBDV (10 μM) treatment alone. In terms of TRPV1 activation, no differences were seen in expression between untreated and LPS-treated organoids. CBD displayed desensitization of TRPV1 in the presence of LPS, and CBDV displayed even greater desensitization except at 10 μM, which increases approximately to baseline levels. This corroborates the current literature in that desensitization of TRPV1 was observed at the lower CBDV concentrations (De Petrocellis et al., 2011). No differences of TMEM119 expression can be seen with LPS-treated organoid in the presence or absence of cannabinoid, except for a slight decrease at 1 μM of cannabinoid. However, at 0.1 and 1 μM, CBD and CBDV downregulate iNOS in the presence of LPS, back to baseline levels, while at 10 μM of cannabinoid, no difference can be seen compared to the LPS-treated organoid. IBA1 expression of LPS-treated organoid is

downregulated in the presence of CBDV while CBD treatment appears to increase IBA1 expression. This suggests that CBDV has an anti-inflammatory effect in regards to microglia activation during neuroinflammation (Ito et al., 2001; Ruan & Elyaman, 2022; Shi et al., 2020; Sonar & Lal, 2019). It should be noted that this is the first finding of TRPV1 present in brain organoids, suggesting the potential to use brain organoids in nociceptive research. Additionally, the presence of innate microglia in brain organoids from self-patterned protocols is virtually unheard of, often requiring post-translational modification or co-cultures to supplement the lack of this specific glial cell type (Del Dosso, Urenda, Nguyen, & Quadrato, 2020). Expression of key ECS components and the alteration of expression of such components following exposure to an inflammatory stimulus and cannabinoids suggest potential of brain organoids as a human *in vitro* model for PD evaluations.

6. CONCLUSION AND FUTURE WORK

Cannabis products have exponentially increased in production, variation, and consumption in the last few decades, especially after its legalization in Canada (*Cannabis Act*, October 2018). This is in part due to the therapeutic benefits of CBD, one of the most well-known and versatile cannabinoids for the treatment of various pathologies. However, the lack of available literature can prove difficult in comprehending the complete pharmacological profile and ensuring safe consumption. Lesser-known cannabinoids such as CBDV have also garnered greater attention as potential antiemetic, analgesic, antiepileptic, neuroprotective, anti-inflammatory, and anxiolytic treatments (Huestis, 2007).

To supplement for the lack of PK and PD data on CBDV, we conducted several human *in vitro* experiments to assess PPB, metabolic stability, intestinal permeation, and inflammatory responses of CBDV. The three-solvent technique allows for the determination of the unbound fraction (f_u), a key determinant in drug distribution, as well as the protein-bound and lipoprotein-bound fractions. The metabolic stability of CBDV was assessed by substrate depletion and using the LESA method with HLMs allowing determination of the true unbound intrinsic clearance ($Cl_{int,u}$). Caco-2 Transwell® assay, the only original and "gold-standard" method employed, is often utilized to assess *in vitro* intestinal permeation. As for PD assessment, 3D cell cultures termed "brain organoids" were cultured from human iPSC for the screening of CBDV and its inflammatory response.

The three-solvent extraction technique was employed to assess PPB of CBDV without the limitation of NSB that is seen in traditional methods. At 25, 50, and 500 ng/mL of CBDV, the albumin-bound and lipoprotein-bound fraction were 59.3-60.5% and 16.5-17.5%, respectively. Approximately 22.9-23.2% of CBDV is unbound in human plasma, therefore the plasma protein binding is not clinically significant as compared to CBD (6.98%) (Taylor et al., 2019). The substrate depletion method to determine the metabolic stability of CBDV was successful in determining $Cl_{int,u}$. Using the LESA method, the Cl_{int} of CBDV was 128 µL/min/mg, therefore making it a high clearance drug and likely indicates primarily metabolism by the liver. Unfortunately, the 21-day permeation study of Caco-2 cells showed limitations as no CBDV (3 µM) could be detected in the receiver compartment. Upon further investigation, a mass balance study showed significant intracellular accumulation of CBDV (90.8 ng/mL). Additionally, in the

absence of Caco-2 cells, only 61.8% of CBDV was detected. Both findings of NSB to plasticware and intracellular accumulation suggest that the Caco-2 Transwell® system may not be suitable for cannabinoids. While the drug intestinal permeation could not be assessed, future work could be improving upon the Caco-2 system or revising our knowledge of apparent permeability using *in vitro* methods.

Our lab was able to produce iPSC-derived brain organoids that self-differentiated into multiple cell types including microglia, as suggested by the consistent detection of microglial markers, TMEM119 and IBA1, unlike various other protocols (Del Dosso et al., 2020). Decreased IBA1 and iNOS from CBDV treatment of LPS-induced brain organoids indicate that CBDV has an anti-inflammatory effect by way of microglia inactivation and decreased nitric oxide, a common biomarker for oxidative stress. The TRPV1 expression with CBDV and CBD treatment was also detected in brain organoid, showcasing active function in the presence and absence of LPS. At low concentration, CBDV was shown to desensitize TRPV1 in the presence of LPS, in line with current knowledge of the drug-receptor response. This indicates that CBDV also exudes anti-inflammatory effects on the brain organoid, as well as the potential of nociceptive research as brain organoids may respond to sensory-based stimuli (e.g., pain). Additionally, with this modified protocol, next steps would be to monitor levels of cytokines (e.g., IL-6, TNF-α) for a better understanding of CBDV's pro-inflammatory and anti-inflammatory response(s) in brain organoids with innate microglia (X. Wang et al., 2022).

Overall, the established PK assays and new 3D cell culture technology provided insight to PK parameters, such as the intrinsic clearance, the unbound fraction, the protein-bound fraction of CBDV, and preliminary inflammatory profile of brain organoids which may contribute to the existing literature. For continued use of CBDV in medicinal and non-medicinal products across all ages, further research is required to establish a safe pharmacological profile.

7. REFERENCES

Abud, E. M., Ramirez, R. N., Martinez, E. S., Healy, L. M., Nguyen, C. H. H., Newman, S. A., … Blurton-Jones, M. (2017). iPSC-Derived Human Microglia-like Cells to Study Neurological Diseases. *Neuron*, *94*(2), 278-293.e9. https://doi.org/10.1016/j.neuron.2017.03.042

Adams, R., Hunt, M., & H. Clark, J. (1940). Structure of Cannabidiol, a Product Isolated from the Marihuana Extract of Minnesota Wild Hemp. I. *Journal of the American Chemical Society*, *62*(1), 196–200. https://doi.org/10.1021/ja01858a058

Agurell, S., Carlsson, S., Lindgren, J., Ohlsson, A., Gillespie, H., & Hollister, L. (1981). Interactions ofΔ 11-tetrahydrocannabinol with cannabinol and cannabidiol following oral administration in man. Assay of cannabinol and cannabidiol by mass fragmentographywith cannabinol and cannabidiol following oral administration in man. Assay of cannab. *Experientia*, *37*(10), 1090–1092. https://doi.org/10.1007/BF02085029

Alhamoruni, A., Lee, A. C., Wright, K. L., Larvin, M., & O'Sullivan, S. E. (2010). Pharmacological Effects of Cannabinoids on the Caco-2 Cell Culture Model of Intestinal Permeability. *Journal of Pharmacology and Experimental Therapeutics*, *335*(1), 92–102. https://doi.org/10.1124/jpet.110.168237

Andersen, J., Revah, O., Miura, Y., Thom, N., Amin, N. D., Kelley, K. W., … Paşca, S. P. (2020). Generation of Functional Human 3D Cortico-Motor Assembloids. *Cell*, *183*(7), 1913-1929.e26. https://doi.org/10.1016/j.cell.2020.11.017

Ao, Z., Cai, H., Havert, D. J., Wu, Z., Gong, Z., Beggs, J. M., … Guo, F. (2020). One-Stop Microfluidic Assembly of Human Brain Organoids to Model Prenatal Cannabis Exposure. *Analytical Chemistry*, *92*(6), 4630–4638. https://doi.org/10.1021/acs.analchem.0c00205

Artegiani, B., & Clevers, H. (2018). Use and application of 3D-organoid technology. *Human Molecular Genetics*, *27*(2), R99–R107. https://doi.org/10.1093/hmg/ddy187

Asha, S., & Vidyavathi, M. (2010). Role of human liver microsomes in in vitro metabolism of drugs-A review. *Applied Biochemistry and Biotechnology*, *160*(6), 1699–1722. https://doi.org/10.1007/s12010-009-8689-6

Aso, E., & Ferrer, I. (2014). Cannabinoids for treatment of alzheimer's disease: Moving toward the clinic. *Frontiers in Pharmacology*, *5 MAR*(March), 1–11. https://doi.org/10.3389/fphar.2014.00037

Bagley, J. A., Reumann, D., Bian, S., Lévi-Strauss, J., & Knoblich, J. A. (2017). Fused cerebral organoids model interactions between brain regions. *Nature Methods*, *14*(7), 743–751. https://doi.org/10.1038/nmeth.4304

Beale, C., Broyd, S. J., Chye, Y., Suo, C., Schira, M., Galettis, P., … Solowij, N. (2018). Prolonged cannabidiol treatment effects on hippocampal subfield volumes in current cannabis users. *Cannabis and Cannabinoid Research*, *3*(1), 94–107. https://doi.org/10.1089/can.2017.0047

Beers, J. L., Fu, D., & Jackson, K. D. (2021). Cytochrome P450–Catalyzed Metabolism of Cannabidiol to the Active Metabolite 7-Hydroxy-Cannabidiol. *Drug Metabolism and Disposition*, *49*, 882–891. https://doi.org/10.1124/dmd.120.000350

Białkowska, K., Komorowski, P., Bryszewska, M., & Miłowska, K. (2020). Spheroids as a type of three-dimensional cell cultures—examples of methods of preparation and the most important application. *International Journal of Molecular Sciences*, *21*(17), 1–17. https://doi.org/10.3390/ijms21176225

Birey, F., Andersen, J., Makinson, C. D., Islam, S., Wei, W., Huber, N., … Pașca, S. P. (2017). Assembly of Functional Forebrain Spheroids from Human Pluripotent Cells. *Nature*, *545*(7652), 54–59. https://doi.org/10.1038/nature22330

Bjarnason, I. (1994). Intestinal permeability. *Gut*, *35*(1 SUPPL.), 18–22. https://doi.org/10.1136/gut.35.1_Suppl.S18

Boggs, D. L., Peckham, A., Boggs, A. A., & Ranganathan, M. (2016). Delta-9-tetrahydrocannabinol and cannabidiol: Separating the chemicals from the '"weed,"' a pharmacodynamic discussion. *Mental Health Clinician*, *6*(6), 277–284. https://doi.org/10.9740/mhc.2016.11.277

Borrelli, F., Pagano, E., Romano, B., Panzera, S., Maiello, F., Coppola, D., … Izzo, A. A. (2014). Colon carcinogenesis is inhibited by the TRPM8 antagonist cannabigerol, a

Cannabis-derived non-psychotropic cannabinoid. *Carcinogenesis*, *35*(12), 2787–2797. https://doi.org/10.1093/carcin/bgu205

Bowman, C. M., & Benet, L. Z. (2018). An Examination of Protein Binding and Protein-Facilitated Uptake Relating to In Vitro-In Vivo Extrapolation. *European Journal of Pharmaceutical Sciences*, *123*, 502–514. https://doi.org/10.1016/j.ejps.2018.08.008

Brian Houston, J. (1994). Utility of in vitro drug metabolism data in predicting in vivo metabolic clearance. *Biochemical Pharmacology*, *47*(9), 1469–1479. https://doi.org/10.1016/0006-2952(94)90520-7

Brownjohn, P. W., Smith, J., Solanki, R., Lohmann, E., Houlden, H., Hardy, J., … Livesey, F. J. (2018). Functional Studies of Missense TREM2 Mutations in Human Stem Cell-Derived Microglia. *Stem Cell Reports*, *10*(4), 1294–1307. https://doi.org/10.1016/j.stemcr.2018.03.003

Calapai, F., Cardia, L., Sorbara, E. E., Navarra, M., Gangemi, S., Calapai, G., & Mannucci, C. (2020). Cannabinoids, blood–brain barrier, and brain disposition. *Pharmaceutics*, *12*(3), 1–15. https://doi.org/10.3390/pharmaceutics12030265

Chagas, M. H. N., Zuardi, A. W., Tumas, V., Pena-Pereira, M. A., Sobreira, E. T., Bergamaschi, M. M., … Crippa, J. A. S. (2014). Effects of cannabidiol in the treatment of patients with Parkinson's disease: An exploratory double-blind trial. *Journal of Psychopharmacology*, *28*(11), 1088–1092. https://doi.org/10.1177/0269881114550355

Chen, L., Deng, H., Cui, H., Fang, J., Zuo, Z., Deng, J., … Zhao, L. (2018). Inflammatory responses and inflammation-associated diseases in organs. *Oncotarget*, *9*(6), 7204–7218. https://doi.org/10.18632/oncotarget.23208

Coe, K. J., & Koudriakova, T. (2014). Metabolic Stability Assessed by Liver Microsomes and Hepatocytes. In G. W. Caldwell & Z. Yan (Eds.), *Methods in Pharmacology and Toxicology: Optimization in Drug Discovery* (2nd ed., pp. 87–99). Totowa, NJ: Humana Press Inc. https://doi.org/10.1007/978-1-62703-742-6_6

Cohen, L. H. (2004). Plasma Protein-Binding Methods in Drug Discovery. In Z. Yan & G. W. Caldwell (Eds.), *Optimization in Drug Discovery: In Vitro Methods* (1st ed., pp. 111–122).

Totowa, NJ: Humana Totowa, NJ. https://doi.org/10.1385/1592598005

De Petrocellis, L., Ligresti, A., Moriello, A. S., Allarà, M., Bisogno, T., Petrosino, S., … Di Marzo, V. (2011). Effects of cannabinoids and cannabinoid-enriched Cannabis extracts on TRP channels and endocannabinoid metabolic enzymes. *British Journal of Pharmacology*, *163*(7), 1479–1494. https://doi.org/10.1111/j.1476-5381.2010.01166.x

Deiana, S., Watanabe, A., Yamasaki, Y., Amada, N., Arthur, M., Fleming, S., … Riedel, G. (2012). Plasma and brain pharmacokinetic profile of cannabidiol (CBD), cannabidivarine (CBDV), Δ 9-tetrahydrocannabivarin (THCV) and cannabigerol (CBG) in rats and mice following oral and intraperitoneal administration and CBD action on obsessive-compulsive behav. *Psychopharmacology*, *219*(3), 859–873. https://doi.org/10.1007/s00213-011-2415-0

Del Dosso, A., Urenda, J. P., Nguyen, T., & Quadrato, G. (2020). Upgrading the Physiological Relevance of Human Brain Organoids. *Neuron*, *107*(6), 1014–1028. https://doi.org/10.1016/j.neuron.2020.08.029

Drożak, P., Skrobas, U., & Drożak, M. (2022). Cannabidiol in the treatment and prevention of Alzheimer's disease – a comprehensive overview of in vitro and in vivo studies. *Journal of Education, Health and Sport*, *12*(9), 834–845. https://doi.org/10.12775/JEHS.2022.12.09.097

FDA. (2018). *Bioanalytical Method Validation: Guidance for Industry*. *Food and Drug Administration (FDA)*. Retrieved from http://www.fda.gov/Drugs/GuidanceComplianceRegulatoryInformation/Guidances/default.htmand/orhttp://www.fda.gov/AnimalVeterinary/GuidanceComplianceEnforcement/GuidanceforIndustry/default.htm

Gaston, T. E., & Friedman, D. (2017). Pharmacology of cannabinoids in the treatment of epilepsy. *Epilepsy and Behavior*, *70*, 313–318. https://doi.org/10.1016/j.yebeh.2016.11.016

Giuliano, C., Jairaj, M., Zafiu, C. M., & Laufer, R. (2005). Direct determination of unbound intrinsic drug clearance in the microsomal stability assay. *Drug Metabolism and Disposition*, *33*(9), 1319–1324. https://doi.org/10.1124/dmd.105.005033

Graf, B. W., & Boppart, S. A. (2010). Imaging and Analysis of Three-Dimensional Cell Culture

Models. *Methods in Molecular Biology*, *591*, 211–227. https://doi.org/10.1007/978-1-60761-404-3_13

Grotenhermen, F., Russo, E., & Zuardi, A. W. (2017). Even High Doses of Oral Cannabidiol Do Not Cause THC-Like Effects in Humans: Comment on Merrick et al. Cannabis and Cannabinoid Research 2016;1(1):102-112; DOI: 10.1089/can.2015.0004. *Cannabis and Cannabinoid Research*, *2*(1), 1–4. https://doi.org/10.1089/can.2016.0036

GW Pharmaceuticals. (2018). GW Pharmaceuticals Announces Preliminary Results of Phase 2a Study for its Pipeline Compound GWP42006 [Press release]. Retrieved 25 April 2021, from https://www.gwpharm.com/about-us/news/gw-pharmaceuticals-announces-preliminary-results-phase-2a-study-its-pipeline-compound

GW Research Ltd. (2015). A study of GWP42006 in people with focal seizures - Part A. ClinicalTrial.gov Identifier: NCT02369471. Retrieved 25 April 2021, from https://clinicaltrials.gov/ct2/show/NCT02369471?term=cannabidivarin&draw=2&rank=5

Hayakawa, K., Mishima, K., Hazekawa, M., Sano, K., Irie, K., Orito, K., … Fujiwara, M. (2008). Cannabidiol potentiates pharmacological effects of Δ9-tetrahydrocannabinol via CB1 receptor-dependent mechanism. *Brain Research*, *1188*(1), 157–164. https://doi.org/10.1016/j.brainres.2007.09.090

Hidalgo, I. J., Raub, T. J., & Borchardt, R. T. (1989). Characterization of the Human Colon Carcinoma Cell Line (Caco-2) as a Model System for Intestinal Epithelial Permeability. *Gastroenterology*, *96*(2), 736–749. https://doi.org/10.1016/S0016-5085(89)80072-1

Hill, A. J., Mercier, M. S., Hill, T. D. M., Glyn, S. E., Jones, N. A., Yamasaki, Y., … Whalley, B. J. (2012). Cannabidivarin is anticonvulsant in mouse and rat. *British Journal of Pharmacology*, *167*(8), 1629–1642. https://doi.org/10.1111/j.1476-5381.2012.02207.x

Hill, T. D. M., Cascio, M. G., Romano, B., Duncan, M., Pertwee, R. G., Williams, C. M., … Hill, A. J. (2013). Cannabidivarin-rich cannabis extracts are anticonvulsant in mouse and rat via a CB1 receptor-independent mechanism. *British Journal of Pharmacology*, *170*(3), 679–692. https://doi.org/10.1111/bph.12321

Hocevar, S. E., Liuc, L., & Duncan, R. K. (2021). Matrigel is required for efficient differentiation of isolated, stem cell-derived otic vesicles into inner ear organoids. *Stem Cell Reports*, *53*(102295), 1–15. https://doi.org/10.1016/j.scr.2021.102295

Houston, J. B., Kenworth, K. E., & Galetin, A. (2003). Typical and Atypical Enzyme Kinetics. In J. Lee, R. S. Obach, & M. B. Fisher (Eds.), *Drug metabolizing enzymes : cytochrome P450 and other enzymes in drug discovery and development* (pp. 211–254). New York: Marcel Dekker.

Hu, M., Ling, J., Lin, H., & Chen, J. (2004). Use of Caco-2 Cell Monolayers to Study Drug Absorption and Metabolism. In Z. Yan & G. W. Caldwell (Eds.), *Optimization in Drug Discovery: In Vitro Methods* (1st ed., pp. 19–35). Totowa, NJ: Humana Totowa, NJ. https://doi.org/10.1385/1592598005

Hubatsch, I., Ragnarsson, E. G. E., & Artursson, P. (2007). Determination of drug permeability and prediction of drug absorption in Caco-2 monolayers. *Nature Protocols*, *2*(9), 2111–2119. https://doi.org/10.1038/nprot.2007.303

Huestis, M. A. (2007). Human cannabinoid pharmacokinetics. *Chemistry and Biodiversity*, *4*(8), 1770–1804. https://doi.org/10.1002/cbdv.200790152

Huestis, M. A., Gorelick, D. A., Heishman, S. J., Preston, K. L., Nelson, R. A., Moolchan, E. T., … Kosten, T. R. (2001). Blockade of effects of smoked marijuana by the CB1-selective cannabinoid receptor antagonist SR141716. *Archives of General Psychiatry*, *58*(4), 322–328. https://doi.org/10.1001/archpsyc.58.4.322

Huestis, M. A., Solimini, R., Pichini, S., Pacifici, R., Carlier, J., & Busardò, F. P. (2019). Cannabidiol Adverse Effects and Toxicity. *Current Neuropharmacology*, *17*(10), 974–989. https://doi.org/10.2174/1570159x17666190603171901

Iannotti, F. A., Hill, C. L., Leo, A., Alhusaini, A., Soubrane, C., Mazzarella, E., … Stephens, G. J. (2014). Nonpsychotropic plant cannabinoids, Cannabidivarin (CBDV) and Cannabidiol (CBD), activate and desensitize Transient Receptor Potential Vanilloid 1 (TRPV1) channels in vitro: Potential for the treatment of neuronal hyperexcitability. *ACS Chemical Neuroscience*, *5*(11), 1131–1141. https://doi.org/10.1021/cn5000524

Ito, D., Tanaka, K., Suzuki, S., Dembo, T., & Fukuuchi, Y. (2001). Enhanced expression of Iba1, ionized calcium-binding adapter molecule 1, after transient focal cerebral ischemia in rat brain. *Stroke*, *32*(5), 1208–1215. https://doi.org/10.1161/01.STR.32.5.1208

Jo, J., Xiao, Y., Sun, A. X., Cukuroglu, E., Tran, H., Göke, J., … Ng, H. H. (2016). Midbrain-like organoids from human pluripotent stem cells contain functional dopaminergic and neuromelanin producing neurons. *Cell Stem Cell*, *19*(2), 248–257. https://doi.org/10.1016/j.stem.2016.07.005

Kargbo, R. B. (2019). TRPV1 Modulators for the Treatment of Pain and Inflammation. *ACS Medicinal Chemistry Letters*, *10*(2), 143–144. https://doi.org/10.1021/acsmedchemlett.8b00618

Klumpers, L. E., & Thacker, D. L. (2019). A brief background on cannabis: From plant to medical indications. *Journal of AOAC International*, *102*(2), 412–420. https://doi.org/10.5740/jaoacint.18-0208

Krieger, T. G., Tirier, S. M., Park, J., Jechow, K., Eisemann, T., Peterziel, H., … Conrad, C. (2020). Modeling glioblastoma invasion using human brain organoids and single-cell transcriptomics. *Neuro-Oncology*, *22*(8), 1138–1149. https://doi.org/10.1093/neuonc/noaa091

Lancaster, M. A., & Knoblich, J. A. (2014a). Generation of cerebral organoids from human pluripotent stem cells. *Nature Protocols*, *9*(10), 2329–2340. https://doi.org/10.1038/nprot.2014.158

Lancaster, M. A., & Knoblich, J. A. (2014b). Organogenesisin a dish: Modeling development and disease using organoid technologies. *Science*, *345*(6194). https://doi.org/10.1126/science.1247125

Lancaster, M. A., Renner, M., Martin, C. A., Wenzel, D., Bicknell, L. S., Hurles, M. E., … Knoblich, J. A. (2013). Cerebral organoids model human brain development and microcephaly. *Nature*, *501*(7467), 373–379. https://doi.org/10.1038/nature12517

Laprairie, R. B., Bagher, A. M., Kelly, M. E. M., & Denovan-Wright, E. M. (2015). Cannabidiol is a negative allosteric modulator of the cannabinoid CB1 receptor. *British Journal of*

Pharmacology, *172*(20), 4790–4805. https://doi.org/10.1111/bph.13250

Lemberger, L., Martz, R., & Rodda, B. (1973). Comparative pharmacology of Δ9 tetrahydrocannabinol and its metabolite, 11 OH Δ9 tetrahydrocannabinol. *Journal of Clinical Investigation*, *52*(10), 2411–2417. https://doi.org/10.1172/JCI107431

Li, A. P. (2005). Preclinical in vitro screening assays for drug-like properties. *Drug Discovery Today: Technologies*, *2*(2), 179–185. https://doi.org/10.1016/j.ddtec.2005.05.024

Linkous, A., Balamatsias, D., Snuderl, M., Edwards, L., Milner, T., Reich, B., … Fine, H. A. (2019). Modeling Patient-Derived Glioblastoma with Cerebral Organoids. *Cell Reports*, *26*(12), 3203–3211. https://doi.org/10.1016/j.celrep.2019.02.063

Lu, H.-C., & Mackie, K. (2016). An introduction to the endogenous cannabinoid system. *Biol Psychiatry*, *79*(7), 516–525. https://doi.org/10.1016/j.biopsych.2015.07.028.

Lucas, C. J., Galettis, P., & Schneider, J. (2018). The pharmacokinetics and the pharmacodynamics of cannabinoids. *British Journal of Clinical Pharmacology*, *84*(11), 2477–2482. https://doi.org/10.1111/bcp.13710

Mansour, A. A., Tiago Gonçalves, J., Bloyd, C. W., Li, H., Fernandes, S., Quang, D., … Biotechnol, N. (2018). An in vivo model of functional and vascularized human brain organoids. *Nat Biotechnol*, *36*(5), 432–441. https://doi.org/10.1038/nbt.4127.An

McGuire, P., Robson, P., Cubala, W. J., Vasile, D., Morrison, P. D., Barron, R., … Wright, S. (2018). Cannabidiol (CBD) as an adjunctive therapy in schizophrenia: A multicenter randomized controlled trial. *American Journal of Psychiatry*, *175*(3), 225–231. https://doi.org/10.1176/appi.ajp.2017.17030325

Mechoulam, R., Shani, A., Edery, H., & Grunfeld, Y. (1970). Chemical Basis of Hashish Activity. *Science*, *169*(3945), 611–612. https://doi.org/10.1126/science.169.3945.611

Minett, T., Classey, J., Matthews, F. E., Fahrenhold, M., Taga, M., Brayne, C., … Boche, D. (2016). Microglial immunophenotype in dementia with Alzheimer's pathology. *Journal of Neuroinflammation*, *13*(1), 1–10. https://doi.org/10.1186/s12974-016-0601-z

Miura, Y., Li, M. Y., Birey, F., Ikeda, K., Revah, O., Thete, M. V., … Pașca, S. P. (2020).

Generation of human striatal organoids and cortico-striatal assembloids from human pluripotent stem cells. *Nature Biotechnology*, *38*(12), 1421–1430. https://doi.org/10.1038/s41587-020-00763-w

Morano, A., Cifelli, P., Nencini, P., Antonilli, L., Fattouch, J., Ruffolo, G., … Giallonardo, A. T. (2016). Cannabis in epilepsy: From clinical practice to basic research focusing on the possible role of cannabidivarin. *Epilepsia Open*, *1*(3–4), 145–151. https://doi.org/10.1002/epi4.12015

Morano, A., Fanella, M., Albini, M., Cifelli, P., Palma, E., Giallonardo, A. T., & Di Bonaventura, C. (2020). Cannabinoids in the treatment of epilepsy: Current status and future prospects. *Neuropsychiatric Disease and Treatment*, *16*, 381–396. https://doi.org/10.2147/NDT.S203782

Muguruma, K., Nishiyama, A., Kawakami, H., Hashimoto, K., & Sasai, Y. (2015). Self-organization of polarized cerebellar tissue in 3D culture of human pluripotent stem cells. *Cell Reports*, *10*(4), 537–550. https://doi.org/10.1016/j.celrep.2014.12.051

Nagarkatti, P., Pandey, R., Rieder, S. A., Hegde, V. L., & Nagarkatti, M. (2009). Cannabinoids as novel anti-inflammatory drugs. *Future Med Chem*, *1*(7), 1333–1349. https://doi.org/10.4155/fmc.09.93

Navarrete, F., García-Gutiérrez, M. S., Jurado-Barba, R., Rubio, G., Gasparyan, A., Austrich-Olivares, A., & Manzanares, J. (2020). Endocannabinoid System Components as Potential Biomarkers in Psychiatry. *Frontiers in Psychiatry*, *11*(April), 1–30. https://doi.org/10.3389/fpsyt.2020.00315

Nawaz, M. S. (2013). Validation and application of a new reversed phase HPLC method for in vitro dissolution studies of rabeprazole sodium in delayed-release tablets. *Journal of Analytical Methods in Chemistry*, (976034), 1–8. https://doi.org/10.1155/2013/976034

Obach, R. S. (1999). Prediction of human clearance of twenty-nine drugs from hepatic microsomal intrinsic clearance data: An examination of in vitro half-life approach and nonspecific binding to microsomes. *Drug Metabolism and Disposition*, *27*(11), 1350–1359.

Ohsawa, K., Imai, Y., Sasaki, Y., & Kohsaka, S. (2004). Microglia/macrophage-specific protein

Iba1 binds to fimbrin and enhances its actin-bundling activity. *Journal of Neurochemistry*, *88*(4), 844–856. https://doi.org/10.1046/j.1471-4159.2003.02213.x

Ozone, C., Suga, H., Eiraku, M., Kadoshima, T., Yonemura, S., Takata, N., … Sasai, Y. (2016). Functional anterior pituitary generated in self-organizing culture of human embryonic stem cells. *Nature Communications*, *7*, 1–10. https://doi.org/10.1038/ncomms10351

Paraíso-Luna, J., Aguareles, J., Martín, R., Ayo-Martín, A. C., Simón-Sánchez, S., Garcıá-Rincón, D., … Galve-Roperh, I. (2020). Endocannabinoid signalling in stem cells and cerebral organoids drives differentiation to deep layer projection neurons via CB1 receptors. *Development (Cambridge)*, *147*(24), 1–12. https://doi.org/10.1242/dev.192161

Parker, L. A., & Limebeer, C. L. (2006). Conditioned gaping in rats: A selective measure of nausea. *Autonomic Neuroscience: Basic and Clinical*, *129*(1–2), 36–41. https://doi.org/10.1016/j.autneu.2006.07.022

Pearson, R. M. (1986). In-vitro techniques: Can they replace animal testing? *Human Reproduction*, *1*(8), 559–560. https://doi.org/10.1093/oxfordjournals.humrep.a136473

Pellegrini, L., Bonfio, C., Chadwick, J., Begum, F., Skehel, M., & Lancaster, M. A. (2020). Human CNS barrier-forming organoids with cerebrospinal fluid production. *Science*, *369*(6500). https://doi.org/10.1126/science.aaz5626

Pham, M. T., Pollock, K. M., Rose, M. D., Cary, W. A., Stewart, H. R., Zhou, P., … Waldau, B. (2018). Generation of human vascularized brain organoids. *Neuroreport*, *29*(7), 588–593. https://doi.org/10.1097/WNR.0000000000001014

Puffenbarger, R. A., Boothe, A. C., & Cabral, G. A. (2000). Cannabinoids inhibit LPS-inducible cytokine mRNA expression in rat microglial cells. *Glia*, *29*(1), 58–69. https://doi.org/10.1002/(SICI)1098-1136(20000101)29:1<58::AID-GLIA6>3.0.CO;2-W

Qian, X., Nguyen, H. N., Song, M. M., Hadiono, C., Ogden, S. C., Hammack, C., … Ming, G. L. (2016). Brain-Region-Specific Organoids Using Mini-bioreactors for Modeling ZIKV Exposure. *Cell*, *165*(5), 1238–1254. https://doi.org/10.1016/j.cell.2016.04.032

Qian, X., Su, Y., Adam, C. D., Deutschmann, A. U., Pather, S. R., Goldberg, E. M., … Ming, G. li. (2020). Sliced Human Cortical Organoids for Modeling Distinct Cortical Layer

Formation. *Cell Stem Cell*, *26*(5), 766-781.e9. https://doi.org/10.1016/j.stem.2020.02.002

Rock, E. M., Sticht, M. A., Duncan, M., Stott, C., & Parker, L. A. (2013). Evaluation of the potential of the phytocannabinoids, cannabidivarin (CBDV) and Δ9-tetrahydrocannabivarin (THCV), to produce CB 1 receptor inverse agonism symptoms of nausea in rats. *British Journal of Pharmacology*, *170*(3), 671–678. https://doi.org/10.1111/bph.12322

Rourke, W. (2019). *Protocol for Drug Permeability Experiment Across Caco-2 or MDCK Cell Lines*. Canada.

Ruan, C., & Elyaman, W. (2022). A New Understanding of TMEM119 as a Marker of Microglia. *Frontiers in Cellular Neuroscience*, *16*(June), 1–4. https://doi.org/10.3389/fncel.2022.902372

Schukking, M., Miranda, H. C., Trujillo, C. A., Negraes, P. D., & Muotri, A. R. (2018). Direct Generation of Human Cortical Organoids from Primary Cells. *Stem Cells and Development*, *27*(22), 1549–1556. https://doi.org/10.1089/scd.2018.0112

Sethi, P. K., Muralidhara, S., Bruckner, J. V., & White, C. A. (2014). Measurement of plasma protein and lipoprotein binding of pyrethroids. *Journal of Pharmacological and Toxicological Methods*, *70*(1), 106–111. https://doi.org/10.1016/j.vascn.2014.06.002

Shi, Y., Sun, L., Wang, M., Liu, J., Zhong, S., Li, R., … Wang, X. (2020). Vascularized human cortical organoids (vOrganoids) model cortical development in vivo. *PLoS Biology*, *18*(5), 1–29. https://doi.org/10.1371/journal.pbio.3000705

Solowij, N., Broyd, S. J., Beale, C., Prick, J. A., Greenwood, L. M., Van Hell, H., … Yücel, M. (2018). Therapeutic Effects of Prolonged Cannabidiol Treatment on Psychological Symptoms and Cognitive Function in Regular Cannabis Users: A Pragmatic Open-Label Clinical Trial. *Cannabis and Cannabinoid Research*, *3*(1), 21–34. https://doi.org/10.1089/can.2017.0043

Sonar, S. A., & Lal, G. (2019). The iNOS activity during an immune response controls the CNS pathology in experimental autoimmune encephalomyelitis. *Frontiers in Immunology*, *10*(APR). https://doi.org/10.3389/fimmu.2019.00710

Stone, N. L., England, T. J., & O'Sullivan, S. E. (2021). Protective Effects of Cannabidivarin

and Cannabigerol on Cells of the Blood–Brain Barrier Under Ischemic Conditions. *Cannabis and Cannabinoid Research*, *X*(X), 1–13. https://doi.org/10.1089/can.2020.0159

Takahashi, K., & Yamanaka, S. (2006). Induction of Pluripotent Stem Cells from Mouse Embryonic and Adult Fibroblast Cultures by Defined Factors. *Cell*, *126*(4), 663–676. https://doi.org/10.1016/j.cell.2006.07.024

Tang, C. (2018). In vitro vs. In vivo: Is One Better? *University Health Network*, p. 1. Retrieved from https://www.uhnresearch.ca/news/vitro-vs-vivo-one-better

Taylor, L., Crockett, J., Tayo, B., & Morrison, G. (2019). A Phase 1, Open-Label, Parallel-Group, Single-Dose Trial of the Pharmacokinetics and Safety of Cannabidiol (CBD) in Subjects With Mild to Severe Hepatic Impairment. *Journal of Clinical Pharmacology*, *59*(8), 1110–1119. https://doi.org/10.1002/jcph.1412

Thion, M. S., Ginhoux, F., & Garel, S. (2018). Microglia and early brain development: An intimate journey. *Science*, *362*(6411), 185–189. https://doi.org/10.1126/science.aat0474

Thomson, J. A., Itskovitz-Eldor, J., Shapiro, S. S., Waknitz, M. A., Swiergiel, J. J., & Marshall, V. S. (1998). Embryonic stem cell lines derived from human blastocysts. *Science*, *282*(5391), 1145–1147. https://doi.org/10.1126/science.282.5391.1145

Trujillo, C. A., Gao, R., Negraes, P. D., Gu, J., Buchanan, J., Preissl, S., … Muotri, A. R. (2019). Complex oscillatory waves emerging from cortical organoids model early human brain network development. *Cell Stem Cell*, *25*(4), 558–569. https://doi.org/10.1016/j.stem.2019.08.002

Venkatachalam, K., & Montell, C. (2007). TRP Channels. *Annu Rev Biochem.*, *76*, 387–417. https://doi.org/10.1146/annurev.biochem.75.103004.142819

Vollner, L., Bieniek, D., & Korte, F. (1969). Haschisch XX1: Cannabidivarin, ein neuer Haschisch-Inhaltsstoff. *Tetrahedron Letters*, *10*(3), 1969.

Vučkovic, S., Srebro, D., Vujovic, K. S., Vučetic, Č., & Prostran, M. (2018). Cannabinoids and pain: New insights from old molecules. *Frontiers in Pharmacology*, *9*(NOV), 1–19. https://doi.org/10.3389/fphar.2018.01259

Wang, S. N., Wang, Z., Xu, T. Y., Cheng, M. H., Li, W. L., & Miao, C. Y. (2020). Cerebral Organoids Repair Ischemic Stroke Brain Injury. *Translational Stroke Research*, *11*(5), 983–1000. https://doi.org/10.1007/s12975-019-00773-0

Wang, X., Lin, C., Wu, S., Zhang, T., Wang, Y., Jiang, Y., & Wang, X. (2022). Cannabidivarin alleviates neuroinflammation by targeting TLR4 co-receptor MD2 and improves morphine-mediated analgesia. *Frontiers in Immunology*, *13*(August), 1–13. https://doi.org/10.3389/fimmu.2022.929222

Whiting, P. F., Wolff, R. F., Deshpande, S., Di Nisio, M., Duffy, S., Hernandez, A. V., … Kleijnen, J. (2015). Cannabinoids for medical use: A systematic review and meta-analysis. *JAMA - Journal of the American Medical Association*, *313*(24), 2456–2473. https://doi.org/10.1001/jama.2015.6358

Xiang, Y., Tanaka, Y., Cakir, B., Patterson, B., Kim, K. Y., Sun, P., … Park, I. H. (2019). hESC-Derived Thalamic Organoids Form Reciprocal Projections When Fused with Cortical Organoids. *Cell Stem Cell*, *24*(3), 487-497.e7. https://doi.org/10.1016/j.stem.2018.12.015

Xiang, Y., Tanaka, Y., Patterson, B., Kang, Y.-J., Govindaiah, G., Roselaar, N., … Park, I.-H. (2017). Fusion of regionally-specified hPSC-derived organoids models human brain development and interneuron migration. *Cell Stem Cell*, *21*(3), 383–398. https://doi.org/10.1016/j.stem.2017.07.007

Yokoi, R., Shibata, M., Odawara, A., Ishibashi, Y., Nagafuku, N., Matsuda, N., & Suzuki, I. (2021). Analysis of signal components < 500 Hz in brain organoids coupled to microelectrode arrays: A reliable test-bed for preclinical seizure liability assessment of drugs and screening of antiepileptic drugs. *Biochemistry and Biophysics Reports*, *28*(July), 101148. https://doi.org/10.1016/j.bbrep.2021.101148

Zamberletti, E., Gabaglio, M., Woolley-Roberts, M., Bingham, S., Rubino, T., & Parolaro, D. (2019). Cannabidivarin Treatment Ameliorates Autism-Like Behaviors and Restores Hippocampal Endocannabinoid System and Glia Alterations Induced by Prenatal Valproic Acid Exposure in Rats. *Frontiers in Cellular Neuroscience*, *13*(August), 1–15. https://doi.org/10.3389/fncel.2019.00367

Zientek, M. A., Goosen, T. C., Tseng, E., Lin, J., Bauman, J. N., Walker, G. S., … Smith, B. J. (2016). In vitro kinetic characterization of axitinib metabolism. *Drug Metabolism and Disposition*, *44*(1), 102–114. https://doi.org/10.1124/dmd.115.065615

Zuardi, A. W. (2008). Cannabidiol : from an inactive cannabinoid to a drug with wide spectrum of action Canabidiol : de um canabinóide inativo a uma droga com amplo espectro de ação. *Revista Brasileira de Psiquiatria*, *30*(3), 271–280. https://doi.org/10.1590/S1516-44462008000300015